

LOW TEMPERATURE PARAMAGNETIC RESONANCE
STUDIES OF THE RARE EARTH GROUP IONS
USING A NEW HIGH SENSITIVITY SPECTROMETER

BY

HARVEY ALLEN BUCKMASTER

A Thesis submitted in partial fulfilment of
the requirements for the degree of
Doctor of Philosophy
in
Physics

We accept this thesis as conforming to the standard required
from candidates for the degree of Doctor of Philosophy

Members of the Department of Physics

The University of British Columbia

November 1955

ABSTRACT

A high sensitivity, wide or narrow band, double field modulation paramagnetic resonance spectrometer operating at a wavelength of 1.25 cm. for use at liquid helium temperatures has been developed which is described in detail. This spectrometer employs a transmission type cylindrical resonant cavity operated in the H_{111} mode. In wide band operation, the magnetic field is modulated at 60 cps. to an amplitude in excess of the resonance line width and at 462.5 kcs. to an amplitude less than or equal to the line width. For narrow band operation only, the high frequency modulation is employed and the static magnetic field is linearly swept. A signal from 10^{-9} grams of diphenyltrinitro phenyl hydrazyl $[(C_6H_5)_2 \cdot N-N \cdot C_6H_2 \cdot (NO_2)_3]$ has been observed at $290^\circ K$. using wide band operation (8 kcs.) indicating that sensitivities of the order of 10^{-12} grams can be achieved with it at $4.2^\circ K$. in narrow band operation (1 cps.). This sensitivity is close to the theoretical value predicted by Bleaney of 10^{-13} grams and is several orders of magnitude greater than that reported for any other paramagnetic resonance spectrometer.

Using this improved sensitivity, higher order transitions $\Delta M = \pm 2, \pm 3$ in dilute gadolinium ethyl sulphate $[4f^7; 8s_{7/2}]$ which were not previously observable, have been studied at $90^\circ K$. as a function of the orientation of the magnetic field with respect to the axis

of symmetry of the crystal. These transitions show that the effect of off-diagonal terms in spin-Hamiltonian have a greater effect on the energy levels than had previously been appreciated from measurements of the $\Delta M = \pm 1$ transitions and help to explain the discrepancies between the calculated and observed zero field splittings. =

An excited state in dilute dysprosium ethyl sulphate $[4f^9; {}^8H_{15/2}]$ has been observed at 4.2°K . with $g_{\parallel} = 5.85 \pm 0.05$ which had previously only been observed at 20°K . with $g_{\parallel} = 5.80 \pm 0.02$ and $g_{\perp} = 8.40 \pm 0.2$.

The line width of dilute praseodymium ethyl sulphate $[4f^2; {}^3H_4]$ has been measured at 4.2°K . and found to be 35 ± 5 gauss showing that the previously observed line width of 200 gauss at 20°K . is due to spin-lattice broadening.

The University of British Columbia

Faculty of Graduate Studies

PROGRAMME OF THE

Final Oral Examination for the Degree of Doctor of Philosophy

of

HARVEY ALLEN BUCKMASTER

B.Sc. (University of Alberta) 1950

M.A. (University of British Columbia) 1952

FRIDAY, DECEMBER 16th, 1955, at 3:00 p.m.

IN ROOM 300, PHYSICS BUILDING

COMMITTEE IN CHARGE

DEAN H. F. ANGUS, *Chairman*

A. D. MOORE

T. E. HULL

B. N. MOYLS

F. H. SOWARD

G. M. VOLKOFF

K. C. MANN

J. B. BROWN

A. M. CROOKER

External Examiner—B. BLEANEY

Clarendon Laboratory, Oxford, England

LOW TEMPERATURE PARAMAGNETIC RESONANCE STUDIES OF THE RARE EARTH GROUP IONS USING A NEW HIGH SENSITIVITY SPECTROMETER

ABSTRACT

A high sensitivity, wide or narrow band, double field modulation paramagnetic resonance spectrometer operating at a wavelength of 1.25 cm. for use at liquid helium temperatures has been developed which is described in detail. This spectrometer employs a transmission type cylindrical resonant cavity operated in the H_{111} mode. In wide band operation, the magnetic field is modulated at 60 cps. to an amplitude in excess of the resonance line width and at 462.5 kcs. to an amplitude less than or equal to the line width. For narrow band operation, only the high frequency modulation is employed and the static magnetic field is linearly swept. A signal from 10^{-9} grams of diphenyl-trinitro phenyl hydrazyl $[(C_6H_5)_2 \cdot N \cdot N \cdot C_6H_2 \cdot (NO_2)_3]$ has been observed at 290°K. using wide band operation (8 kcs.) indicating that sensitivities of the order of 10^{-12} grams can be achieved with it at 4.2°K. in narrow band operation (1 cps.). This sensitivity is close to the theoretical value of 10^{-13} grams predicted by Bleaney and is several orders of magnitude greater than that reported for any other paramagnetic resonance spectrometer.

Using this improved sensitivity, higher order transitions $\Delta M = \pm 2, \pm 3$ in dilute gadolinium ethyl sulphate $[4f^7; {}^8S_{7/2}]$ which were not previously observable, have been studied at 90°K. as a function of the orientation of the magnetic field with respect to the symmetry axis of the crystal. These transitions show that the effect of off-diagonal terms in spin-Hamiltonian have a greater effect on the energy levels than had previously been appreciated from measurements of the $\Delta M = \pm 1$ transitions and help to explain the discrepancies between the calculated and observed zero field splittings.

An excited state in dilute dysprosium ethyl sulphate $[4f^9; {}^6H_{15/2}]$ has been observed at 4.2°K. with $g_1 = 5.85 \pm 0.05$ which had previously only been observed at 20°K. with $g_1 = 5.80 \pm 0.02$ and $g_2 = 8.40 \pm 0.2$.

The line width of dilute praseodymium ethyl sulphate $[4f^2; {}^3H_4]$ has been measured at 4.2°K. and found to be 35 ± 5 gauss showing that the previously observed line width of 200 gauss at 20°K. is due to spin-lattice broadening.

PUBLICATIONS

Radial Matrix Elements for the Quadrupole Transition with the Morse Potential.

Canadian Journal of Physics. 30, 314 (1952).

A New Paramagnetic Resonance Spectrometer.

(Co-author H. E. D. Scovil), Canadian Journal of Physics
(submitted for publication).

▲ $M=\pm 2$ Transitions in Dilute Gadolinium Ethyl Sulphate.

Canadian Journal of Physics (submitted for publication).

▲ $M=\pm 3$ Transitions in Dilute Gadolinium Ethyl Sulphate.

Canadian Journal of Physics (submitted for publication).

GRADUATE STUDIES

Field of Study: Physics

Electromagnetic Theory.....	W. Opechowski
Quantum Mechanics.....	G. M. Volkoff
Magnetism.....	W. Opechowski
Electronics.....	H. E. D. Scovil
Special Relativity Theory.....	W. Opechowski
Quantum Theory of Radiation.....	F. A. Kaempffer
Advanced Quantum Mechanics.....	{ W. Opechowski G. M. Volkoff F. A. Kaempffer

Other Studies:

Continuous Groups.....	S. A. Jennings
Network Theory.....	A. D. Moore
Theory of Functions of a Real Variable.....	R. D. James
Theory of Functions of a Complex Variable.....	W. H. Simons
Theory of Algebraic Numbers.....	B. N. Moyls
Modern Algebra.....	D. Derry
Integral Equations and Eigenvalue Equations.....	T. E. Hull

ACKNOWLEDGMENTS

The research described in this thesis was supported by the National Research Council of Canada through research grants to Dr. Scovil and the award of two Studentships (1952-3, 1953-4) and a Fellowship (1954-5) along with Summer Scholarships (1952, 53, 54, 55) to the author. I am also indebted to N.R.C. for making it possible for me to continue my studies after the completion of this thesis by the award of an Overseas Postdoctorate Fellowship.

It is not possible to adequately express the deep appreciation which I owe to Dr. H.E.D. Scovil. Without the motivation through his active interest, stimulating discussion, and general help, this research could not have been completed.

I should like to express my sincere gratitude to all my teachers, both at the University of British Columbia and at the University of Alberta, for increasing my knowledge and enthusiasm for physics.

The members of the low temperature group, Dr. J.M. Daniels, Dr. J.B. Brown and Mr. H. Zerbst, deserve special acknowledgment for their help in the design of low temperature equipment and for supplying the liquid helium required for some of the experiments described in this thesis.

I am indebted to Dr. K.C. Mann for the loan of a current regulator which was used with the electromagnet

during the final experiments.

The donation of a billet of soft steel for the electromagnet by the Steel Company of Canada Ltd. is acknowledged.

The equipment used could not have been designed and constructed so adequately without the interest, help and cooperation of the members of the Physics Department shop; Mr. A.J. Fraser, Mr. W. Morrison, Mr. W. Maier, Mr. E. Price and Mr. J. Lees. Grateful acknowledgment is also made to Miss A. Redlick, Mr. D. Watts and Mr. J. Elliott for drafting most of the diagrams and to Miss E. Staf and Miss P. Wood for typing the final draft of this thesis.

I wish to express my appreciation to all my fellow students who contributed in innumerable ways.

...

TERMINOLOGY

The following conventions, definitions, abbreviations and symbols are adhered to in this thesis.

- Conventions:
- a. 2.64 refers to subsection 4 of section 6 of Chapter II.
 - b. (III,7) refers to equation 7 which occurs in Chapter III. All equations are numbered consecutively from the beginning of Chapter I to the end of Chapter IV.
 - c. Bleaney (B8) refers to a reference by Bleaney which occurs as the eighth reference in the "B" section of the bibliography when these are arranged in alphabetical order. Minor references occur as (E1).

- Definitions:
- a. Half line width refers to the full width of a resonance line at half intensity.
 - b. Room temperature means 290°K. , oxygen temperature 90°K. , nitrogen temperature 78°K. , hydrogen temperature 20°K. and helium temperature 4.2°K.

Abbreviations:

Symbols:

Constants: The meanings of all symbols employed in this thesis are the same as those in the

list issued by the Physical Society of London unless defined otherwise and all values of constants are taken from the International Critical Tables.

.....

TABLE OF CONTENTS

	Page
INTRODUCTION	
A. Methods of Measuring the Paramagnetic Properties of Matter	i
B. Magnetic Properties of Matter in the Solid State	iii
CHAPTER I - QUANTUM THEORY OF PARAMAGNETISM	1
1.1 - Introduction	1
1.2 Paramagnetic Resonance Phenomena	3
1.21 The resonance conditions	3
1.22 The fine structure	4
1.23 The hyperfine structure	7
1.3 Line Width	8
1.31 Spin - lattice interaction	9
1.32 Spin - spin interaction	10
1.4 Energy Levels of the Ion	12
1.41 General Hamiltonian	13
1.42 Hamiltonian of the free ion in magnetic field	14
1.43 Ion in the crystalline electric field	16
1.44 Matrix elements of the crystalline field	20
1.5 Spin - Hamiltonian	23
1.51 Axial symmetry about z-axis	24
1.52 Hyperfine structure	27
1.53 Non-axial symmetry	28
1.54 S-State ions	29

	Page
1.55 Anomalous case	30
CHAPTER II - PARAMAGNETIC RESONANCE SPECTROMETERS . .	33
2.1 Introduction	33
2.2 General Requirements	33
2.3 Noise	37
2.4 General Classification	41
2.5 Point-to-Point Spectrometer	43
2.6 Frequency Modulation Spectrometers	43
2.61 Line Shape Spectrometer	44
2.62 Balanced Bridge Spectrometer	44
2.7 Field Modulation Spectrometers	45
2.71 Bolometer Spectrometer	45
2.72 Superheterodyne Spectrometer	46
2.73 Video Spectrometer	47
2.74 Double Field Modulation Spectrometer	47
2.8 Comparison of Techniques	51
CHAPTER III - Experimental Apparatus	53
3.1 Introduction	53
3.2 Microwave Apparatus	53
3.21 Wave Guide Components	54
3.22 Microwave Power Generator	55
3.23 Detectors	56
3.24 Cavity Resonators	56
3.25 Wavelength Measurement	57
3.26 Klystron Stabilization	58
3.3 Magnetic Field Equipment	58
3.31 Design and Construction of the Electromagnet	58

	Page
3.32 Performance of the Electromagnet	60
3.33 Electromagnet Power Sources	62
3.34 Magnetic Field Measurements	63
3.35 Low Frequency Modulation	65
3.36 High Frequency Modulation	66
3.4 Detection Apparatus	69
3.41 Single Modulation	69
3.42 Double Modulation	70
3.43 Video Display	71
3.44 Narrow Band Operation	72
3.5 Auxiliary Electronic Apparatus	72
3.51 Calibrator	72
3.52 Frequency Meter	73
3.53 Power Supplies	73
3.6 Low Temperature Apparatus	74
3.61 Single Modulation Head	74
3.62 Double Modulation Head	76
3.63 Helium Recovery System	81
3.7 Crystals	82
3.8 Performance	84
CHAPTER IV - EXPERIMENTAL RESULTS	87
4.1 Introduction	87
4.2 Gadolinium Ethyl Sulphate	88
4.21 Theory	89
4.22 Experimental Results For Dilute Gadolinium Ethyl Sulphate	91

	Page
4.3 Line Width of Praseodymium Ethyl	
Sulphate at 4.2°K.	98
4.4 Excited State in Dysprosium Ethyl	
Sulphate at 4.2°K.	99
4.5 Future Experiments	100

LIST OF ILLUSTRATIONS

Facing Page

Fig. 1a	Energy level diagram of the ground state splittings of Cr^{3+} in a crystalline electric field with predominantly cubic symmetry but with a small component of trigonal symmetry	5
Fig. 1b	Energy level diagram, $S = 3/2$, magnetic field parallel to the axis of crystalline field showing the allowed transition . . .	55
Fig. 2	Energy level diagram, $S = 1/2$, $I = 5/2$ in a strong magnetic field showing the allowed transitions	7
Fig. 3a	Point-to-point paramagnetic resonance spectrometer.	43
Fig. 3b	Video paramagnetic resonance spectrometer .	43
Fig. 4	Balanced bridge paramagnetic resonance spectrometer	44
Fig. 5	Bolometer paramagnetic resonance spectrometer	45
Fig. 6	Superheterodyne paramagnetic resonance spectrometer	46
Fig. 7	Double field modulation paramagnetic resonance spectrometer	47
Fig. 8	Block diagram of 1.25 cm. microwave apparatus	54
Fig. 9	Block diagram of a cavity type klystron frequency stabilizer	58

Fig. 10	Block diagram of current regulator for electromagnet	62
Fig. 11	Block diagram of proton resonance unit. . .	64
Fig. 12	Block diagram of slotted resonant cavity .	67
Fig. 13	Block diagram of double modulation detection system	70
Fig. 14	Cross-section of K band resonator	75
Fig. 15a	Diagram of double Kovar seal	80
Fig. 15b	Diagram of sandwich type insulated vacuum seal	80
Fig. 16	Helium recovery and vacuum system	81
Fig. 17	Crystal structure of the rare earth ethyl sulphates	83
Fig. 18	$\Delta M = \pm 2$ transitions in gadolinium ethyl sulphate as function of the angle with symmetry axis of the crystal	96

LIST OF TABLES

		<u>Facing Page</u>
TABLE I	The Transition Groups Of The Periodic Table	v
TABLE II	The Ground States Of The Free Ions Of The Iron And Rare Earth Groups	vi
TABLE III	The Values of ρ and H Satisfying Kramer's Doublet Relation When $g = 2$	35
TABLE IV	The Relative Characteristics And Sensitiv- ities Of Paramagnetic Resonance Spectrometers	51
TABLE V	Experimental Data $\Delta M = \pm 1$ Transitions For Dilute Gadolinium Ethyl Sulphate at 290°K.	95
TABLE VI	Experimental Data $\Delta M = \pm 1$ Transitions of n Dilute Gadolinium Ethyl Sulphate at 90°K.	95
TABLE VII	"g" Values And Splitting Parameter For Dilute Gadolinium Ethyl Sulphate From $\Delta M = \pm 1$ Transitions	95
TABLE VIII	Experimental Data $\Delta M = \pm 2$ Transitions For Dilute Gadolinium Ethyl Sulphate At 90°K.	96
TABLE IX	$\Delta M = \pm 2$ Transitions For Dilute Gadolinium Ethyl Sulphate As Function Of Angle Be- tween Direction Of Magnetic Field And Crystal Symmetry Axis At 5° Intervals	96

TABLE X	Values of g_{\parallel} And g_{\perp} And Splitting Parameters For Dilute Gadolinium Ethyl Sulphate From $\Delta M = \pm 2$ Transitions At 90°K	96
TABLE XI	$\Delta M = \pm 3$ Transitions For Dilute Gado- linium Ethyl Sulphate As Function Of Angle Between Direction Of Magnetic Field And Crystal Symmetry Axis At 5° Intervals.	97
TABLE XII	Values of g_{\parallel} And g_{\perp} And Splitting Parameters For Dilute Gadolinium Ethyl Sulphate From $\Delta M = \pm 3$ Transitions At 90°K	97

LIST OF PLATES

Facing Page

Plate	I	a. "g" marker signal from video spectrometer	49
		b. "g" marker signal from video spectrometer with r.f. field modulation on	49
		c. "g" marker signal from double field modulation spectrometer with linear detector	49
		d. 10^{-9} grams "g" marker signal from double field modulation spectrometer with linear detector	49
Plate	II	General view of experimental apparatus	53
Plate	III	View of microwave components	55
Plate	IV	View of electromagnet showing d.c. coils, modulation coils and spectrometer head with the dewars in the gap	60
Plate	V	View showing shielding of r.f. amplifier and detector with shields removed . . .	71
Plate	VI	View of the double modulation head with the dewars in the magnetic field . . .	74
Plate	VII	View of helium temperature single modulation head	76

Plate VIII	View of the double modulation head with the dewars removed	77
Plate IX	a. Structure on $\Delta M = \pm 1$ transitions due to lattice defects and pairs of Gd^{+3} ions	97
	b. 4 of 5 $\Delta M = \pm 3$ transitions near crossover point	97
	c. $\Delta M = \pm 2$ transitions near crossover point	97
	d. 6 $\Delta M = \pm 2$ transitions at magnetic field orientation where total separ- ation is 500 gauss	97
Plate X	General view of experimental apparatus .	109
Plate XI	General view of microwave bench	110

.....

INTRODUCTION

A. Methods Of Measuring The Paramagnetic Properties
Of Matter

In this thesis, we shall be concerned with those magnetic properties of ions of the rare earth group, which can be measured using paramagnetic resonance. Magnetic resonance is a branch of radio frequency spectroscopy which is important for solid state studies. It can be classified into (a) nuclear, (b) ferromagnetic, (c) antiferromagnetic and (d) paramagnetic resonance. The first is concerned with nuclear dipoles while the remainder are concerned with electronic dipoles. (b) and (c) deal with magnetic systems where the electronic dipoles are strongly coupled together by exchange forces while in (d) the electronic dipoles are loosely coupled together; each paramagnetic ion is considered individually.

There is one important difference between optical and radio frequency spectroscopy. The former deals with spectra which are due to the absorption and spontaneous emission of radiation with Einstein emission, which is stimulated by the presence of radiation of the same frequency, of at most secondary importance. The latter is only concerned with the absorption and stimulated emission of radiation.

As the energy $h\nu$ of the radio frequency quantum is always much smaller than the thermal energy kT , the number

of occurring processes of absorption is only slightly larger than the number of occurring processes of stimulated emission. This net surplus, which is inversely proportional to the temperature T_s , characterizing the statistical distribution over the energy levels concerned, is what is detected in an experiment.

The magnetic moment of an ion arises from contributions by electronic and nuclear dipoles; the effect of the former predominating. A study of magnetism from the microscopic viewpoint consequently deals with the properties of electrons and nuclei.

The paramagnetic properties of ions have been investigated by measurements of the (a) susceptibility, (b) specific heat, (c) gyromagnetic ratio, (d) Faraday effect, (e) paramagnetic relaxation and (f) paramagnetic resonance. All but the last of these methods, study the magnetic properties of electrons in atoms or ions from the macroscopic viewpoint. In ionic crystals, these properties depend upon the behaviour of the occupied lower electronic states, in particular, their separation, their relative position and their anisotropic behaviour in a magnetic field. Paramagnetic resonance, since it is essentially a spectroscopic method, studies these same properties from the microscopic viewpoint which enables it to differentiate between impurities. This is of great value for studies of the ions of the rare earth group where it is difficult to obtain pure

compounds. Moreover, it is orders of magnitude more sensitive than any of the other methods. Consequently, it can deal with very small quantities of paramagnetic substances which is also of importance for rare earth group studies. This sensitivity is sufficient to permit the perturbing effects of the nuclear spin and nuclear electric quadrupole moment to be detected. This is particularly advantageous since this method can be used to determine nuclear spins, ratio of the magnetic moments of two isotopes of the same atom and nuclear moments of those atoms which are not easily accessible to other methods.

Unfortunately, it suffers from several disadvantages. Single crystals of suitable size, which are required for accurate work, cannot always be grown. Certain substances cannot be investigated because there are no allowed transitions between the levels which give rise to the paramagnetism. At present, information can be obtained only about the ground state. Recent work indicates that resonances between the ground state and the first excited state may be detected.

B. Magnetic Properties Of Matter In The Solid State

In the solid state, atoms are very close together and consequently strong forces of interaction exist between them. For pure elements, there is an exchange interaction between the valence electrons. In non-metals, the valence electrons are paired with spins opposing and this produces no magnetic

effect. In pure metals, the valence electrons form an electron gas since they are no longer bound to the atom. The remaining closed shells exhibit no magnetic properties because of the Pauli exclusion principle. It can be shown by consideration of Fermi-Dirac statistics or exchange demagnetization that the electron gas has only a very feeble magnetic moment.

Paramagnetism is found in solids only when some of the atoms contain an incomplete electron shell. In ionic crystals the tendency is to form ions with completed shells (inert gas configuration). Hence in such compounds only those elements which have incomplete d or f shells are paramagnetic, since in these elements incomplete shells remain after their normal valency requirements are satisfied.

In covalent crystals and covalent complexes the tendency is to form bonds, each bond containing a pair of electrons with opposed spins. Hence, such crystals are not normally paramagnetic. The electrons in an incomplete d shell frequently take part in covalent bonding, the atoms involved exhibiting an abnormal valency (coordination bond). Thus, many atoms which would be paramagnetic in an ionic crystal, are diamagnetic in a covalent crystal. In particular, covalent compounds of the 3d and 4f series are generally paramagnetic and there are reasons for believing that many typical ionic crystals (e.g. $\text{CsTi}(\text{SO}_4)_2 \cdot 12\text{H}_2\text{O}$) are not purely ionic, but that the paramagnetic ion is partly

TABLE I

Transition Groups of the Periodic Table

<u>Group</u>	<u>Z</u>	<u>Incomplete Shell</u>	<u>n</u>
Iron	21 to 29	3d ⁿ	1 - 10
Palladium	38 to 46	4d ⁿ	0 - 10
Rare Earth	57 to 71	4f ⁿ	0 - 14
Platinum	72 to 78	5d ⁿ	2 - 9
Actinide	88 to 96 (?)	6d ⁿ	0 - 8 (?)

covalently bonded. Conversely, there are some purely covalent compounds which exhibit paramagnetism, e.g. NO which has 15 electrons and hence must have at least one of these electrons unpaired.

In the pure metals of these groups, the exchange forces play the predominant role in penetrating the inner shells and usually produce exchange demagnetization. It is possible for these forces to align the spins of the electrons producing exchange magnetization which results in the metal having a permanent magnetic moment, i.e. ferromagnetism. This occurs with certain elements of the iron group such as iron, cobalt and nickel.

The five transition groups of the periodic table are listed in Table I.

The palladium, platinum and most actinide group elements appear to form covalently bound compounds which generally exhibit no paramagnetism except in complexes. The iron and rare earth groups form many ionic compounds which exhibit paramagnetism and hence these groups have been studied extensively. In Table II, the ions of these two groups are listed together with their configuration of the incomplete shell and the ground state as given by the Hundt rules. These rules, which determine the lowest-lying term for a given configuration, are

1. a. Of all the terms allowed by the Pauli principle, that one with the maximum multiplicity lies lowest (the multiplicity is equal to

TABLE II

The Ground States of the Free Ions of the Iron and
Rare Earth Groups

Ion	<u>Electronic Configuration</u>	<u>Ground State Free Ion</u>
Ti ³⁺ , V ⁴⁺	3d ¹	² D _{3/2}
V ³⁺	3d ²	³ F ₂
Cr ³⁺ , V ²⁺	3d ³	⁴ F _{3/2}
Mn ³⁺ , Cr ²⁺	3d ⁴	⁵ D ₆
<u>Iron</u> <u>Group</u> Fe ³⁺ , Mn ²⁺	3d ⁵	⁶ S ₀
Fe ²⁺	3d ⁶	⁵ D ₄
Co ²⁺	3d ⁷	⁴ F _{9/2}
Ni ²⁺	3d ⁸	³ F ₄
Cu ²⁺	3d ⁹	² D _{5/2}
Zn ²⁺	3d ¹⁰	¹ S ₀
<hr/>		
La ³⁺	4f ⁰	¹ S ₀
Ce ³⁺	4f ¹	² F _{5/2}
Pr ³⁺	4f ²	³ H ₄
Nd ³⁺	4f ³	⁴ I _{9/2}
Pm ³⁺	4f ⁴	⁵ I ₄
Sm ³⁺	4f ⁵	⁶ H _{5/2}
<u>Rare</u> <u>Earth</u> Eu ³⁺	4f ⁶	⁷ F ₈
Gd ³⁺	4f ⁷	⁸ S _{7/2}
Tb ³⁺	4f ⁸	⁷ F ₆
Dy ³⁺	4f ⁹	⁸ H _{15/2}
Ho ³⁺	4f ¹⁰	⁵ I ₈
Er ³⁺	4f ¹¹	⁴ I _{15/2}
Tm ³⁺	4f ¹²	³ H ₆
Yb ³⁺	4f ¹³	² F _{7/2}
Lu ³⁺	4f ¹⁴	¹ S ₀

$2S + 1$ where S is the total spin quantum number).

- b. If several terms have the same maximum multiplicity, that term with the greatest L lies lowest (L is the total electronic orbital quantum number).
2. Multiplets arising from a configuration consisting of less than half of the electrons in a completed subgroup are usually normal (smallest J lowest) and those from a configuration consisting of more than half are usually inverted (largest J lowest). (Multiplets are terms formed through the various combinations of a given S and L and are characterized by the quantum number $J = L + S$).

CHAPTER I

QUANTUM THEORY OF PARAMAGNETISM

An excellent summary of both the experimental and theoretical aspects of paramagnetic resonance is contained in the review article by Bleaney and Stevens (B11). A complementary review by Bowers and Owens (B16), containing a summary of all the experimental results to date, is at present in press. In this chapter, the theoretical work described in these review articles together with general theoretical papers by Bleaney (B7,8,10) and Abragam and Pryce (A1) and specific theoretical papers on the rare earth group ions by Elliott and Stevens (E1,2,3,S7) are summarized. Since the research described in this thesis is experimental, emphasis is placed on those aspects of the theory which are necessary to describe the results reported in Chapter IV. These results are concerned with only rare earth group ions. No mention is made of those aspects of the theory which are applicable to covalent complexes. This aspect is considered in papers by Stevens (S9), and Abragam and Pryce (A1) amongst others.

1.1 Introduction

The magnetic moment of a paramagnetic ion is due to the orbital and spin angular momentum of the unpaired

electrons which determine the energy levels of the ion. It is not unreasonable to expect that these energy levels will be altered when the magnetic ion is surrounded by other ions and water dipoles. These interactions with the other constituents of the crystal are of three types.

The ion is subjected to a strong inhomogeneous electric field called the crystalline or Stark field which is due to the other constituents of the crystal. The main symmetry of this field is determined by the crystal structure; however it is not unusual that the distortions from this symmetry have a profound effect on the energy levels. The effects of the crystalline electric field is to lift some of the degeneracy of the energy levels of the free ion. This effect will be discussed in 1.4.

It is possible that the effect of an exchange between the electrons of the paramagnetic ion and the other electrons of the crystal will alter the energy levels. Such exchange interactions, which can be calculated only approximately, will be mentioned in 1.31.

The third interaction couples the paramagnetic ions together into a 'spin' system. It will be considered in 1.32.

If the distance between the paramagnetic ions is increased by dilution, then the last two interactions are decreased and it is only necessary to consider the effect of the crystalline electric field. We then speak of magnetically very 'dilute' salts.

1.2 Paramagnetic Resonance Phenomenon

1.21 The Resonance Condition

When an ion possessing a magnetic moment, and therefore having a degenerate ground state, is placed in a steady magnetic field, the degeneracy is lifted and the levels undergo a Zeeman splitting. An oscillating magnetic field of suitable frequency will induce transitions between the Zeeman levels if these are allowed.

The precession frequency of the magnetic moment about the axis of the steady magnetic field H is given by

$$\nu = g \cdot \left(\frac{e}{4\pi mc} \right) \cdot H \quad (1)$$

where g is the spectroscopic splitting factor. g is one if only orbital motion of the electrons exists and precession frequency is then the same as that given by the classical theorem of Larmor which is proved in Van Vleck (V3).

If a circularly polarized magnetic field is also applied such that it also rotates about H in synchronism with the angular momentum vector, it will exert a constant couple on the latter, eventually causing it to turn over and reverse its projection on H . This "flipping over" is accompanied by an absorption of energy from the radiation field.

Quantum mechanically, a free ion with resultant angular momentum J in a magnetic field H has energy levels corresponding to the various spatial orientations of J with

energies $Mg\beta H$, where M is the electronic quantum number and β is the Bohr magneton.

The selection rule for magnetic dipole transitions is $\Delta M = \pm 1$. These transitions can be induced by a frequency such that

$$h\nu = g\beta H \quad (2)$$

which is identical to (1,1) since

$$\beta = \frac{eh}{4\pi mc} \quad (2a)$$

When a system of ions is in thermal equilibrium with their surroundings, the lowest energy states have the greater population. Since transitions up and down have equal a priori probability, the net result of the application of resonance radiation is a gain in energy from the radiation field, and a shift towards a more equal population of the various levels. This corresponds to an increase in the temperature of the system which is sometimes called the "spin" temperature as differentiated from the "lattice" temperature. The resonance absorption can be detected by the loss of energy from the radiation, which causes a damping of the tuned circuit in which the paramagnetic substance is placed.

1.22 The Fine Structure

The degeneracy of the ground state of a paramagnetic ion in a crystal is usually lifted by the crystalline electric field and other interactions, eg. σ for Cr^{3+} in

FIGURE 1b
ENERGY LEVEL DIAGRAM: $S = 3/2$

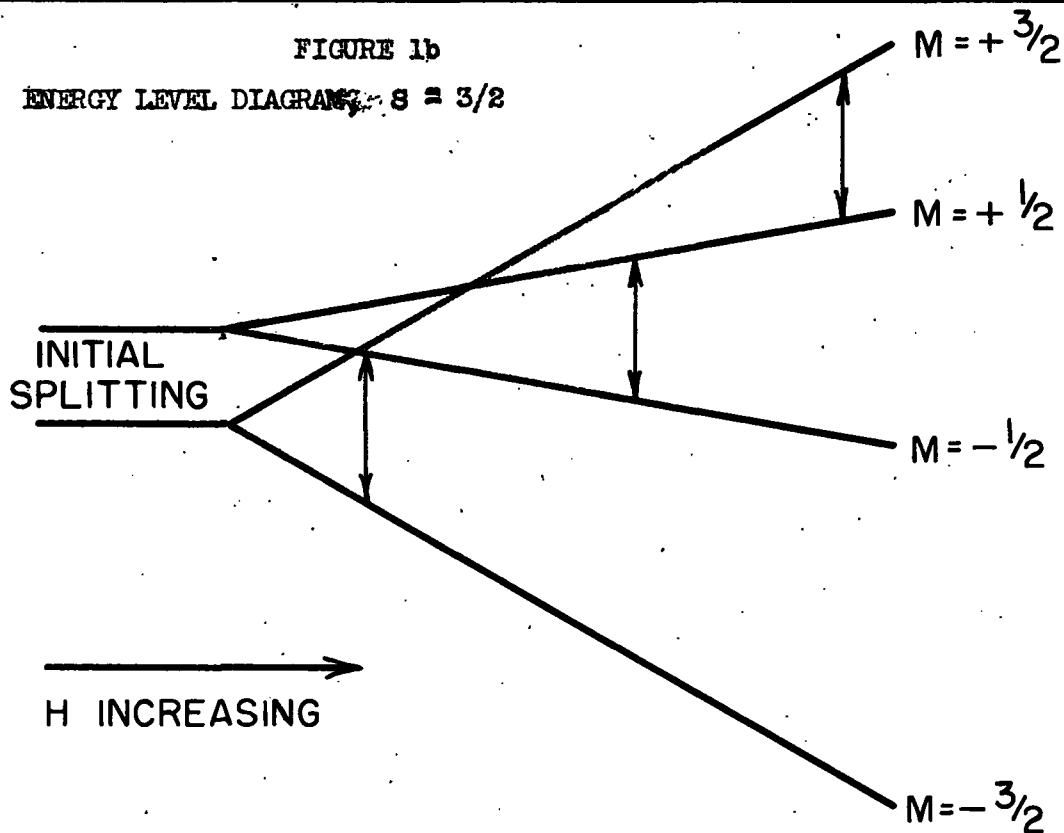
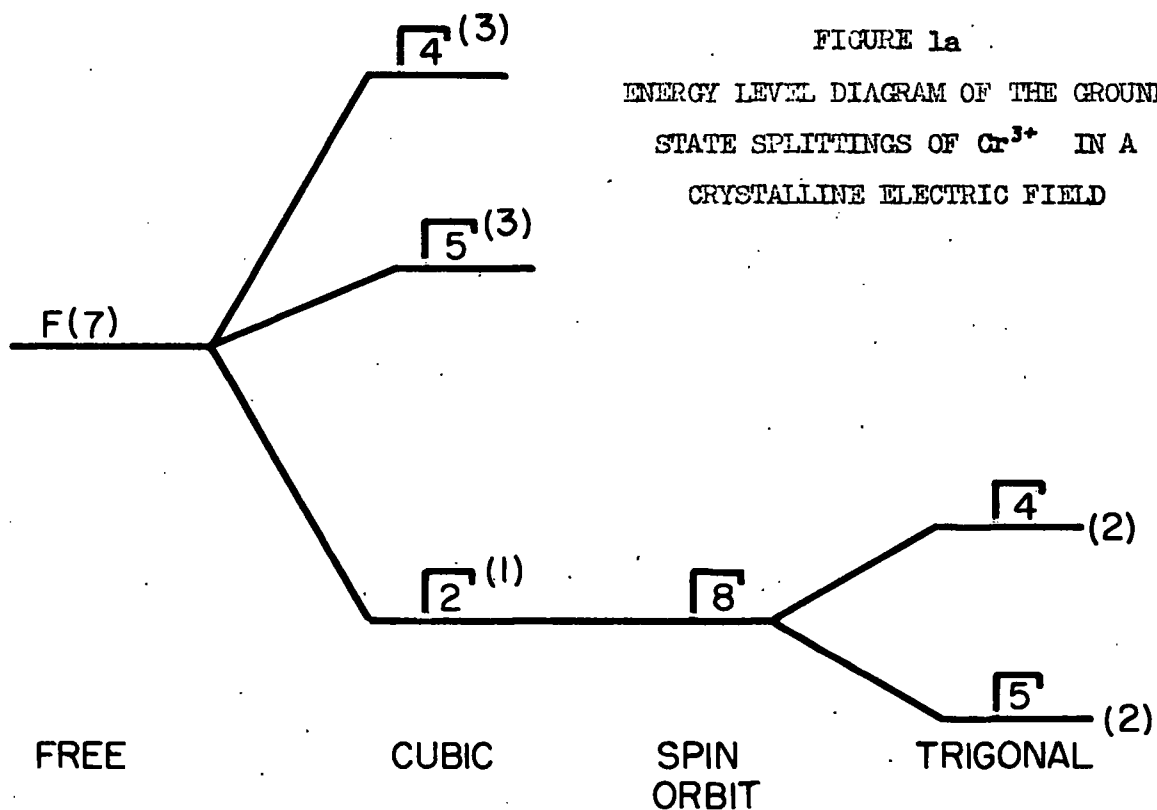


FIGURE 1a
ENERGY LEVEL DIAGRAM OF THE GROUND STATE SPLITTINGS OF Cr^{3+} IN A CRYSTALLINE ELECTRIC FIELD



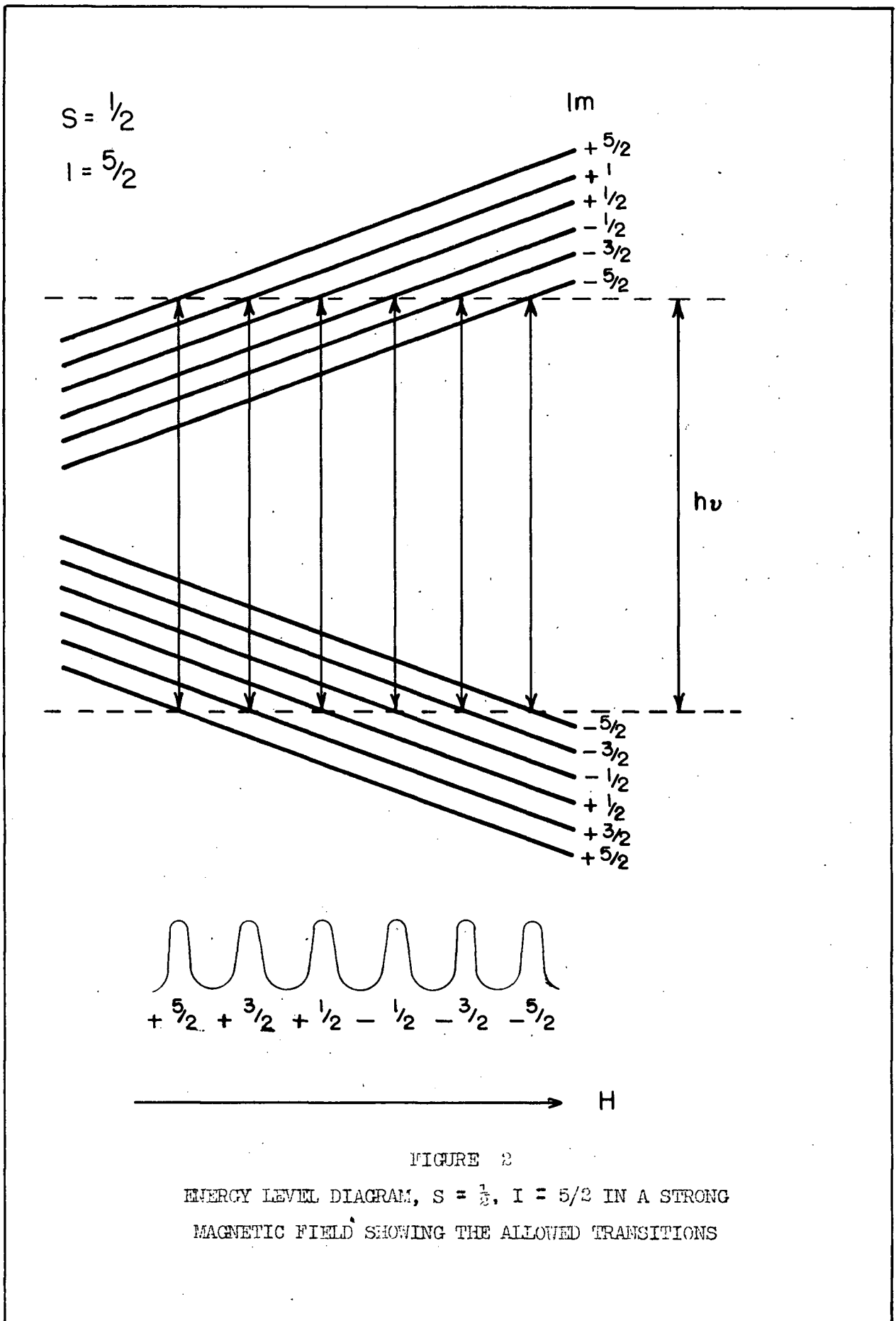
$\text{Cr}(\text{NH}_3\text{CH}_3) \cdot (\text{SO}_4)_2 \cdot 12\text{H}_2\text{O}$, the Cr^{3+} ion is surrounded by a distorted octahedron of water molecules which produce an electric field with predominantly cubic symmetry but with a small component of trigonal symmetry. The seven-fold degenerate orbital ground state of the free Cr^{3+} ion is split into a singlet and two triplets by the cubic component of the field, the singlet lies lowest. Taking into account the spin of $3/2$ this level has four-fold degeneracy and is split into two doublets by spin-orbit coupling. It can be shown (Kramer's Theorem) that if the number of electrons in an ion is odd, all levels are doublets and hence magnetic. If the number of electrons is even, the levels may be singlets which are non-magnetic. Although the energy difference between the lowest and the next higher orbital level is $0(10^4)\text{cm}^{-1}$ and corresponds to an optical frequency, the splitting of the two lowest spin doublets is $0(.2)\text{cm}^{-1}$ and corresponds to a microwave frequency. In Figure 1a, an energy level diagram of these splittings of the ground state of Cr^{3+} is given.

In such a case, it would be possible, in principle, to measure this splitting directly by varying the frequency of the applied microwave radiation until an absorption is observed. However, it is experimentally usually simpler to apply a magnetic field, to vary the splittings and examine the spectrum as a function of field at constant frequency (2.2). In principle, it is possible to pass from high field

measurements to the zero field splittings.

As an example of this, we consider an ion of spin $3/2$ with an initial splitting between the doublets $M = \pm 1/2$ and $\pm 3/2$ due to the crystalline electric field. The axis of quantization is taken to be the same as the axis of the field. When the magnetic field is applied parallel to the axis, the energy levels diverge linearly as is shown in Figure 1b. This is related to the fact that the axis of precession does not change when the field is applied. The selection rule is $\Delta M = \pm 1$ (magnetic dipole transition). The central lines are stronger since they are due to transitions between states for which the projection of the magnetic moment on the direction of the microwave magnetic field is greatest.

When the external magnetic field is applied at an angle to the axis of the crystalline field there is no unique axis of quantization because there is competition between the two fields. In the limiting case of very large magnetic fields, the actual states tend towards those defined by using the direction of this field as the axis of quantization. It is convenient to describe the actual states using the same quantum numbers as for very large magnetic fields. Because the actual states are not pure states of axial quantization, the selection rule $\Delta M = \pm 1$ no longer holds strictly and "forbidden" lines ($\Delta M = \pm 2, \pm 3$, etc.) appear. These are strongest when the splittings due to the external magnetic field and the crystalline electric field are about the same.



Their intensity and position vary in a rather complicated manner with the angle between these two axes.

1.23 The Hyperfine Structure

Hyperfine structure is observed in paramagnetic resonance when the nucleus of the paramagnetic ion possesses a resultant angular momentum and hence a nuclear magnetic moment which will interact with the magnetic field of the electrons. This hyperfine structure is perturbed when the nucleus also possesses an electric quadrupole moment which will interact with the electric field gradient at the nucleus.

The nuclear magnetic moment will take up $2I + 1$ orientations in the field of the surrounding electrons. The external magnetic field is neglected since it is several orders of magnitude smaller (10^3 gauss). If a microwave magnetic field is applied, transitions will occur when the electron magnetic moment changes its orientation. The nuclear magnetic moment will not change its orientation because it is very small. These changes in the orientation of the field acting on the nucleus will change the energy of interaction and will differ for each of the $2I + 1$ nuclear orientations thus splitting each electronic transition into $2I + 1$ components of equal intensity and spacing. In Figure 2, the situation is illustrated when $S = \frac{1}{2}$ and $I = \frac{5}{2}$. The allowed transitions correspond to

$$\Delta M = \pm 1 \text{ and } \Delta m = 0.$$

The effect of the nuclear electric quadrupole moment is to make the hyperfine structure more complex when the external magnetic field is at an angle to the symmetry axis of the crystal. It tries to align the nucleus along the symmetry axis and the complexity arises from the fact that the magnetic field of the electrons will be simultaneously trying to align it in the direction of the external magnetic field. When the two fields are perpendicular, it can be shown that the total number of possible lines is $6I - 1$ and that they are of unequal intensity.

1.3 Line Width

The resolution of the spectra in paramagnetic resonance spectroscopy, is not limited by instrumental effects, but rather by the crystalline environment. Interactions between the paramagnetic ions and the lattice and between the various ions themselves are the principal causes of line width. It is convenient to treat these interactions in terms of relaxation effects, characterizing them by relaxation times: spin-lattice relaxation time and spin-spin relaxation.

Paramagnetic relaxation effects may be studied using frequencies of the order of the reciprocal of the relaxation time. At such frequencies, the lines are not resolved, and the line width at half intensity is of the

order of $1/\tau$ sec^{-1} where τ is the relaxation time. Such phenomena has been reviewed by Cooke (C3).

In paramagnetic resonance, where the lines are resolved because higher frequencies are employed, it is usually necessary to reduce the line width to improve the resolution. To achieve this, it is necessary to understand the underlying processes which we will now outline.

1.31 Spin - Lattice Interaction

The inverse of the spin-lattice relaxation time is a measure of the rate at which a spin reverses direction and gives or receives a quantum of energy to the lattice. If the lifetime of a state is τ then by the uncertainty principle its energy is uncertain to the order of h/τ and hence the line should have approximately this breadth. Two theories have been developed. The first is semi-classical, based on a collision model.

Two processes are assumed to occur. One is a direct process in which quanta of energy are absorbed or emitted by the lattice. It is of the first order, but only lattice waves of a certain frequency are effective since it is a resonance process. In the second, the lattice waves are non-elastically scattered by the magnetic ions, giving a quasi-Raman effect of second order. The intensity of the lattice waves of low frequency which give rise to first order processes is proportioned to T , while the number of Raman processes is proportioned to T^2 for $T \gg \theta$ and T^1

for $T \ll \theta$ where θ is the Debye temperature of the lattice. Experimentally, it has been found that at helium temperatures the first order processes may predominate while at higher temperatures the Raman processes predominate.

Quantum mechanically, it is necessary to consider the effect of an oscillating crystalline electric field caused by lattice vibrations which will couple with the orbital momentum of the magnetic ions. It has been suggested that the coupling between the lattice waves and the spins is produced by spin-orbit coupling. It has also been found that the spin-lattice relaxation time is strongly dependent on the separation between the ground state and the first excited state; τ is longer as the separation increases. Spin-lattice relaxation is the predominant line broadening mechanism at high temperatures, but at temperatures below about 10° K, it is usually negligible compared with the spin-interaction.

1.32 Spin-Spin Interaction

The other broadening process is due to the interaction of the magnetic dipoles, which may be assumed to be situated in a rigid lattice at low temperature. General theories have been developed by Pryce and Stevens (P3) and Van Vleck (V4) on the assumption that the spin-lattice relaxation time is long and that the effect of the thermal motion in broadening the resonance line is negligible. Two

types of interaction between magnetic ions are identified; the dipole-dipole and exchange.

Semi-classically, each ion may be regarded as a gyroscopic magnet; i.e. its angular and magnetic moments are parallel, located at a fixed point in space and in an external magnetic field H of fixed direction. They will precess about this direction and can be regarded as equivalent to a magnet fixed in this direction together with a magnet rotating in a plane perpendicular to it. If any magnet A is considered, the steady field ~~at~~ it will be the resultant of the external field and the internal steady field of the fixed magnets associated with all the other magnets. A will therefore precess about this resultant field with a frequency equal to γH where γ is its gyromagnetic ratio and H is the resultant steady field. There will be a spread in the precessional frequencies due to the variation in the value and orientation of H from magnet to magnet which will result in a broadening of the line called "steady field broadening."

If two magnets have the same precessional frequencies, the rotating field from one will be at the correct frequency to induce transitions in the other, whereas if the two magnets have different precessional frequencies, the rotating fields have little effect. Magnets with the same precessional frequencies tend to induce transitions in each other, reducing their life-times in given states and

this broadening the resonance line. Such broadening is called "resonance broadening."

The quantum mechanical treatment based on these concepts enables the area and second and fourth moments to be calculated. In the treatment due to Van Vleck (V4), it is found that exchange contributes to the fourth moment. Exchange between similar ions narrows the moment lines while exchange between dissimilar ions will broaden it. Exchange arises from the coulomb interaction between electrons. It can be shown that this can be replaced by an interaction between their spins of the form $\frac{1}{4} J(1 + 4\vec{S}_1 \cdot \vec{S}_2)$. In the theory of Pryce and Stevens (P3), exchange also enters the second moment, because it is probably more realistic. Since exchange has not been found to play any role in ions of the rare earth group we do not consider this aspect any further.

1.4 Energy Levels Of The Ion

The principal features of paramagnetic resonance phenomena was outlined in 1.2. From that discussion, one might be tempted to feel that this phenomena is well understood. Fortunately, the fact that each ion in each crystalline electric field must be considered on its own merit makes the investigation of paramagnetic phenomena a prolific source of experimental and theoretical problems.

1.41 General Hamiltonian

The Hamiltonian for a paramagnetic ion in a crystal can be written as the sum of a number of terms whose effect on the energy of the ion are in decreasing order of magnitude. An exact solution is usually obtained for the largest term and the effect of the remaining terms taken into account by perturbation calculations. The order of precedence of these terms varies with the ion under consideration. For ions of the rare earth group in a crystalline solid subjected to a magnetic field, the Hamiltonian is

$$H = H_F + H_{LS} + H_V + H_H + H_{\mu_N} + H_Q + H_W$$

where H_F is the Hamiltonian for the free ion

H_{LS} is the effect of the spin-orbit coupling

H_V is the effect of the crystalline electric field

H_H is the effect of the external magnetic field

H_{μ_N} is the effect ^{of the} interaction of the nuclear magnetic moment with the magnetic field

H_Q is the interaction of the nuclear electric quadrupole moment

H_W is the interaction of the nucleus with the magnetic field of the electrons

For the iron group $H_V \gg H_{LS}$

whereas for the rare earth group $H_{LS} \gg H_V$. This is due to the fact that 3d electrons are not as well shielded as

the 4f electrons. This is verified by the fact that the optical absorption spectral lines of the rare earth group atoms are very sharp. Another way of expressing this is to say that the 4f wave functions do not project very far outside of the atom and so only slightly overlap the other atoms even in the solid state. To a good approximation, the rare earth ions in the solid state may be considered as free.

1.42 Hamiltonian Of The Free Ion In Magnetic Field

The terms which occur in the Hamiltonian of the free ion in a magnetic field may be enumerated in order of decreasing magnitude. They are as follows:

- a. The coulomb interactions of the electrons with the nucleus (assumed fixed) and with each other.

$$H_F^1 = \sum_i \left(\frac{p_i^2}{2m} - \frac{Ze^2}{r_i} \right) + \sum_{i \neq j} \frac{e^2}{r_{ij}}$$

- b. The magnetic interactions between the electron spins and the orbits may be written in the form

$$H_F'' = \sum_{jk} \left(a_{jk} \vec{l}_j \cdot \vec{s}_k + b_{jk} \vec{l}_i \cdot \vec{l}_k + c_{jk} \vec{s}_i \cdot \vec{s}_k \right)$$

according to Van Vleck (V3). Pryce (P4) has used a spin-spin interaction of the form

$$H_F''' = \sum_{jk} 4 \beta^2 \left[\frac{\vec{s}_j \cdot \vec{s}_k}{r_{jk}^3} - 3 \frac{(\vec{r}_{jk} \cdot \vec{s}_j) \cdot (\vec{r}_{jk} \cdot \vec{s}_k)}{r_{jk}^5} \right]$$

to describe the interactions between the electrons spins which is based on the usual form

of dipole-dipole coupling. The orders of magnitude are $10^2 - 10^3 \text{ cm}^{-1}$ for the spin-orbit coupling and $0(1) \text{ cm}^{-1}$ for the spin-spin coupling.

- c. The interaction with the external magnetic field is

$$H_{\text{LS}} = \sum_i \frac{eh}{4\pi mc} (\vec{l} + 2\vec{s})_i \cdot \mathbf{H} = \beta (\vec{L} + 2\vec{S}) \cdot \mathbf{H}$$

where the diamagnetic term

$$\frac{e^2 H^2}{8mc^2} \cdot \sum_i (x^2 + y^2)_i$$

is omitted, because it causes only a shift in these levels without altering their relative separation. The associated energy is $0(1) \text{ cm}^{-1}$.

- d. The interaction between the magnetic moment of the nucleus and the magnetic field set up by the orbital and spin moments of the electrons is

$$H = 2\gamma\beta\beta_N \sum_i \left[\frac{(\vec{l}_i - \vec{s}_i) \cdot \vec{I}}{r_i^3} + 3 \frac{(\vec{r}_i \cdot \vec{s}_i) \cdot (\vec{r}_i \cdot \vec{I})}{r_i^5} \right] + \frac{8\pi}{3} \delta(r_i) \vec{s}_i \cdot \vec{I}$$

The last term is always zero unless there are S-electrons present, in which case the other terms are zero. The energy is $0(10^{-2}) \text{ cm}^{-1}$.

- e. The electrostatic interaction between the electrons and the nuclear electric quadrupole moment is

$$H_q = \frac{e^2 Q}{2I(2I-1)} \cdot \sum_i \left[\frac{\vec{I}(\vec{I}+1)}{r_i^3} - \frac{3(\vec{r}_i \cdot \vec{I})^2}{r_i^5} \right]$$

which is of magnitude $O(10^{-4})\text{cm}^{-1}$. The interaction of the nuclear quadrupole moment with the crystalline electric field is usually negligible.

- f. The direct interaction of the nuclear moment with the external field is

$$H_N = - \gamma \beta_N H \cdot I$$

and has the magnitude $O(10^{-4})\text{cm}^{-1}$.

- g. The interaction of crystalline electric field is

$$H_V = - \sum_i e V(x_i, y_i, z_i)$$

Its order of magnitude has already been discussed in 1.41. This term will be considered in detail in 1.43.

1.43 Ion In The Crystalline Electric Field

We shall now consider the effect of the interaction of the free ion with the crystalline electric field which was mentioned in 1.42g. In a crystal, a paramagnetic ion is subjected to a strong, inhomogeneous electric field which is usually called the crystalline electric field. This field arises from the effect of the other constituents of the crystal and consists of two components: a. static and b. fluctuating. The latter, which is due to the thermal vibration of the lattice, has a negligible effect on the energy levels and usually contributes only to the line width.

The static component is never exactly known because it depends on the charge distribution, the orientation of

the water dipoles and the overlapping of the electron clouds. If the crystal structure is known from X-ray data then, to a first approximation, the field will have the same symmetry as the crystal structure. This field will produce a Stark splitting of the energy levels of the free ion thereby removing some of the $2J + 1$ degeneracy. The degree to which this degeneracy is lifted has been shown by Bethe (B4) to depend on the symmetry of the field.

We now follow the discussion of this in Bijl (B5). The application of group theory is based on the fact that Schrodinger's equation is invariant under certain transformations of the variables of the system. Such transformations always constitute a group which may be called the symmetry group of the system. The wave functions of an n -fold degenerate energy level will thus be linearly transformed amongst themselves by a transformation of the symmetry group, i.e. the wave functions transform according to an n -dimensional representation of the group. The representation is irreducible, if the n -dimensional space spanned by these wave functions does not contain an invariant subspace. An irreducible representation of degree $(2J + 1)$, D_J , of the space rotation group is induced by the $(2J + 1)$ wave functions of an atom having an angular momentum J .

When such an atom is placed in a crystal, its symmetry group is no longer the space rotation group but one

of lower symmetry which is a sub-group of the original group. The wave functions of the atom now transform according to a representation of this new group. In general, this representation D_J will be reducible and hence contain invariant subspaces. An irreducible representation of the new group is realized in each of its invariant subgroups. There is no reason why the wave functions belonging to different irreducible representations should have the same energy and in general this is true. The original levels of the free ion will be split, in a crystal, into a number of other levels which can be classified according to the irreducible representations of the new group contained by the original representation; this number will be equal to the number of irreducible representations of the new group.

If J is half integer, the representations are double valued and the levels remain degenerate even with fields of lowest symmetry. Here "Kramers" degeneracy always remains, which can only be removed by a magnetic field. We thus see that group theory will give the type of level that can occur, the number of levels and with additional information the relative spacings of the energy levels.

Perturbation calculations are necessary to obtain the magnitude of the splittings. Only one splitting need be computed if the relative separations have been obtained from group theory. For perturbation theory, the crystalline electric field must be known. If we assume that this potential satisfies Laplace's equation then it can be expanded in

spherical harmonics.

$$V = \sum_{n,m} A_n^m r^n Y_n^m(\theta, \phi) \quad (3)$$

where $Y_n^m(\theta, \phi)$ is normalized to unity and defined as

$$Y_n^m(\theta, \phi) = (-1)^n \left[\frac{(2n+1)(n-|m|)!}{2(n+|m|)!} \right]^{1/2} \frac{1}{\sqrt{2\pi}} P_n^m(\cos\theta) e^{im\phi} \quad (4)$$

$$\text{where } P_n^m(x) = \frac{(1-x^2)^{m/2}}{2^n n!} \frac{d^{n+m}}{dx^{n+m}} (x^2-1)^n \quad (4a)$$

The number of terms in (I,3) can be reduced considerably by the following arguments. For d-electrons, all terms for which $n > 4$ will have zero matrix elements while for f-electrons, the same is true when $n > 6$. This arises from the fact that in the evaluation of integrals of the form $\int \chi^* V \psi dt$ where χ and ψ are electron wave functions, the density $\chi^* \psi$ can be expanded in spherical harmonics and does not contain terms where $n > 2l$ (l is the quantum number for the orbital angular momentum). By the orthogonality of spherical harmonics, the integral vanishes if V is a spherical harmonic with $n > 2l$. Similarly, if n is odd, the integral is zero because the product $\chi^* \psi$ is unchanged by the substitution $x, y, z \rightarrow -x, -y, -z$ whereas V reverses sign. The term for $n = 0$ is dropped because it is an additive constant.

To reduce the number of terms further, we must consider the symmetry properties of the surroundings. For the rare earth ethyl sulphates, with which we are concerned,

there is threefold axis of rotation symmetry and a reflection symmetry plane which is usually denoted by C_{3h} . Elliott and Stevens (E1) have shown that for this symmetry V can be written as

$$\begin{aligned}
 V = & A_0 + A_2^0 (3z^2 - r^2) + A_4^0 (35z^4 - 30r^2z^2 + 3r^4) \\
 & + A_6^0 (231z^6 - 315r^2z^4 + 105r^4z^2 - 5r^6) \\
 & + A_6^6 (x^6 - 15x^4y^2 + 15x^2y^4 - y^6) \quad (6)
 \end{aligned}$$

We now define the types of symmetry from the subscript m of the spherical harmonic which determine the various potentials. If $m = 0$ the spherical harmonic has axial symmetry, while if $m = \pm 2$ it has rhombic symmetry, $m = \pm 3$ trigonal symmetry and $m = \pm 4$ tetragonal symmetry. Any potential containing terms of different symmetry is said to have an overall symmetry, which is the greatest symmetry common to all the terms.

1.44 Matrix Elements Of The Crystalline Field

The method of calculating the matrix elements of the crystalline field potentials for ions of the rare earth group has been discussed in detail by Stevens (S7) and Elliott and Stevens (E1, E2, E3). In this section we shall outline their general method of attacking this problem.

To evaluate the matrix elements of the crystalline field, it is necessary to find representations in which the states are eigenstates of the total angular momentum J and

to determine the matrix elements joining states in different J manifolds. These states are formed by taking linear combinations of determinantal product states of $4f$ one-electron states. The rare earth group ions show Russell - Saunders coupling so the product states are first combined to form states for which L and S are constants i.e. $|4f^n; L, S, J\rangle$. These are then combined into states for which J is constant i.e. $|4f^n; L, S, J, J_z\rangle$. Since the basic product states are generally not known, it is simpler to determine the matrix elements using methods which do not require this information.

These methods are based on the fact that within a manifold of states for which J is a constant, there are simple relations between the matrix elements of potential operators and the appropriate angular momentum operators. Thus, for example, inside a manifold for which J is constant

$$\sum (3J_z^2 - r^2) \equiv \alpha \bar{r}^2 [3J_z^2 - J(J+1)] \quad (7)$$

These relations can be verified using Wigner coefficients.

Having established the above relations, it is then necessary to determine the multiplying factor. This is done by using the fact that the potential functions do not show any dependence on the spin, so that similar operator equivalents hold inside manifolds in which L is constant. A convenient state in L, S, J, J_z quantization is chosen and expressed in L, S, J_z, S_z quantization and an equation obtained by equating the two expectation values of the function.

Another state in L, S, L_z, S_z quantization is then chosen and expressed in one electron product states and again expectation values are equated. In this way, sufficient relations are obtained to determine the factors in terms of radial integrals over $4f$ wave functions.

We now consider the calculation of matrix elements coupling states in different J manifolds. It is no longer possible to use operator equivalents and so the Wigner coefficients are used directly. The variation of the matrix elements with J_z is obtained in the same way as above. To calculate the multiplying constant, it is convenient to regard the potential, say V_6^0 , as a component of a vector in a D_6 space with $m = 0$. For the example $\langle J, J_z | V_6^0 | J+2, J_z \rangle$ the coefficient of $|J, J_z \rangle$ in $V_6^0 | J+2, J_z \rangle$ is equal to a constant multiplying the appropriate Wigner coefficient. It will be independent of J_z and hence can be calculated from values of J_z .

Elliott and Stevens (E1, E2, E3) have extended the above work of Stevens (S7) by showing general methods of finding the ground state of an ion of the rare earth group in any crystalline field. Detailed calculations are done for the ethyl sulphates. The effects of the nuclear spin and quadrupole moment are also taken into account.

An important general theorem has been proved by Elliott and Stevens (E2). It states that

$$\frac{g_{\parallel}}{g_{\perp}} = \frac{A}{B} \quad (8)$$

where A, B are defined in (I,13) and holds when the states which describe a doublet are eigenstates of the total angular momentum. This relation is a constant for an ion independent of its environment and the degree with which it holds is a good indication of whether or not it is a good approximation to assume that the crystalline field splitting is small compared with the separation of the levels of the free ion. Experimentally, it is more likely to hold in the second half of the 4f-shell where the first excited level is well removed and implies that the hyperfine structure should be isotropic when measured at constant frequency.

1.5 Spin-Hamiltonian

It is difficult to calculate many of the parameters which are involved in the total Hamiltonian as it has been discussed in 1.4. Furthermore, when they can be evaluated, the accuracy is poorer than can be obtained experimentally. Consequently, a more convenient means of discussing experimental results which also permits their correlation with other types of magnetic measurements has been introduced. Abragam and Pryce (A1) have shown that the behaviour of the energy levels of a paramagnetic ion can be represented in the following phenomenological manner. This semi-empirical representation is called the "spin" Hamiltonian. It is based

upon the concept of an "effective" spin S which is obtained by equating the multiplicity of the lines observed to $2S$.

In the remainder of this section, the various spin-Hamiltonians that have found successful application will be considered. The eigenvalues in terms of the adjustable parameters will also be given.

1.51 Axial Symmetry About z - Axis. Bleaney (B7)

$$\mathcal{H} = g_{\parallel} \cdot \beta \cdot H_z S_z + g_{\perp} \cdot \beta \cdot (H_x S_x + H_y S_y) + D \left[S_z^2 - \frac{1}{3} S(S+1) \right] \quad (9)$$

where g_{\parallel} and g_{\perp} are the values of the spectroscopic splitting factor parallel and perpendicular to the z -axis. The term in D represents the effect of the initial splitting due to the crystalline field.

In strong fields where $g\beta H \gg D$, it is convenient to choose the axes so that elements in S_x and S_y do not occur in the major term $g\beta H \cdot S$ of the spin-Hamiltonian. If g is anisotropic, this is equivalent to choosing the axis about which the spin precesses as the new z -axis. If the magnetic field H makes an angle θ to the symmetry axis of the crystal, then the allowed transitions are $\Delta M = \pm 1$.

For the transition $M \leftrightarrow M-1$ we obtain

$$h\nu = g\beta H + \frac{D}{2} (2M-1) \left[3 \frac{g_{\parallel}^2}{g^2} \cdot \cos^2 \theta - 1 \right] - \left(\frac{D g_{\parallel} g_{\perp} \cos \theta \sin \theta}{g^2} \right)^2 \cdot \frac{1}{2g\beta H_0} \cdot [4S(S+1) - 24M(M-1) - 9]$$

$$+ \left(\frac{D g_{\perp}^2 \sin^2 \theta}{g^2} \right)^2 \cdot \frac{1}{8 g \beta H_0} \cdot [2S(S+1) - 6M(M-1) - 3] \quad (10)$$

$$\text{where} \quad g^2 = g_{\parallel}^2 \cos^2 \theta + g_{\perp}^2 \sin^2 \theta \quad (10a)$$

This shows that the fine structure results in a splitting into $2S$ lines which are equally spaced in the first approximation. The spacing varies with angle, falling to zero where $\left(\frac{g_{\parallel}}{g}\right) \cos \theta = \frac{1}{\sqrt{3}}$. This equal spacing is disturbed by second order effects which vanish in strong fields or along the symmetry axis. In the absence of the fine structure splitting, all of the lines would coincide at a field $H = H_0$ which is used as the second order perturbation denominator. It is easy to see that the spectrum is the same independent of whether the measurements are made at constant frequency, as is the case in practice, or at constant magnetic field.

The intensity of these lines is

$$P = \frac{\pi \nu^2 (g' \beta H')^2}{4kT} \cdot \frac{N}{2S+1} \cdot [S(S+1) - M(M-1)] \cdot F(\nu, \nu_0, \Delta \omega) \quad (11)$$

where P is the power absorbed in the crystal

N is the number of paramagnetic ions

H' is the amplitude of the microwave field

$$H' \cos 2\pi \nu t$$

g' is the effective g value along the normal to the axis along which the spin precesses.

$F(\nu, \nu_0, \Delta\nu)$ is a 'shape factor' depending on the line width

$F(\nu', \nu_0, \Delta\nu) \approx 1/\Delta\nu$ where $\Delta\nu$ is the half width at half intensity.

It has been assumed that H' is normal to g' . In practice, H' is normal to H and hence is at an angle to g' resulting in a small error in the absolute intensities but none in the relative intensities.

Transitions corresponding to changes in M of greater than one have been observed which are weaker in intensity by a factor of the order of $(D/H)^2$ and vanish only if the external field is parallel to the symmetry axis. The intensity formulae are complicated, and show little dependence on the angle between the external and microwave magnetic fields. For $\Delta M = \pm 2$, the position of a line corresponding to the transition $M \leftrightarrow M-2$ is

$$h\nu = 2g\beta H + 2D(M-1) \left[3 \frac{g_{\parallel}^2}{g^2} \cdot \cos^2 \theta - 1 \right]$$

$$- \left(\frac{Dg_{\parallel} g_{\perp} \cos \theta \sin \theta}{g^2} \right)^2 \cdot \frac{2}{g\beta H_0} \cdot [4S(S+1) - 24M(M-2) - 33]$$

$$+ \left(\frac{Dg_{\perp}^2 \sin^2 \theta}{g^2} \right)^2 \cdot \frac{1}{2g\beta H_0} \cdot [2S(S+1) - 6M(M-2) - 9] \quad (12)$$

where H_0 has the same significance as for the $\Delta M = \pm 1$ transitions.

1.52 Hyperfine Structure Bleaney (B8)

$$\mathcal{H} = AS_z I_z + B(S_x I_x + S_y I_y) + P \left[I_z^2 - \frac{1}{3} I(I+1) \right] - \gamma \beta_N \mathbf{H} \cdot \mathbf{I} \quad (13)$$

where A, B correspond to the interaction between the nuclear magnetic moment and the magnetic field of the incomplete electron shell. P is due to the interaction of the nuclear electric quadrupole moment with the gradient of the electric field at the nucleus. The last term takes into account the direct effect of the external magnetic field on the nuclear magnetic moment.

If this Hamiltonian is added to that of 2.51 (I,9) then the strong allowed transitions are those for which $\Delta m = 0$ and the position of the line $(M, m) \leftrightarrow (M-1, m)$ is found by adding to the right hand side of (I,10) the quantity.

$$\begin{aligned} & K m + \frac{B^2}{4g\beta H_0} \cdot \frac{A^2 + K^2}{K^2} \cdot [I(I+1) - m^2] \\ & + \frac{B^2}{2g\beta H_0} \cdot \frac{A}{K} \cdot m (2M-1) \\ & + \frac{1}{2g\beta H_0} \cdot \left(\frac{A^2 - B^2}{K} \right)^2 \cdot \left(\frac{g_{\parallel} g_{\perp}}{g^2} \right)^2 \sin^2 \theta \cos^2 \theta m^2 \\ & + \frac{P^2}{2KM(M-1)} \cos^2 \theta \sin^2 \theta \cdot \left(\frac{ABg_{\parallel} g_{\perp}}{K^2 g^2} \right)^2 \cdot m [4I(I+1) - 8m^2 - 1] \\ & - \frac{P^2}{8KM(M-1)} \sin^4 \theta \cdot \left(\frac{Bg_{\perp}}{Kg} \right)^4 \cdot m [2I(I+1) - 2m^2 - 1] \end{aligned} \quad (14)$$

$$\text{where } K^2 g^2 = A^2 g_{\parallel}^2 \cos^2 \theta + B^2 g_{\perp}^2 \sin^2 \theta \quad (14a)$$

In the first approximation, the nuclear interaction splits each electronic transition ^{into} $(2I + 1)$ equally spaced components with separation K between successive lines. There is no first order effect from the quadrupole interaction if $P \ll B$. The second order effects of the quadrupole term are important since they produce a change in the spacing of the hyperfine lines, which means that P can be determined. If H is at angle with the symmetry axis of the crystal, the quadrupole interaction will break down the ordinary selection rule $\Delta m = 0$ when $P \approx K$ and the new selection rules are $\Delta m = 0, \pm 1, \pm 2$. The intensity of the $\Delta m = \pm 1, \pm 2$ transitions are of the order of $(P / K)^2$ compared with the $\Delta m = 0$ transitions. Bleaney (B7) discusses these effects in great detail.

1.53 Non-Axial Symmetry

If the symmetry of the crystalline electric field is not axial, then additional terms in the spin Hamiltonian must be introduced to account for their departure. It is usual to use terms of the form $E(S_x^2 - S_y^2)$. Their effect is taken into account by second order perturbation calculations. Fortunately, for most of the resonance spectra observed to date, few departures from axial symmetry have been encountered.

1.54 S - State Ions

When the orbital state of the free ion has no degeneracy the spin-Hamiltonian is quite different. According to the Hund rule, this will occur whenever an unfilled electronic shell is half filled i.e. Mn^{2+} , Fe^{3+} $[3d^5, 6s_{5/2}]$ and Gd^{3+} , Eu^{2+} $[4f^7, 8s_{7/2}]$

We follow the treatment of Stevens (S8). We already know from group theory (1.43) that the spin-Hamiltonian should only contain even powers of S_x , S_y and S_z and that it should also reflect the same symmetry as that of the crystal. We start with a given value of S and a certain field symmetry and consider the even powers of S_x^n , etc. It can then be shown that expressions where $n > n_1$ are expressible with terms where $n \leq n_1$. In this manner it has been shown by Bleaney and Stevens (B11) that with cubic symmetry and spin $5/2$ and no nuclear spin

$$\mathcal{H} = g\beta H \cdot S + 1/6 a \left[S_x^4 + S_y^4 + S_z^4 - 1/5 S(S+1)(3S^2 + 3S - 1) \right] \quad (15)$$

In a similar manner, Elliott and Stevens (E1) have found that the following spin-Hamiltonian

$$\begin{aligned} \mathcal{H} = & g\beta H \cdot S + A^0_2 \left[3S_z^2 - S(S+1) \right] \\ & + A^0_4 \left[35S_z^4 - 30S(S+1)S_z^2 + 25S_z^2 - 6S(S+1) + 3S^2(S+1)^2 \right] \\ & + A^0_6 \left[231S_z^6 - 315S(S+1)S_z^4 + 735S_z^4 + 105S^2(S+1)^2 S_z^2 \right] \end{aligned}$$

$$\begin{aligned}
& - 525 S(S+1)S_z^2 + 294 S_z^2 - 5 S^3 (3+1)^3 \\
& + 40 S^2(S+1)^2 - 60 S(S+1) \\
& + A^6_6 \left[(S_x+i S_y)^6 + (S_x-i S_y)^6 \right]
\end{aligned} \tag{16}$$

will fit the experimental results for dilute gadolinium ethyl sulphate and magnesium nitrate when the external magnetic field is parallel to the symmetry axis of the crystal.

1.55 Anomalous Case

In a number of resonance spectra, it has been observed that, contrary to expectation, (B10, C4) the maximum intensity occurs when the microwave magnetic field was parallel to the steady magnetic field producing the Zeeman splittings. This phenomena has been explained in the following way. The ground state of such ions is a doublet whose levels contain states differing in J_z by unity but the normal type of resonance transition is not allowed since the matrix elements of J_x and J_y between the two states are zero. A distortion of the crystalline lattice produced by the Jahn-Teller effect (J1) (C4) will remove the degeneracy of the levels, admixing the states of the two levels, permitting allowed transitions when the microwave and Zeeman magnets fields are parallel.

This situation occurs for $\text{Pr}^{3+} \left[4f^2, 3H_4 \right]$. It has been studied by Bleaney and Scovil (B10) in the dilute

ethyl sulphate and Cooke and Duffus (6A) in the dilute magnesium nitrate. It has also been found by Bleaney, Elewellyn, Pryce and Hall (Bl4) to occur in plutonium diluted with $(\text{UO}_2)\text{Rb}(\text{NO}_3)_2$.

These workers have found that the resonance results can be interpreted using the following spin-Hamiltonian and fictitious spin $S = 1/2$

$$\mathcal{H} = g_{\parallel} \beta H_z S_z + A S_z I_z + P \left[I_z^2 - 1/3 I(I+1) \right] + \Delta_x S_x + \Delta_y S_y \quad (17)$$

where $\Delta^2 = \Delta_x^2 + \Delta_y^2$ (17a)

and the allowed transitions are given by

$$h \nu = \left[(g_{\parallel} \beta H \cos \theta + Am)^2 + \Delta^2 \right]^{1/2} \quad (18)$$

where θ is the angle H makes with the crystal axis and effect of quadrupole interaction term has been neglected.

The last two terms represent the effect of departure of the crystalline electric field from the full symmetry associated with the crystal structure.

The line shape of such transitions is always asymmetric; the intensity rises slowly on the low field side and falls sharply on the high field side. It can be accounted for by assuming a random distribution of strains in the crystal, giving a Gaussian distribution centred on zero for the distortion parameters Δ_x and Δ_y . If the

transition probability is assumed to be proportional to Δ , the sharp cut-off in the intensity on the high field side corresponds to the Gaussian distribution of the distortion energy. Consequently, the correct place to experimentally measure the position of each resonance is at the high field limit.

CHAPTER II

PARAMAGNETIC RESONANCE SPECTROMETERS

2.1. Introduction

To perform an experimental study of paramagnetic resonance phenomena, a suitable spectrometer is required. The design will be determined by the type of experiment to be performed, the sensitivity required, equipment available, finances available and the taste of the designer. The fundamental objective in spectrometer design is usually to achieve maximum sensitivity. In this chapter, the basic principles of spectrometer design and their application by various designers are discussed in detail. The object of this survey was to gain an understanding of the limitations of the existing designs in the hope that a new spectrometer of greater sensitivity could be designed. Such a spectrometer has been developed and constructed. Its design is described in this chapter. (2.74).

Finally, a comparison is made of existing types of spectrometers on the basis of sensitivity, stability, type of operation, and ease of operation.

2.2. General Requirements

The essential requirements of any paramagnetic resonance spectrometer are to place a paramagnetic substance

(usually a crystal) in a region where it can absorb electromagnetic radiation, to apply a magnetic field, and to detect any absorption of power from the radiation field as a function of the magnetic field strength.

A versatile spectrometer should operate over a wide range of temperatures. The temperature at which an investigation is carried out will depend on the relaxation times of the substance under consideration. (B11). The best signals are obtained when the relaxation time τ is long enough to permit the absorption of energy but not so long as to cause saturation. This is usually of $0(10^{-6})$ seconds and can be obtained at room or oxygen temperatures for chemical compounds containing ions of the iron group whereas the rare earth group ions, with the exception of gadolinium, require hydrogen or helium temperatures.

Paramagnetic resonance spectrometers are generally operated at microwave frequencies since it is theoretically desirable (S2) to split the energy levels as far apart as possible. Moreover, the sensitivity is proportional to the operating frequency (II,20). Large magnetic fields are consequently required if the ground state is a Kramer's doublet. Table III shows the corresponding values of ν and λ for different values of H when $g = 2$, i.e. free electron.

Table III

$$h\nu = g \beta H \quad \nu \text{ kilomegacycles} = 2.8040 H_{\text{kilogauss}}$$

H_{Oersteds}	256.63	1069.9	3,566.3	8,918.8	10,699.0
ν_{kmcs}	1	3	10	25	30
λ_{cm}	30	10	3.0	1.2	1.0

Experiments are performed in small magnetic fields using radio frequency techniques when information about the various terms in the Hamiltonian and the ground state energy levels is desired. This region will not be considered in this thesis although much work is still required before a complete understanding of resonance phenomena is achieved.

Measurement techniques at microwave frequencies were highly refined during the war as a result of the importance placed on the development of radar. These war-time investigations have been fully documented and published as the Radiation Laboratory Series. This material has been found to be a valuable source of information on microwave and electronic techniques. The circuitry is of the distributed parameter type, instead of the lumped parameter type used at radio frequencies. The application of these techniques to gas spectroscopy has been reviewed by

Bleaney (B6), and Gordy (G1) and to paramagnetic resonance by Bleaney and Stevens (B11).

The existence at the end of the war of large quantities of radar equipment at 10, 3, and 1.25 cm. led to its exploitation for scientific purposes. Consequently, most gas and paramagnetic resonance spectroscopy has been performed at these wavelengths.

In paramagnetic resonance, it is necessary to place the sample in a high Q tuned cavity because (a) the sample is usually a small, single crystal and the highest sensitivity is obtained by concentrating the microwave magnetic field in it. Saturation effects are increased by doing this; however, they are not as serious as in gas spectroscopy because here we are dealing with the transition probabilities associated with magnetic dipoles ($\sim 10^{-20}$ emu.) rather than with electric dipoles ($\sim 10^{-10}$ emu.), and (b) the sample should be located in a strong, homogeneous static magnetic field.

Most paramagnetic resonance spectrometers are operated at constant frequency due to the limited tuning range of microwave power sources (K4) and because high Q tuned cavities are required. It is convenient to lock the frequency of the source electrically to the frequency of the cavity (P3), R2). Resonances are thus investigated as a function of magnetic field at constant frequency.

To gain information concerning the relation between the crystal symmetry axis and the direction of the crystal-line electric field, it is necessary to rotate either the

crystal about one of its axes or the magnetic field with respect to the microwave magnetic field. Rotation of the crystal in the cavity has the disadvantage that it upsets the tuning of the cavity. This necessitates rechecking the tuning after each rotation and remeasuring the frequency. If the external magnetic field is rotated then the intensity of the signal is a function of the rotation since it is proportional to the square of the sine of the angle between the magnetic field and the microwave magnetic field. It is preferable but not essential to be able to perform both of these operations.

2.3 Noise

The sensitivity of all measurements is limited by spontaneous fluctuations called noise which are a manifestation of the statistical nature of physical phenomena. For electronic measurements, this noise is due to the random motion of the electrons. Noise originating from mechanical vibration is not considered although it may be troublesome to eliminate. We assume that any sources of mechanical vibration can be eliminated.

Electronic noise in a paramagnetic resonance spectrometer arises from three sources.

- a. Klystron or oscillation noise
- b. Detector or converter noise
- c. Amplifier noise

In general, reflex klystrons are used as the source of microwave power in paramagnetic resonance spectroscopy because of their frequency stability (3.26). We confine ourselves to a few comments about the noise generated in them. The theory of the noise in reflex klystrons is discussed by Knipp and Kuper (K4) and van der Ziel (V2). It is sufficient to mention the following pertinent experimental facts.

1. The noise-signal power ratio is decreased only slightly when operating at frequencies below the centre of a mode whereas it increases by at least a factor of two at the high frequency half-power point.

2. Provided that the oscillator is not overloaded and properly matched, the noise signal power ratio is independent of the mode of operation. Slight improvement may be obtained by the use of higher modes i.e. less negative reflector voltages.

3. The noise-signal power ratio decreases as the intermediate frequency is increased.

It is usually found that klystron noise does not appreciably affect the total noise of those systems in which we are interested and, hence, we will not consider it further.

In the microwave region, semi-conductor crystal diodes are generally used as power detectors or frequency converters. A bolometer can be used as a power detector. It does not suffer from the "flicker" or excess noise

effects that occur in crystals; however, the upper limit of its frequency response is about 100 cycles. A spectrometer using a bolometer is considered in 2.71.

The theory of semi-conductor noise has been discussed by Torrey and Whitmer (T2) and van der Ziel (V2), amongst others. Three noise components can be distinguished: Johnson or thermal, shot and flicker. The first two are independent of frequency and fairly well understood. No satisfactory theoretical explanation of "flicker" noise has been advanced. It has been found experimentally, that the "flicker" noise power is inversely proportional to the frequency and that it is of the same magnitude as the Johnson and shot noise at a frequency $0(10^6)$ cycles. It would, thus, be desirable to operate the crystal converter at frequencies in excess of 10^6 cycles if minimum crystal noise were the only experimental consideration. It should be noted that this upper frequency limit has been set in a wide range from 10^6 to 2×10^7 cycles. It can be shown that the integrated "flicker" noise in a given bandwidth is reduced by a factor of $0(10^3)$ when the band centre is changed from 10^2 cycles to 10^6 cycles. This calculation is based on the assumption that the amplitude of the signal displayed on the oscilloscope is proportional to the power absorbed in the cavity by the transition. This means that the crystal converter operates as a square law detector when the amplitude of the modulation of the power level is small compared with the power level. This assumption is justified by the

fact that the relative intensities of the observed signals agree with the square of the transition probabilities for the transitions. It has not been directly verified experimentally. Little improvement is gained above this ^{frequency} because the "flicker" noise is probably negligible.

The electronic amplifiers used with crystal video detectors or converters can be easily designed to have noise figures of about 2 db. at frequencies up to 10 mcs. Since the overall noise figure of the crystal converter and amplifier is about 15 db, very slight improvement is achieved by decreasing the noise figure of the amplifier. This means that the matching network between the crystal and the input stage at low frequencies (< 10 mcs) is non-critical and considerable mismatch can be tolerated without introducing adverse effects on the overall noise figure of the system (S9,V5,L1). Both Valley & Wallman (V1) and van der Ziel (V2) give a comprehensive analysis of the problems of noise and the design of matched low noise figure input amplifiers for crystal detectors.

From the above considerations it should be obvious the ultimate achievable sensitivity of a paramagnetic resonance spectrometer is determined by the crystal noise.

It follows that one of the primary design objectives is to detect the resonance signal at a frequency where the noise from the crystal converter can be minimized.

2.4. General Classification

Having discussed the problems which must be considered the design of a paramagnetic resonance spectrometer, we now classify the existing designs.

If video presentation of resonance phenomena is desired then either the frequency or the magnetic field must be repetitively swept, in time, over a small region of frequency or field. This leads to the classification according to whether frequency or field modulation is employed.

The alternative to video is recorder presentation. In theory, it should be possible to sweep linearly in either frequency or magnetic field, as is done in nuclear magnetic resonance, and hence record detector output as a function of either frequency or magnetic field. It has already been mentioned that the frequency cannot be swept over a sufficient range with a reflex klystron and in any case the tuned cavity would have to be simultaneously kept in tune with the klystron. At microwave frequencies, the magnetic field is always swept when paramagnetic resonance phenomena is displayed on an automatic pen recorder.

Video and recorder display can be best classified by the term band width. It has been shown (S10) that the bandwidth required to reproduce accurately the line shape of the resonance phenomena must be about 100 times the repetition frequency of the modulation. Video and wide band operation are synonymous terms. The band width also depends on the

amplitude of the modulation. As the amplitude or frequency is increased the bandwidth must correspondingly be increased, since it is proportional to

$$\frac{dH_1}{dt} = A_1 \omega_1 \cos \omega_1 t \quad (19)$$

where H_1 is the amplitude of the field modulation at time T

A_1 is the maximum amplitude of the field modulation

ω_1 is the frequency of the field modulation

Strandberg (S10) gives an analysis of this effect. When recorder display is utilized, the bandwidth can be greatly reduced without affecting the line shape. Hence the term narrow band operation. The band width can then be of the order of 1/100th the modulation frequency. Here, also, the signal amplitude depends on the amplitude of the modulation and should be less than or equal to the line width of the signal (S4) if undesirable effects are to be eliminated.

Stability is a design criterion, which is related to band-width considerations. In general, the stability of a system must be increased as the bandwidth is decreased since, although the sensitivity is greater in narrow band operation, the time required to obtain the same amount of information as in wide band operation is increased. It is convenient to speak of short and-or long term stability thus relating stability and bandwidths.

Another useful design criterion is the concept of reproducibility. This is always closely related to the

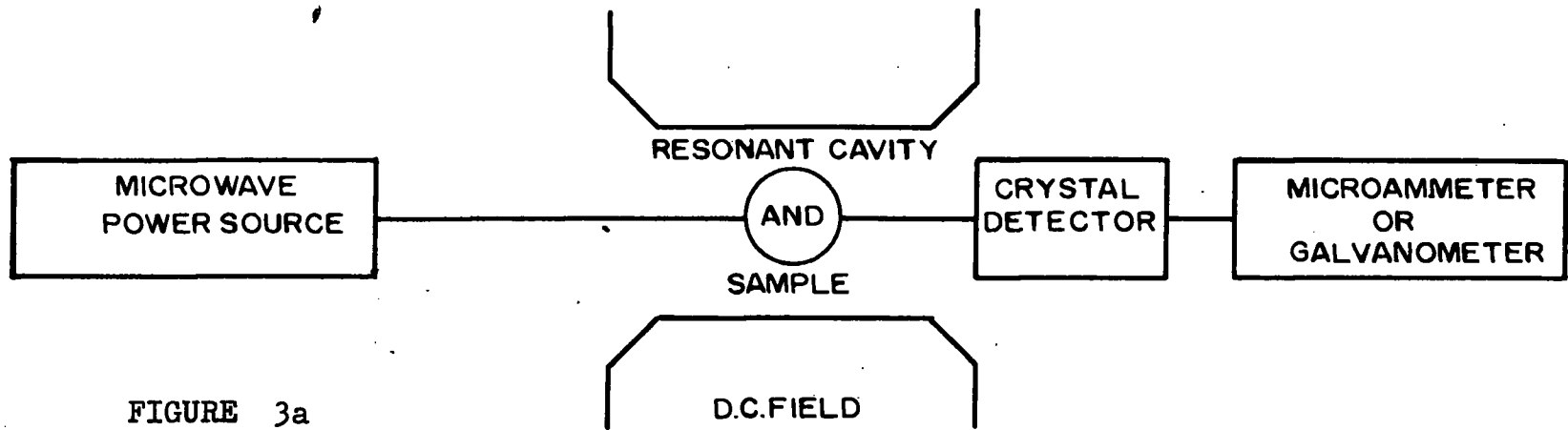


FIGURE 3a

POINT-TO-POINT PARAMAGNETIC RESONANCE SPECTROMETER

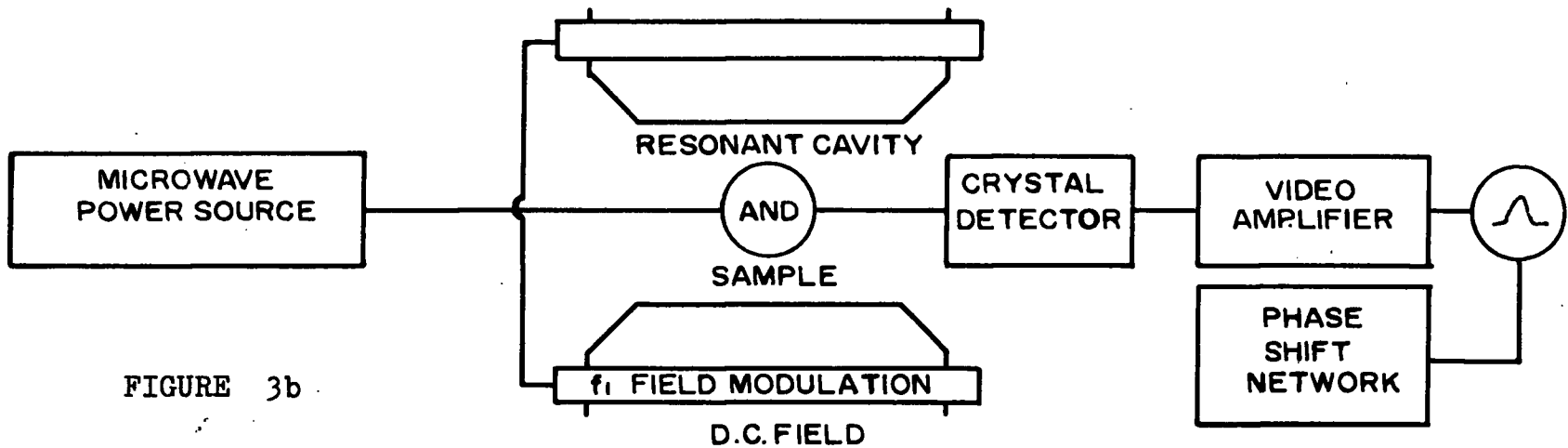


FIGURE 3b

VIDEO PARAMAGNETIC RESONANCE SPECTROMETER

accuracy with which measurements can be made. In general, it is desirable to have the reproducibility greater than the accuracy although it is not infrequent that the accuracy is limited by the reproducibility.

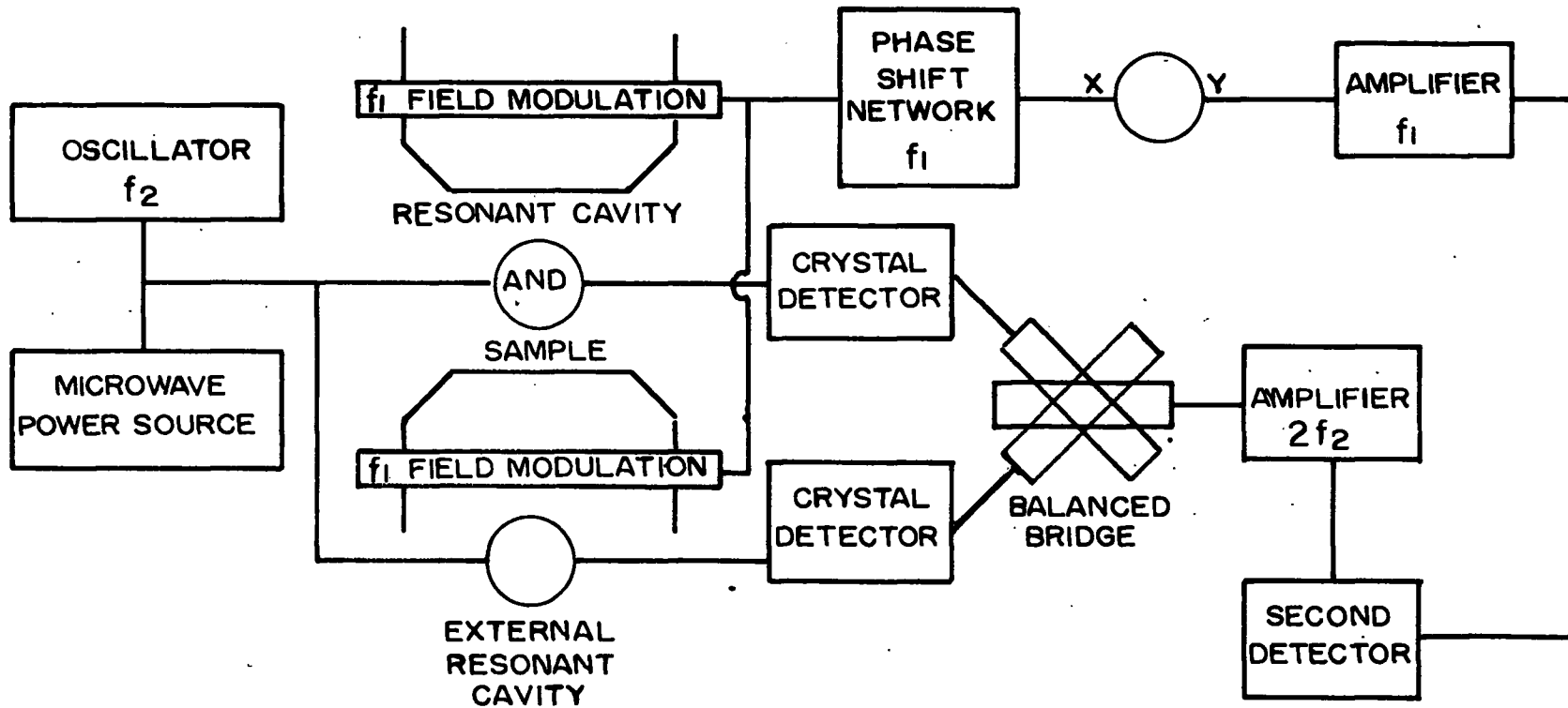
2.5. Point-to-Point Spectrometer

The point-to-point method fulfills the basic requirements of a spectrometer but is considered obsolete because of the slowness with which results can be obtained. A block diagram of its components is shown in Figure 3a. Two types of operation are possible; either the reflection or transmission coefficient of the resonant cavity can be measured as a function of magnetic field strength. Bleaney and Stevens (B11) give the necessary formulae for calculating the magnetic absorption with this method. Although it is very slow and tedious this is probably the best method of obtaining accurate data about the shape of resonance lines.

2.6. Frequency Modulation Spectrometers

Frequency modulation spectrometers employ either electrical or mechanical methods of modulating the output frequency of the klystron. The mechanical method introduces mechanical instabilities which manifest themselves as electrical instabilities i.e. noise. Frequency modulation of a klystron introduces an excess of low frequency noise which severely limits the sensitivity of the system. Moreover, the power varies considerably over a mode. Consequently,

FIGURE 4



BALANCED BRIDGE PARAMAGNETIC RESONANCE SPECTROMETER

such systems are not very satisfactory from the point of view of sensitivity. Also the stability is poor.

2.61. Line Shape Spectrometer

Weidner and Whitmer (W1) have constructed a frequency modulated spectrometer. Since the modulation repetition rate is very low (1 cps) it is essentially an automatic recording d.c. or point-to-point spectrometer and, hence, has the same sensitivity. Similarly, it also has the advantage of accurately reproducing line-shapes on a recorder.

2.62. Balanced Bridge Spectrometer

Bagguley and Griffiths (B1) have developed a frequency modulation system employing a balance method which uses two resonant cavities. A block diagram of this spectrometer is shown in Figure 4. This method was developed with the aim of eliminating the "flicker" noise in the crystal detector since the reflector was modulated at 1 mcs. The system has a number of inherent disadvantages. For optimum sensitivity, the Q of the two cavities should be the same. This is not possible since one cavity contains a sample which loads it decreasing its Q . Moreover, since most experiments are performed at low temperatures, the Q 's of the cavities would not be the same even if they were both unloaded except at the expense of duplication of low temperature equipment. The use of two crystal converters also increases the noise figure of the system. This spectrometer appears to be no

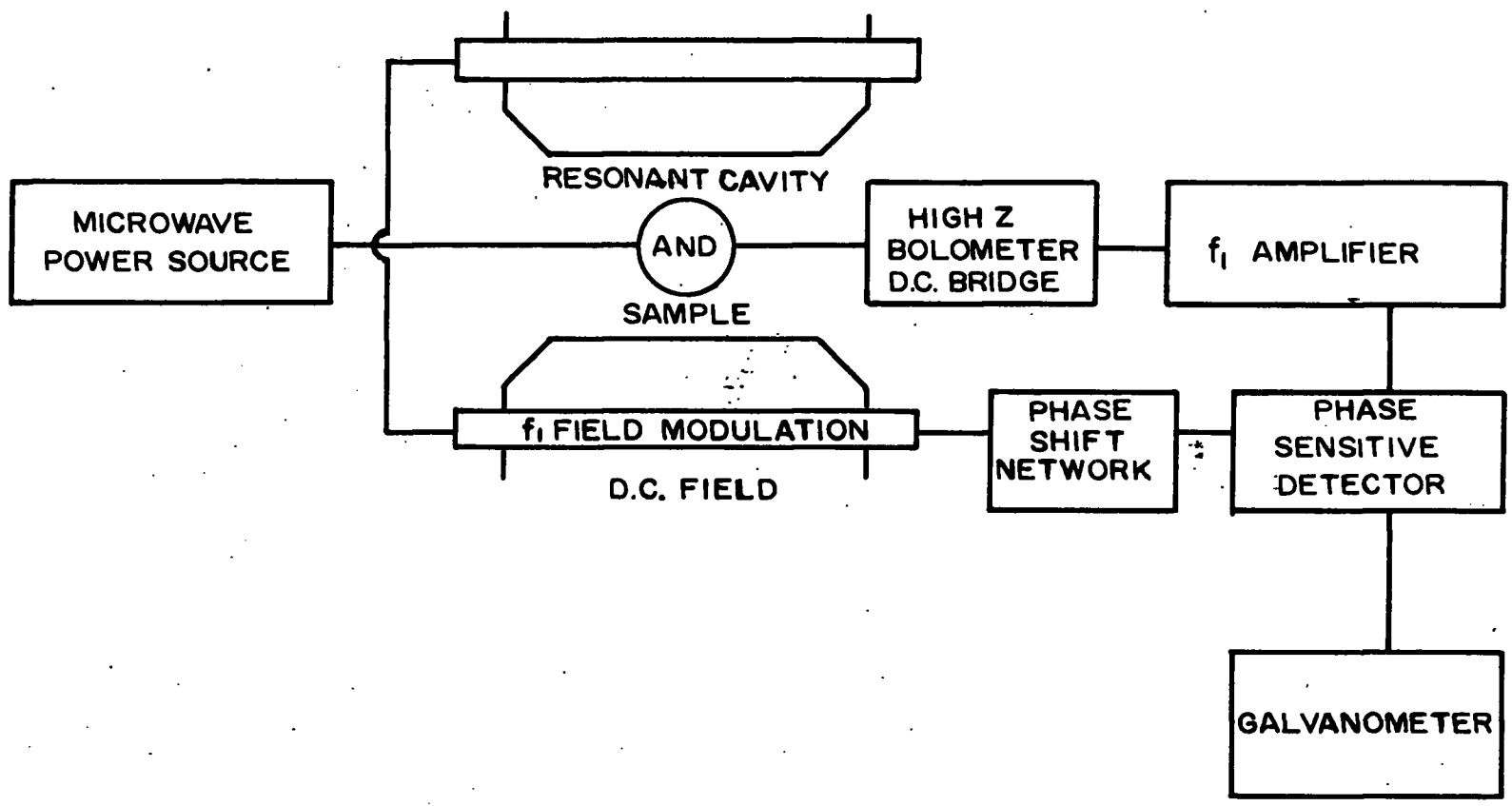


FIGURE 5

BOLOMETER PARAMAGNETIC RESONANCE SPECTROMETER

more sensitive than a video spectrometer and suffers from the disadvantage that it is much more difficult to operate and is less stable.

2.7. Field Modulation Spectrometers

In a field modulation spectrometer, the frequency of the klystron is fixed and preferably locked to the resonant frequency of the cavity. The amplitude of the field modulation is greater than the half line width in wide band operation and about equal to or less than it in narrow band operation. Field modulation eliminates the excessive noise and instabilities introduced by frequency modulation. However, it is more difficult to eliminate the crystal "flicker" noise using this technique. One successful method of achieving this is described in 3.74. This difficulty arises from the fact that it is impossible to modulate the field of an electromagnet to the amplitude required at frequencies much in excess of one kilocycle because of the a.c. hysteresis loss in the iron of the magnet. The detection must occur at low frequencies where the crystal converter is excessively noisy.

2.71. Bolometer Spectrometer

A paramagnetic gas resonance spectrometer using a bolometer has been developed by Beringer and Castle (B2,B3). A block diagram of this arrangement is shown in Figure 5. This is probably the most sensitive spectrometer that has been developed because there is no problem of excess crystal

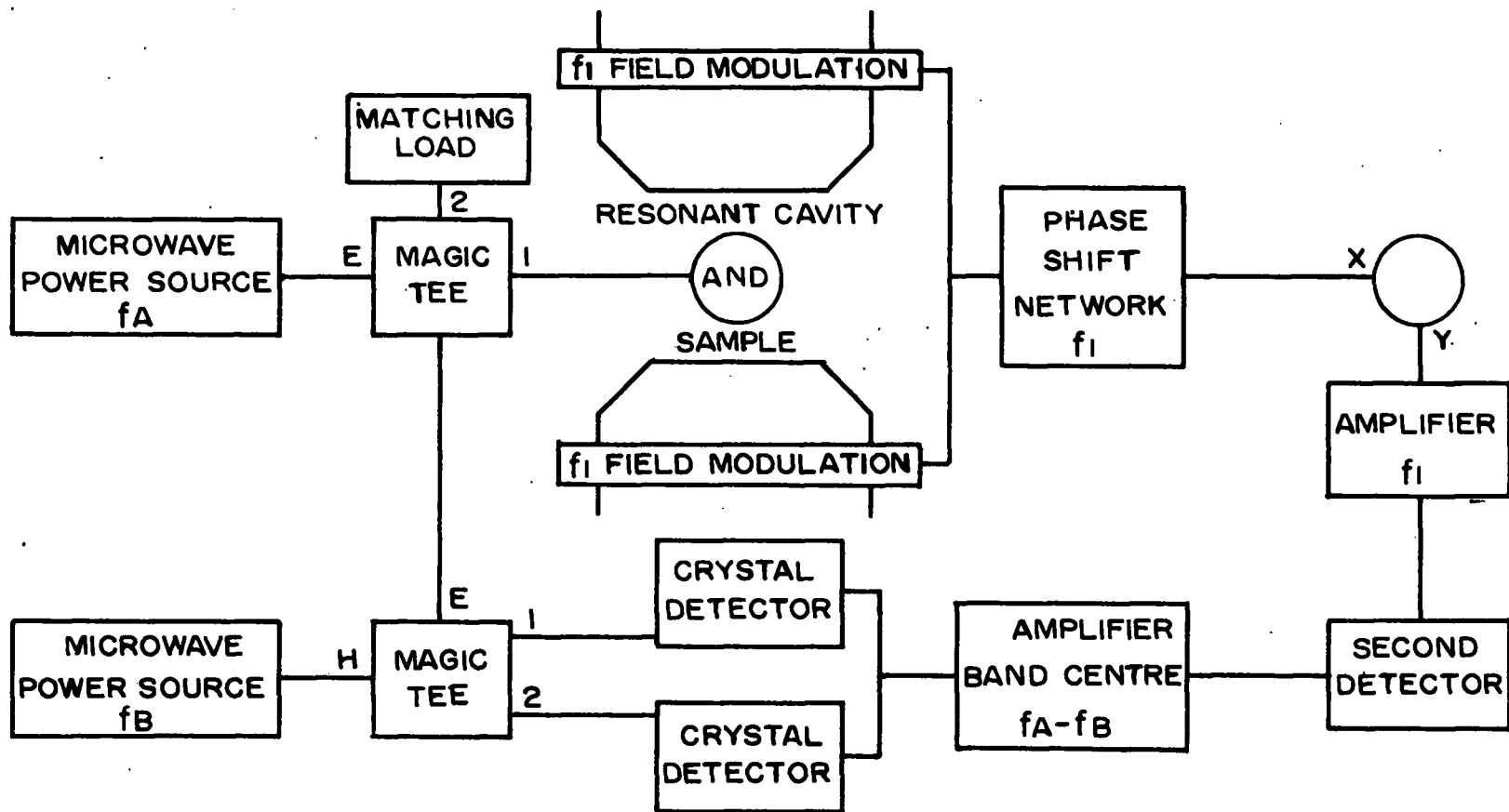


FIGURE 6

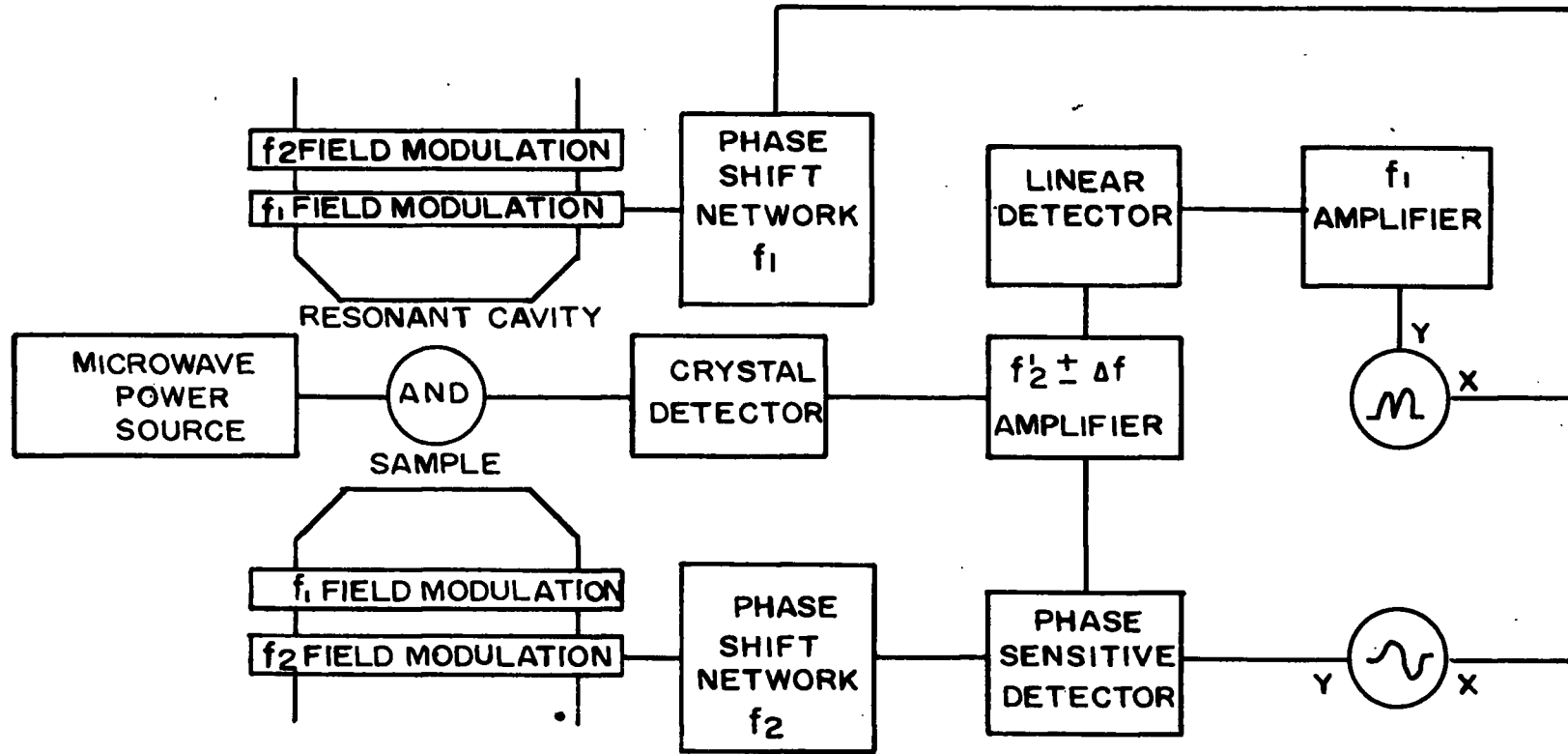
SUPERHETERODYNE PARAMAGNETIC RESONANCE SPECTROMETER

noise. However, it does suffer from the disadvantage that it can only be used for narrow band operation due to the limited frequency response of a bolometer (T2). Moreover it requires critical adjustment to keep in balance and is not too stable since a d.c. bridge is employed. It is rather strange that, in view of its reported sensitivity, it has only been used to study paramagnetic resonance in gases (B11).

2.72. Superheterodyne Spectrometer

The application of the superheterodyne principle to paramagnetic resonance spectrometer design has been discussed by several authors. Theoretically, it should be a very sensitive method but in practice it falls short of this limit by a wide margin, suffering seriously from instability since not only must one klystron be locked to the resonant frequency of the cavity but another klystron must be locked at a constant frequency difference to the first one. Furthermore, excessive noise seems to be introduced at the crystal converter. This noise is probably due to low frequency beats between the two signals which are caused by the fact that any oscillator does not generate a monochromatic spectrum (finite Q of tank circuit). Theoretically, the use of a balanced mixer should eliminate such noise (T2,M3) but this does not seem to be achieved in practice. A block diagram of a superheterodyne used by Schneider and England (S1) is shown in Figure 6. Recently, Hirshon and Fraenkel (H4) have reported an improved version. They have taken extreme care to

FIGURE 7



DOUBLE FIELD MODULATION PARAMAGNETIC RESONANCE SPECTROMETER

stabilize the system; but unfortunately it suffers from large spurious instabilities which limit its sensitivity.

2.73. Video Spectrometer

The single modulation or video spectrometer is the simplest and fastest instrument to operate and is probably the most widely used (B11, S2). A large block diagram of one is shown in Figure 3b. It can be used on wide or narrow band; however, its sensitivity is poor since the modulation frequency is limited to below 10^3 cycles (2.7) and hence "flicker" crystal noise is a serious problem. Its stability is relatively good.

2.74. Double Field Modulation Spectrometer

The double modulation spectrometer shown in Figure 7 and developed by the author in this laboratory (S3) has all the advantages of the video type (simplicity, stability, wide and narrow band operation) with the added advantage of greatly increased sensitivity since it eliminates most of the excess crystal noise. The principle of its design is not new. It was tried in microwave gas spectroscopy by Hartz and van der Ziel (H1) without notable success. While we were in the process of applying it to paramagnetic resonance spectroscopy at microwave frequencies, Smaller and Yasaitis (S5) reported the successful application of it to paramagnetic resonance spectroscopy at radio frequencies (10 mcs - 500 mcs).

In their application, it was used to eliminate flicker noise in the amplification system. The gain in sensitivity achieved at radio frequencies by this method is not large. Moreover, since the limiting sensitivity is proportional to the detection frequency, we will not consider their method further. At radio frequencies, this technique is really only a complicated approach to eliminating the "flicker" noise in the electronic tubes. This effect can be eliminated much more simply by modulating at a single frequency in excess of 10^6 cycle since there is no iron necessary to produce the required magnetic fields, which otherwise complicates the matter.

In a video type spectrometer, the magnetic field is modulated at a frequency f_1 (usually less than 100 cycles) with amplitude H_1 (greater than the line width at half amplitude). If the output of the crystal converter is applied, after amplification, on the Y plates of an oscilloscope and the X plates are modulated at the frequency f_1 with the proper phase then any resonances in the region $(H \pm H_1)$ where H is the magnetic field, are displayed on the screen as stationary signals.

If we also modulate the magnetic field at a frequency f_2 with amplitude H_2 (less than or equal to the line width), feed the output of the crystal converter into an amplifier with band centre at f_2 and band width of about $100 f_1$, redetect at video frequencies and apply this signal

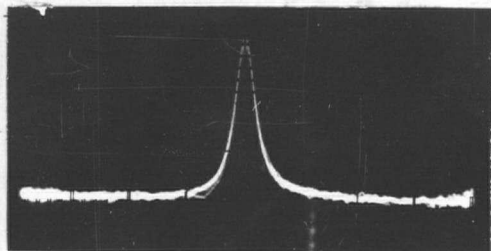


PLATE Ia

"g" marker signal from
video spectrometer

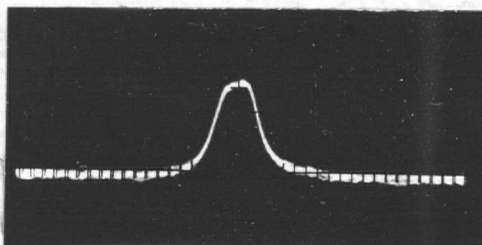


PLATE Ib

"g" marker signal from
video spectrometer with
r.f. field modulation on

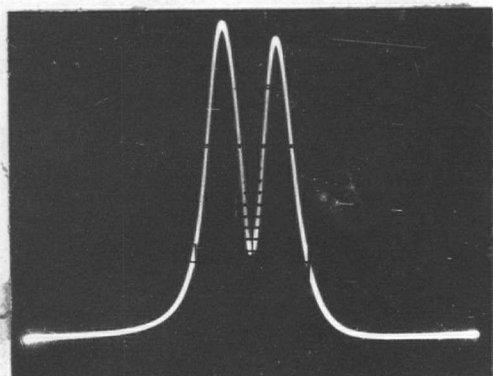


PLATE Ic

"g" marker signal from
double field modulation
spectrometer with linear
detector

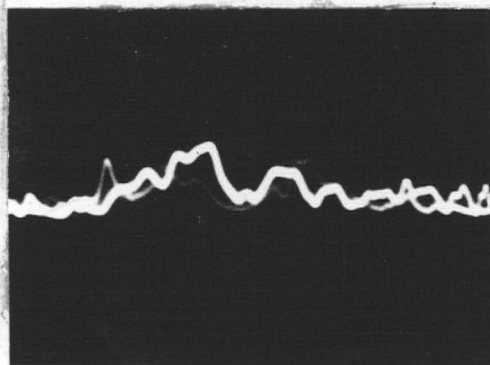


PLATE Id

10^{-9} grams "g" marker
signal from double field
modulation spectrometer
with linear detector

to the Y plates, the derivative or modulus of the derivative of any resonance signal in the region $H \pm H_1$ will be displayed on the screen depending on whether a phase sensitive or linear second detector is used (H3,K1,C1).

The choice of the frequency f_2 depends on two factors:

- a. It should be above 1 mcs to enable the crystal converter to operate in a region where the excess noise is negligible;
- b. It should be less than the line width of the resonance signal in frequency units. For dilute hydrated crystals this is about 16 gauss or 25 mcs. In free radical or deuterated crystals, it may be as small as 1 or 2 gauss or about 3 mcs.

Hence, the choice of a frequency of about 1 mcs for f_2 will satisfy both of the above conditions.

It can be shown that the use of a frequency of one megacycle for f_2 should result in an improvement of sensitivity of $O(10^3)$ over that obtained by the use of a single field modulation, of low frequency. Plate 1a. and c. shows oscillograms of a signal obtained from $O(10^{-5})$ grams of "g" marker (diphenyl-trinitro phenyl hydrazyl) $[(C_6H_5)_2 \cdot N \cdot NC_6H_2 \cdot (NO_2)_3]$ on both single and double modulation. The signal-to-noise ratios are 50:1 and $5 \cdot 10^4:1$ respectively. The theoretical improvement in sensitivity is thus experimentally verified. In Plate 1b, the "g" marker resonance is also shown when detected with the

single modulation spectrometer but with the high frequency modulation applied to an amplitude equal to the line width. It can be clearly seen that the amplitude of the signal has been decreased by a factor of two verifying that the amplitude of this modulation is actually equal to the line width. Plate 1d. shows an oscillogram of 10^{-9} grams of "g" marker with a signal-to-noise ratio of 2:1. All of these signals were obtained at room temperature using wide band operation (8 kilocycles). The use of a radical as a calibration signal is convenient since the resonance is due to an almost free electron [$g_{\text{radical}} = 2.0038$ (H5) and $g_{\text{electron}} = 2.0028$]. and the magnetic concentration is large (T3).

The sensitivity achieved using this method in wide band operation is greater than that obtained using any other technique in wide or narrow band operation except that of Beringer and Castle (B2). Unfortunately, we have not had the time to construct the apparatus necessary for narrow band operation. Theoretically, an improvement of $10^2 - 10^3$ should be possible using a narrow band phase sensitive detector. In practice a factor of 50 is considered good since instabilities rather than noise now limit the sensitivity. This would indicate that the ultimate sensitivity of a double modulation spectrometer should be about 10^{-12} grams in narrow band operation. The double modulation technique described here is much easier to apply in narrow band operation because of its inherently greater electrical stability. Stability in narrow band operation of a video spectrometer

Table IV
Comparison of Different Types of Paramagnetic Resonance Spectrometer

Type	Ref.	Operation		Mass Sensitivity M min				Stability
		Bandwidth		Wide Band (10^4 cps)		Narrow Band (1 cps)		
		Wide	Narrow	Mmin (GRAMS)	T (°K)	Mmin (GRAMS)	T (°K)	
Theoretical	B11	Yes	Yes	4×10^{-10}	290°	4×10^{-12}	290°	
				1×10^{-10}	20°	1×10^{-12}	20°	
				5×10^{-11}	4°	5×10^{-13}	4°	
Point-to-Point	B11	No	Yes			1×10^{-6}	290°	Fair
D.C. Recorder	W1	No	Yes			1×10^{-6}	290°	Fair
Balanced Bridge	B1	Yes	Yes	1×10^{-7}	290°			Poor
Bolometer	B2	No	Yes			5×10^{-10}	290°	Good
Superheterodyne	S1, H4	Yes	Yes	1×10^{-7}	290°	5×10^{-9}	290°	Fair
Single Field Modulation (Video)	B11 S2	Yes	Yes	5×10^{-7}	290°	Calculated		Good
				1×10^{-7}	20°			
				5×10^{-8}	4°	5×10^{-10}	4°	
Double Field Modulation	S3	Yes	Yes	1×10^{-9}	290°	Calculated		Very Good
				1×10^{-10}	4°			

is determined by the stability of the microwave power level at the crystal converter. The double modulation spectrometer is less sensitive to fluctuations in the microwave power level because the signal is first detected at high frequencies and then redetected. Signals of good stability have been observed with the double modulation spectrometer which, when examined simultaneously with the video spectrometer, could hardly be studied because of microphonic difficulties. This also explains why the cavity can be allowed to fill with liquid helium when the double modulation spectrometer is used. This cannot be permitted if satisfactory stability is to be obtained with the video spectrometer. It should be further noted that visual integration of signals increases the apparent sensitivity of wide band operation.

2.8. Comparison Of Techniques

Table IV is arranged to show the characteristics and sensitivities of all the known paramagnetic resonance spectrometers.

The theoretical sensitivity has been calculated using the formula derived by Bleaney and Stevens (B11)

$$\chi_{\min} = \frac{V}{\pi Q_0} \left[\frac{NF \cdot kT \cdot df}{P_1} \right]^{1/2} \quad (20)$$

where V is the effective volume of the cavity defined by

$$\int H^2 dv = H_1^2 V \quad (20a)$$

Q_0 is the unloaded Q of the cavity

NF is the noise figure of the receiver

P_1 is the available power from the microwave oscillator

df is the effective bandwidth of the receiver

To convert from χ_{\min} to the minimum detectable mass, we require the equation

$$\chi'' = \frac{\pi \nu g'^2 \beta^2 N [S(S+1) - M(M-1)] f(\nu)}{8 kT(2S+1)} \quad (21)$$

for the $M \leftrightarrow M-1$ transition where

N is the number of paramagnetic ions

S is the spin of the ion

ν is the frequency at which the resonance is observed

β is the Bohr magneton ($\beta = \frac{eh}{4\pi mc}$)

g' is the spectroscopic splitting factor

$f(\nu)$ is the normalized line shape function

and the gram atomic weight of the paramagnetic ion.

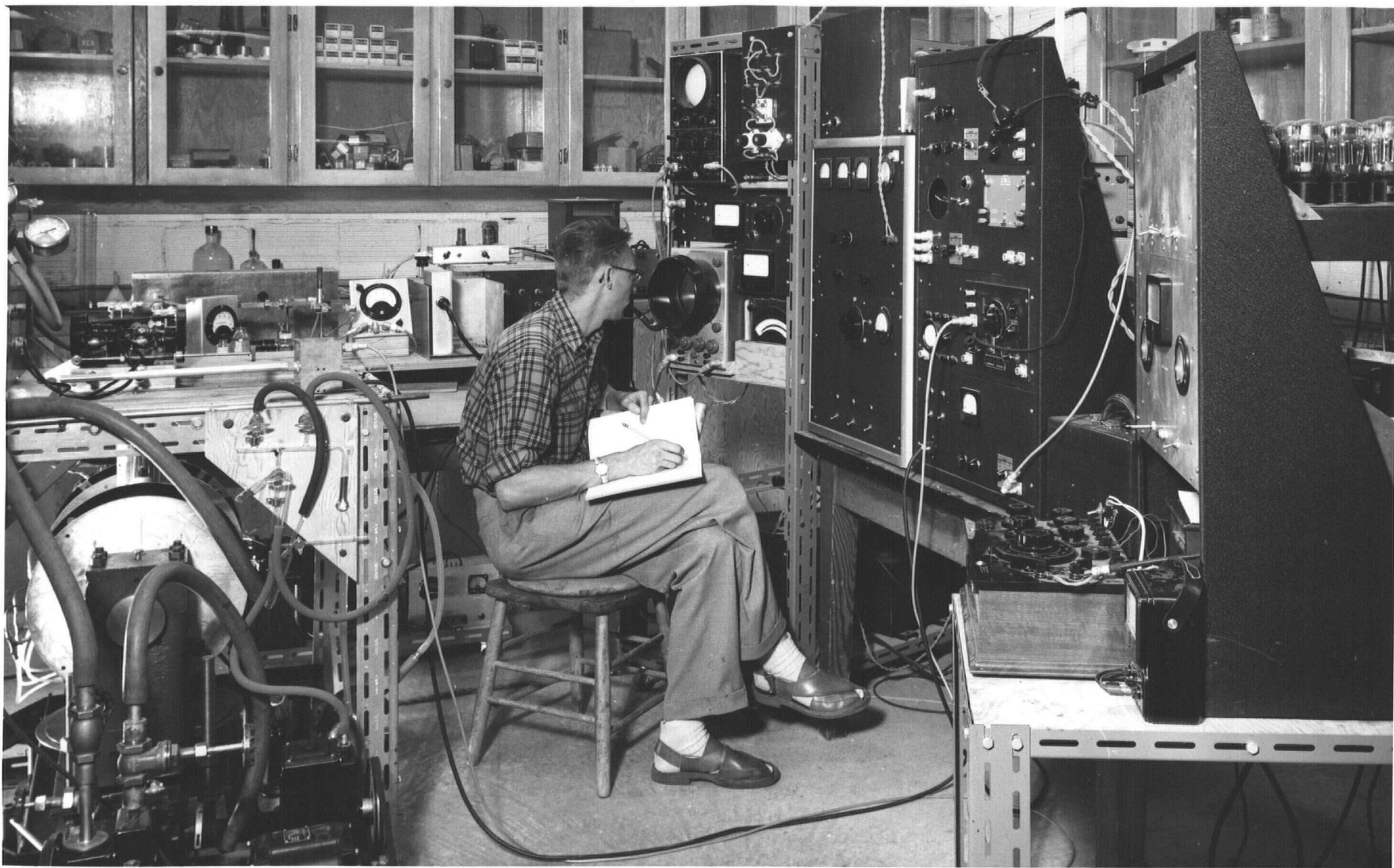
The following values have been used in the numerical calculation

$S = 1/2$, $\nu = 25,000$ mcs; $g = 2$, $Q_0 = 5000$, $df = 1$ cps, 10^4 cps.

$V = 1$ cc, $T = 4^\circ, 20^\circ, 290^\circ$ K., $P_1 = 40$ milliwatts N.F. = 10

$\nu/\Delta\nu \approx 10^3$ for a dilute hydrated crystal, 100 for gram

ionic weight. All published sensitivities have been normalized using these values.



facing page 53

PLATE II · General view of experimental apparatus ·

CHAPTER III

EXPERIMENTAL APPARATUS

3.1. Introduction

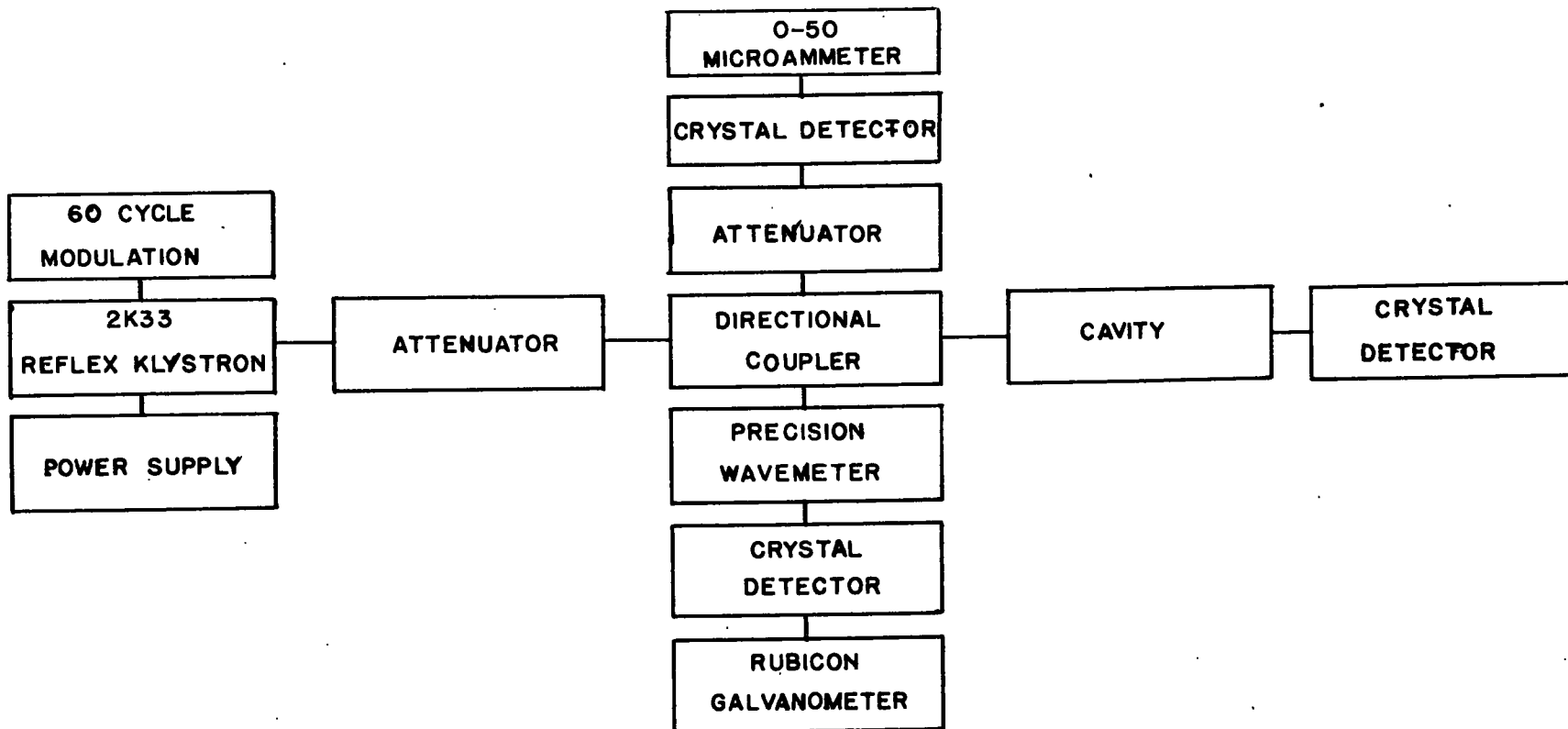
In this chapter, the components of the wide band, double modulation spectrometer developed to perform the experiments described in Chapter IV are described in detail. Since it can also be operated (with a slight modification) as a wide band, single modulation spectrometer, we shall describe the components required for both at the same time and indicate, where it is necessary, those which are unique to one mode of operation or the other.

Both function from room to helium temperature. Block diagrams are employed to illustrate the design principles used and the actual circuit diagrams are collected together in Appendix 1. Two general views of the apparatus are shown in Plates II and IX.

Chronologically, the single modulation spectrometer, which is of standard design, was constructed first and the double modulation spectrometer was developed from it.

3.2 Microwave Apparatus

Identical microwave components are required for the single and double modulation spectrometers with the



BLOCK DIAGRAM OF 1.25CM. MICROWAVE APPARATUS

FIGURE 8

exception of the tuned cavity in which the sample under investigation is placed. The choice of the frequency of operation was dictated by two considerations.

- a. the availability of apparatus in this laboratory from the microwave gas spectroscopy group, and
- b. the ability to operate over the widest range of "g" values.

Consequently, the spectrometers operate at about 25 kmcs. or 1.2 cm. The photograph in Plate III shows the general arrangement of the microwave components. The block diagram in Figure 8 shows the same arrangement.

3.21. Wave Guide Components

The attenuators, "E" bends, "H" bends, crystal detectors, "magic" T's, tapered section, directional couplers, and straight sections employed have been designed from the data in Montgomery (M3) and constructed in this laboratory. Electroplating techniques have been found useful in some instances. It was considered economical to use commercial contact flanges RG - 425/U. 18 inch lengths of commercial flexible waveguide are utilized to connect the microwave equipment to and from the spectrometer head to which the cavity is attached. This enables the cavity to be moved in and out of the magnetic field without breaking the microwave circuit and has considerable advantage when experiments are performed using liquid helium (3.62).

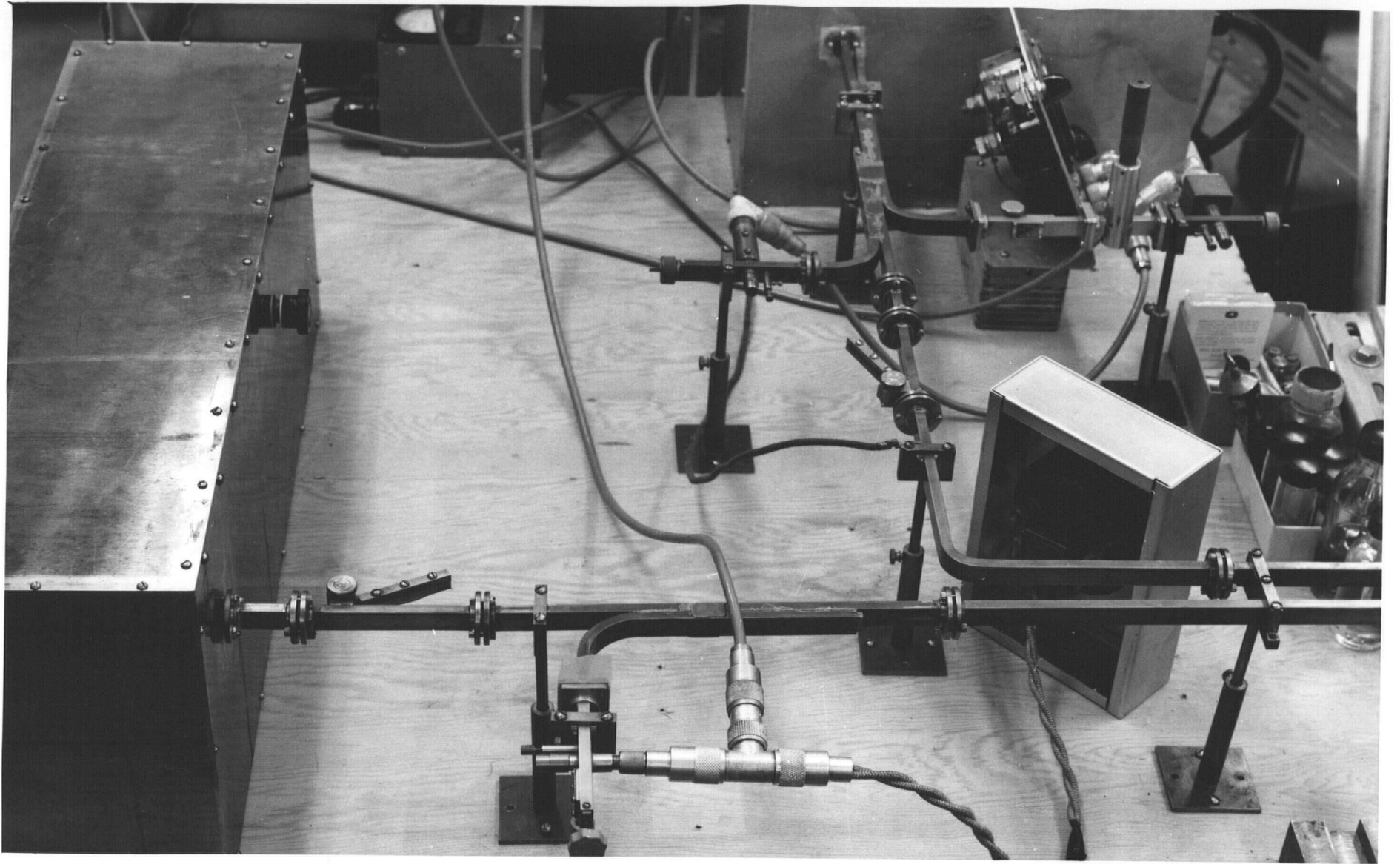


PLATE III · View of microwave components ·

3.22. Microwave Power Generator

A paramagnetic resonance spectrometer requires a radiation source which

- a. generates an essentially monochromatic spectrum,
- b. possesses both long and short term frequency and power stability (1 part 10^5)
- c. generates sufficient power (100 milliwatts)
- d. can be tuned over a reasonable frequency range (10%)
- e. generates a minimum amount of noise.

The most satisfactory source of microwave power in the 1.2 cm region which approximately satisfies these conditions is the 2K 33A. reflex klystrons. This type of tube is fully discussed in (K4).

It is essential, if stable, noiseless operation is to be obtained, to mount the klystron at least six feet from the electromagnet and to shield it in a brass box since its operation is severely affected by stray static and a.c. magnetic fields. This box is clearly shown in Plates III and IX. There are particularly troublesome when the double modulation technique is employed since the stray r.f. field is large. Improved temperature stability is another advantage of the brass box.

A high stability, low ripple power supply is essential if conditions a, b and c are to be satisfied. A power supply of standard design for the 2K 33A with a

voltage stabilization factor of 10^3 and about 1 millivolt r.m.s. of noise and hum has been constructed. The filament is d.c. heated by a 6.3 volt storage cell to prevent 60 ν frequency modulation. Vacuum diodes, inserted between the reflector and cathode and grid and cathode, prevent these elements of the klystron from becoming positive with respect to the cathode and destroying the tube because of excess beam current and secondary emission from the reflector. A fuse in the cathode also limits the cathode current. To facilitate finding the resonant frequency of the cavity, provision is made to modulate the klystron reflector at 60 cycles.

For improved stability, it has been found useful to lock the frequency of the klystron to the frequency of the tuned cavity. Such a system is described in 3.26.

3.23. Detectors

Broad band crystal detector mounts have been constructed (3.21). The $1N26$ silicon crystal converter is the only unit designed to operate at 25 kmcs. Specially selected, low noise temperature, low conversion loss units were obtained to ensure a minimum noise figure for the entire system.

3.24. Cavity Resonators

Cylindrical 1.2 cm. resonant cavities operating in the H_{111} mode have been designed from the data in

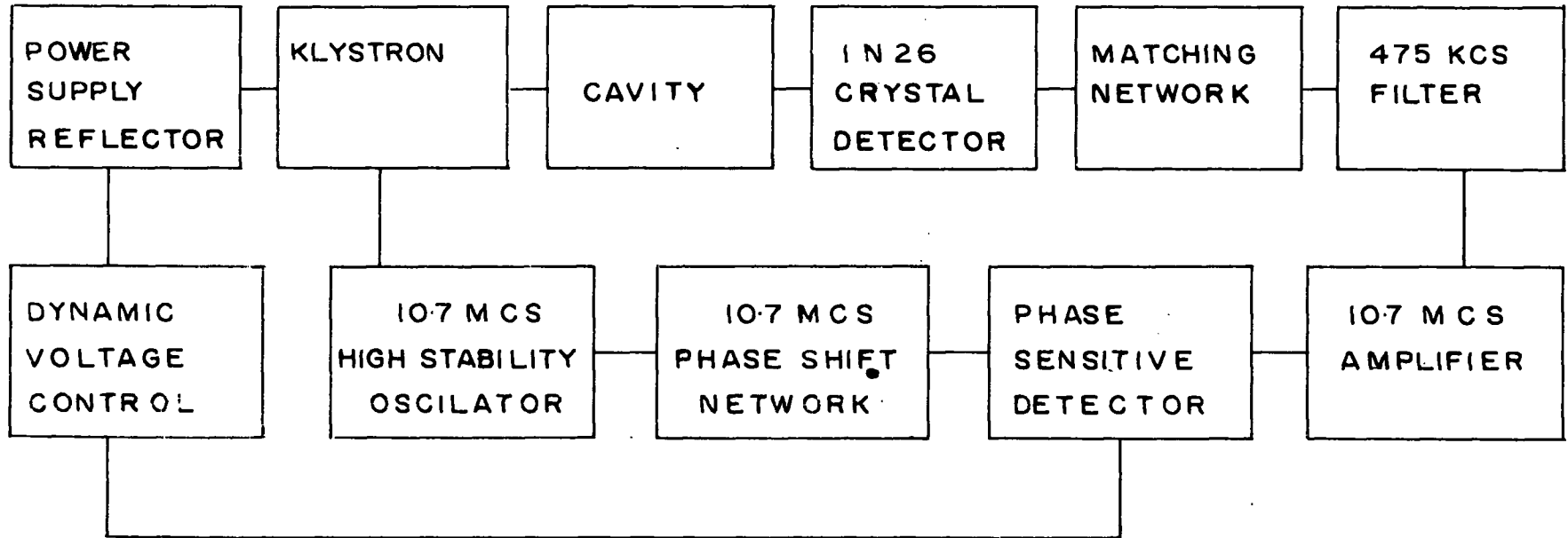
Montgomery (M3). They can be tuned by means of a threaded end plunger with the proper choke termination. This mode concentrates the microwave magnetic field at the ends of the cylinder where the sample may be conveniently mounted on the face of the tuning plunger, ensuring maximum sensitivity because most of the magnetic field is then concentrated in the sample. The Q of the cavity is decreased from $O(10^4)$ to $O(10^3)$ by heavy coupling to reduce instabilities caused by microphonics and to permit the crystal converter to operate with optimum signal-to-noise.

To employ the double modulation technique, it is necessary to slot the walls of the cavity in a plane through the axis of the cylinder. The microwave current in the H_{111} mode flows in planes parallel to this cut and, hence, the Q of the cavity is not affected by its presence, provided it is not too wide (< 0.020 inch). The introduction of the high frequency modulation current inside the cavity by means of this slot will be considered in 3.5. A diagram of a slotted cavity is shown in Figure 12 and an actual one can be seen in the photograph in Plate **VIII**

3.25. Wavelength Measurement

A commercial, transmission type wavemeter is employed to measure the wavelength of the microwave radiation. It will measure frequencies in the range from 22.20 - 27.00 kmcs. with an accuracy of 1 part in 10^4 .

FIGURE 9



BLOCK DIAGRAM OF A CAVITY TYPE
KLYSTRON FREQUENCY STABILIZER

The calibration has been carefully checked (M2) using the microwave frequency standard (accuracy 1 part in 10^7) available in this laboratory (M1).

3.26. Klystron Stabilization

It has been found convenient to stabilize the frequency of the 2K33A reflex klystron using a modification of the Pound (P2) stabilization circuit developed in this laboratory (R2). This stabilizer, which is shown in Figure 9, locks the frequency of the klystron to that of the tuned cavity and will follow changes in the resonant frequency of it.

3.3. Magnetic Field Equipment

The design, construction and performance of the equipment required to produce, control and measure the various magnetic fields required for a double modulation spectrometer are described in this section.

3.31. Design And Construction Of The Electromagnet

A small electromagnet, suitable for a paramagnetic resonance spectrometer, has been designed and constructed. Flexibility and economy were the major design considerations.

At 25 kmcs. a field of 9000 gauss is required to observe paramagnetic resonance absorptions when $g = 2$ and 18,000 gauss when $g = 1$. It is advantageous to be able to observe resonances over as large a range of g values as

possible. The field homogeneity should be about 0.01% over the volume of the samples which are about 2 mm. on edge if line widths of one gauss are to be observed. The air gap is determined by the diameter of the cavity and the temperature at which the experiment is to be performed. At room temperature, where no dewars are required, the gap can be 0.600 inches since the outside diameter of the cavity is 0.580 inches. Using standard sizes of glass, the smallest outside diameter of the tail of a dewar into which the cavity will fit is 0.900 inches. At helium temperatures, two dewars, one inside the other, are required and the outside diameter becomes 1.250 inches. Since experiments were planned involving $g = 1.5$ at helium temperatures, a field of 12 kilogauss in a gap of 1.270 inches is required. Satisfactory homogeneity can be obtained with 2 inch diameter pole faces although 4 inch faces would be better. It is also advantageous to be able to rotate the magnetic field (2.2).

On the basis of the above considerations, an electromagnet has been designed, which has the following features;

- a. Adjustable gap up to 3 inches
- b. Interchangeable 4 inch cylindrical and 2 inch tapered pole faces
- c. Adjustable shims on the pole faces to improve the homogeneity (R1)
- d. Rotatable magnet yoke (360°)
- e. Calibrated scale with 0.5° divisions to

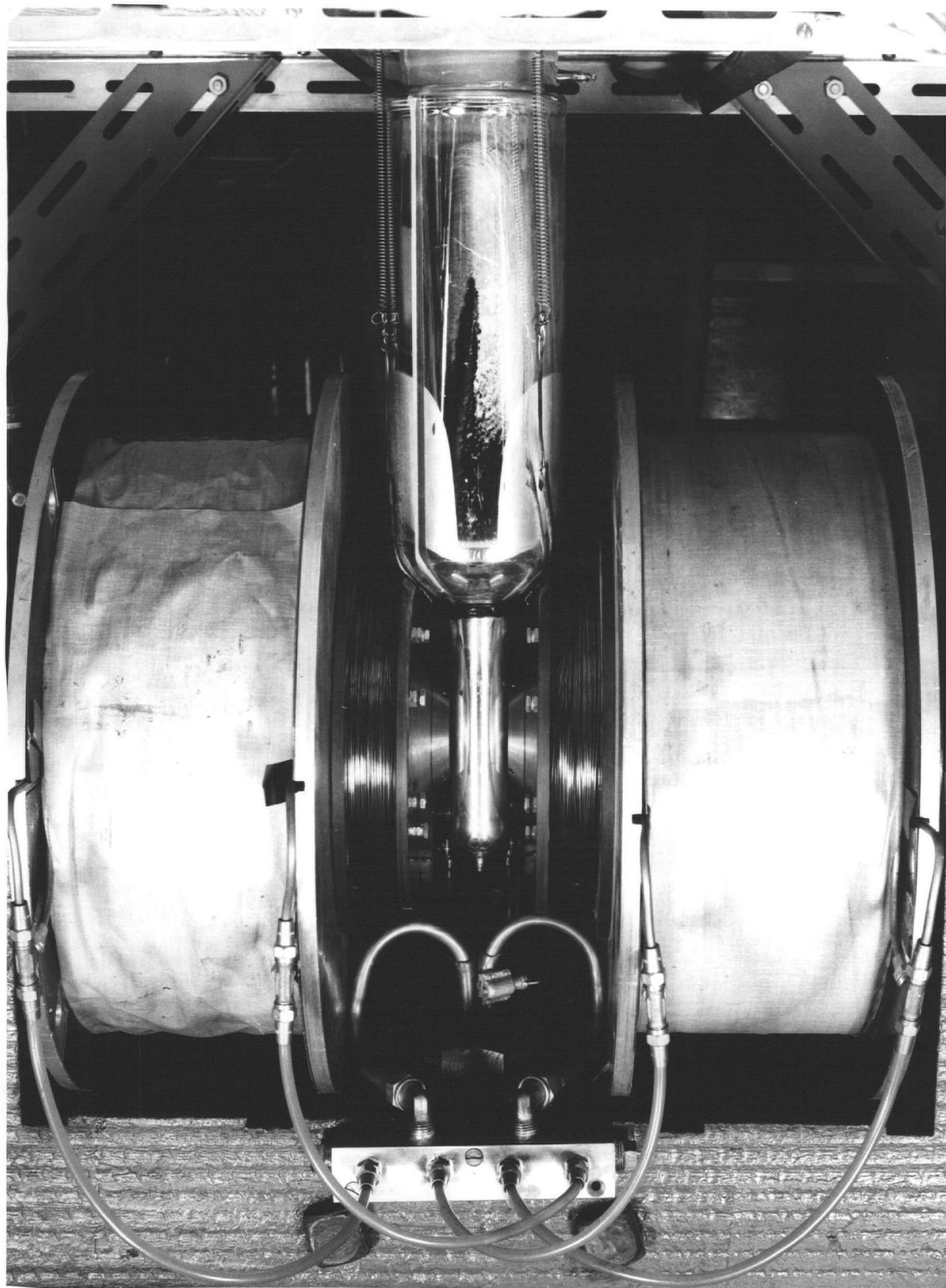


PLATE IV · View of electromagnet

facing page 60

measure rotation.

- f. Vertical level adjustment
- g. Trolley mounting for ease of moving
- h. Adjustable pads to level and position trolley
- i. Water cooling

A view of the magnet is shown in Plate IV with the spectrometer head and dewars in the gap.

The yoke and pole pieces were made from a high quality soft steel billet donated by The Steel Company of Canada Ltd. with the following chemical specifications. 0.05%C, 0.010%P, 0.025%S, 0.08%Mn, 0.002%Si. The yoke was fabricated by Ross and Howard Ltd. and the remainder of the unit was constructed in the department machine shop.

It was estimated that 40,000 ampere-turns would be sufficient to obtain 15,000 gauss in a 1 inch gap assuming $H_{\text{iron}} = 80$ ampere-turns / inch. Since a 125 volt 16 ampere D.C. generator was available, the magnet impedance coils were matched to it. Each coil was wound with 3,300 turns of #13 double glass insulated copper wire and has a resistance of 16 ohms. When the coils are connected in parallel, a magnetization force of 52,000 ampere-turns is available.

Two layers of 3/16" diameter copper tubing are used to cool each coil.

3.32. Performance Of The Electromagnet

Using the two inch tapered pole faces, it is possible to obtain a field of 13,000 gauss in a gap of 1.27

inches, and 18,000 gauss in 0.920 inches. This permits g values down to 1.5 to be observed at helium temperatures and to 1 at oxygen temperatures.

Line widths of 3.7 gauss have been observed for " g " marker in agreement with the reported value (H_5) which confirms that the homogeneity is adequate. Using samples of mineral oil, $3/8$ " long $3/16$ " diameter, very prominent wiggles (3.34) (B_{14}, B_{15}) on the proton resonance absorption are observed with the 4 inch diameter pole faces. They are just visible with the 2 inch faces indicating that the homogeneity is considerably poorer.

From the shape of the magnetisation curve, it is evident that the ultimate field obtainable is limited by saturation of the iron inside the current coils rather than of the pole faces. This effect is due to the large leakage factor which is produced by shape of the magnet window necessary for a paramagnetic resonance spectrometer. Tapered pole pieces or 6 inch diameter pieces with tapered faces would improve this greatly.

When a current of 9 amperes flows in each of the coils, the temperature of the cooling water rises from 12°C . to 35°C . showing that there is not adequate thermal contact between the cooling coils and the wire. More cooling surface would be required if improved long term stability were desired. For maximum stability, the magnet current is left at about 6 amperes for an hour in advance of an experiment to allow the magnet to reach thermal equilibrium.

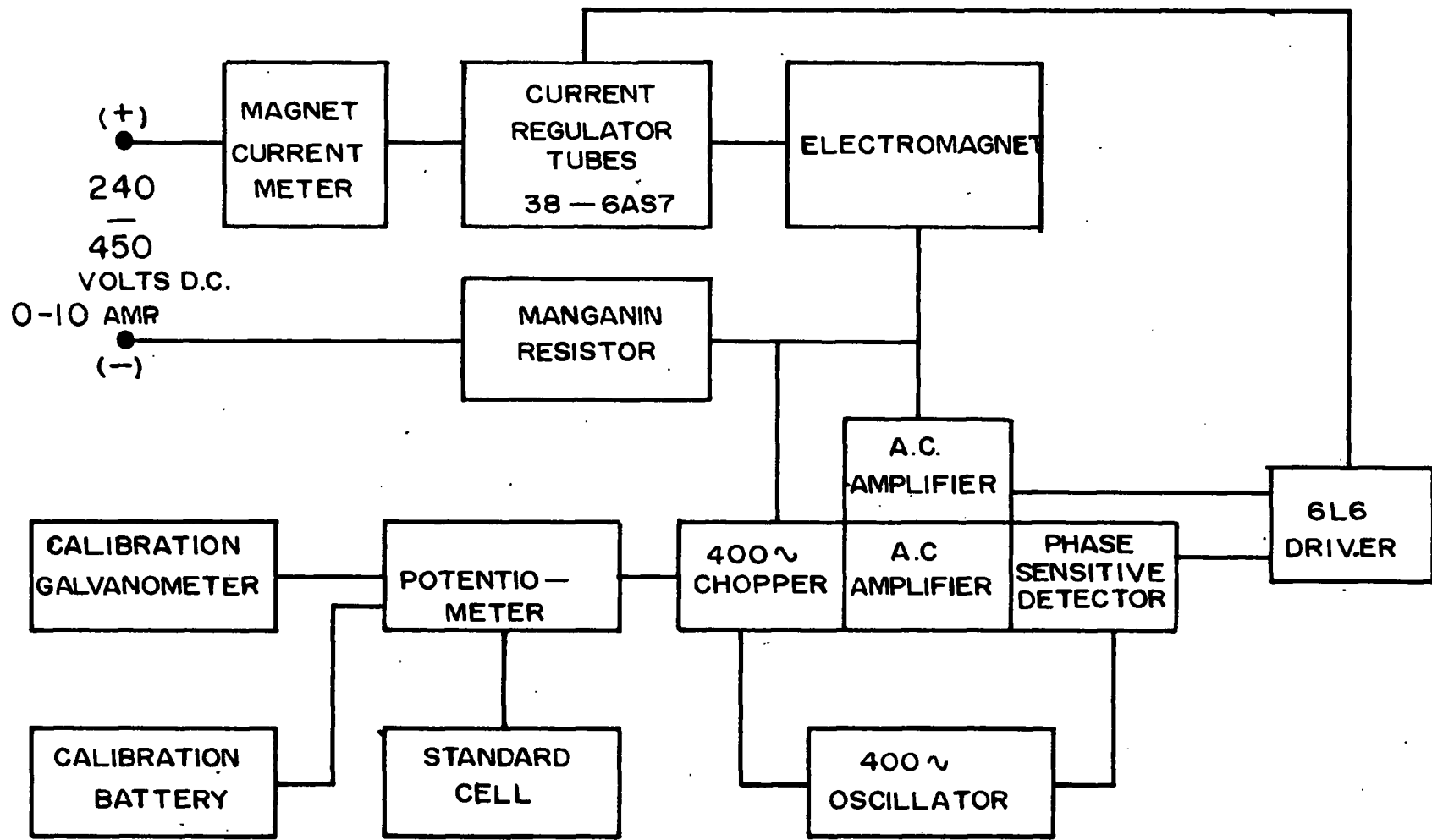


FIGURE 10
BLOCK DIAGRAM OF CURRENT REGULATOR FOR ELECTROMAGNET

3.33. Electromagnet Power Sources

Two power sources have been used with the electromagnet. When a non-stabilized magnetic field reproducible to 1% is sufficient, a one kilowatt motor generator unit producing 16 amps at 125 volts is used. It has the advantage that a large range of magnetic fields can be examined quickly. Current control is obtained by varying the resistance in the field coil.

When accurate measurements are performed, it is necessary to stabilize the magnet current. Since the accuracy of frequency measurements is 1 part 10^4 , it is necessary to stabilize the current and to also reproduce any required current to the same accuracy. A block diagram of the current stabilizer used is shown in Figure 10. The stabilization factor is 1 part 10^4 however, the reproducibility is only 5 parts 10^4 . The accuracy of resonance measurements is consequently limited by the reproducibility.

When the current stabilizer is used, the d.c. power is obtained from two 150 volt 400 ampere D.C. motor-generator units in the Physics Building. The output of one is stacked on top of the other in order to obtain the necessary voltage. When still higher voltages are required, the output of the 1 kva. motor-generator, mentioned above, is stacked on top of the other two.

3.34. Magnetic Field Measurements

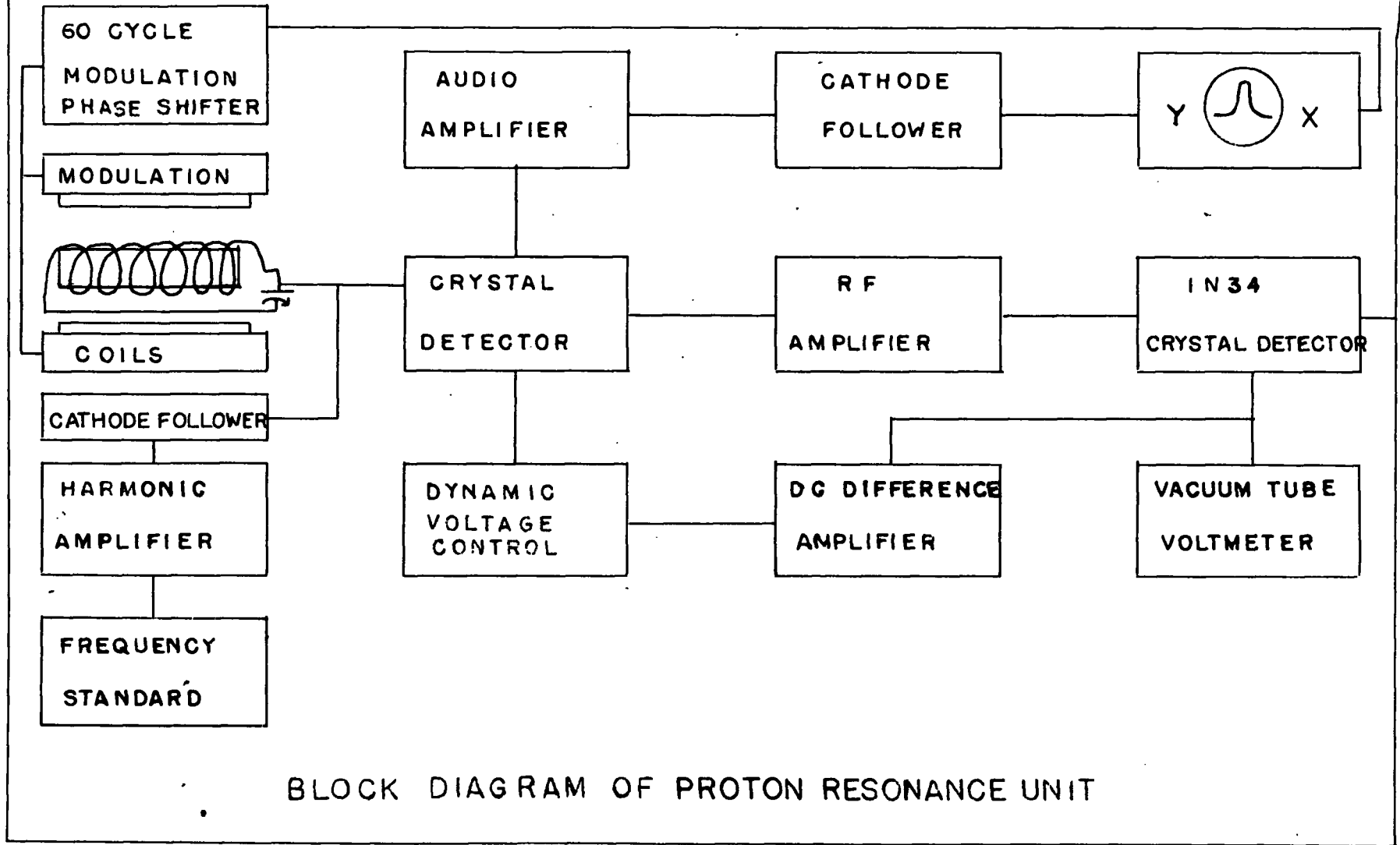
Three methods of measuring magnetic fields have been employed.

- a. Flip coil
- b. Proton resonance
- c. Comparison with known lines.

Where 1% accuracy is sufficient, a flip coil and ballistic galvanometer or fluxmeter is used.

With the proton resonance method, the precision is determined by the accuracy with which frequencies $0(10)$ mcs. can be measured (1 part 10^5 is easily obtainable). If a combined paramagnetic resonance and proton head is used, then it is limited by precision with which the proton resonance can be superimposed on the paramagnetic resonance (1 part 10^4). This method has the advantage that the field is measured simultaneously with the resonance. Inaccuracy is introduced by the fact that the paramagnetic sample and the proton sample are not in the same part of the magnetic field. With a homogeneous magnetic field this objection is not serious since the two samples can be arranged within one centimeter of each other. Unfortunately, this technique cannot be employed at helium temperatures unless solid proton samples are used. This necessitates a more complicated proton head, the line width is greater (10 gauss) and the accuracy is correspondingly poorer (5 part 10^4). Consequently, the usual procedure at helium temperatures is to calibrate the field in advance,

FIGURE 11



BLOCK DIAGRAM OF PROTON RESONANCE UNIT

using a proton head, or else to place the proton head outside the dewars.

The theory and application of nuclear magnetic resonance to the measurement of magnetic fields has been discussed in the literature by numerous authors (B15,B16,K3,S2,C2,K5). The gyromagnetic ratio of the proton has been very accurately determined (T1) ($\gamma_p = 0.234865 \pm 0.000004$ kilogauss/megacycle). Consequently, the proton can be used for accurate field measurements up to 15 kilogauss (63 mcs). Above this frequency, Lithium signals are used (K5).

The proton magnetic field spectrometer shown in Figure 11 is an improved version of one used at Clarendon Laboratory (S2). An important feature is an automatic oscillation level regulator which enables optimum signal-to-noise ratio to be maintained over a wide range of frequencies. Provision to monitor the oscillation level continuously is also made. Four plug-in coils, each covering about one octave of frequency, allow the magnetic field to be measured from 1,000 to 16,000 gauss. The oscillation frequency is measured with a BC-221AH war surplus frequency meter (3.52). The proton resonance head can be seen on the left-hand side of the photograph in Plate IX.

Since it was found to be difficult to reproduce magnetic field measurements to the accuracy desired (1 part 10^4) with the proton spectrometer because of the difficulty of interchanging identically the positions of the paramagnetic sample and the proton sample, it was considered more accurate

to make use of the measurements of known absorptions obtained with a combined proton and paramagnetic resonance head and to calibrate the magnetic field from these. Reproducible results, accurate to 5 parts in 10^4 , can be obtained using this method in conjunction with proton resonance measurements. Unfortunately, the double modulation spectrometer does not permit the inclusion of a proton head for mechanical reasons. Moreover, shielding of the proton resonance head from the 462.5 kcs high frequency modulation would be a formidable task.

3.35. Low Frequency Modulation

Two Helmholtz coils, each wound on bakelite bobbins with 350 turns of #20, H.F. insulated, copper wire, supply the low frequency modulation field. The current is obtained from the 60 cycle mains and is controlled by a variac. The voltage drop across a one-ohm resistance in series with the two coils drives the X plates of the oscilloscope. A variable phase shift network is introduced to ensure that the two signals obtained from each half of the sinusoidal sweep can be brought into coincidence. The amplitude of the field modulation is obtained by calibrating the current in the coils measured with a substandard ammeter against the voltage induced in a search coil placed in the centre of the magnet gap. Since the a.c. hysteresis depends on the magnitude of the d.c. field, calibrations must be made at different magnetic fields. Magnetic fields in the interval $H \pm H_1$ where H is the magnetic field

and H_1 is the amplitude of the field modulation are displayed on the horizontal trace of the oscilloscope, however, since the sweep is sinusoidal rather than linear, fields within this interval are sinusoidally related.

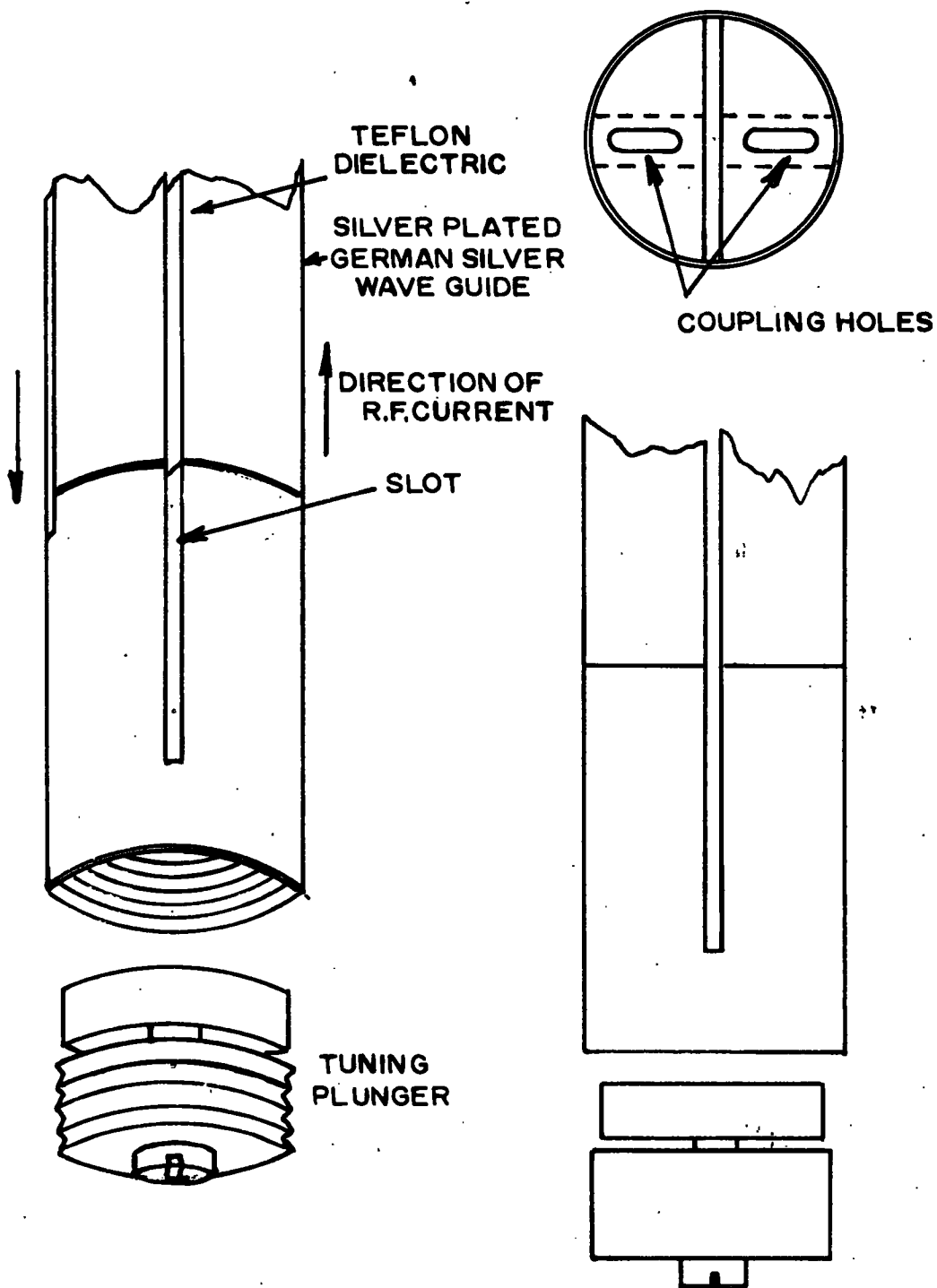
3.36. High Frequency Modulation

There are three possible methods of producing the high frequency magnetic field at the crystal site:

- a. Helmholtz type coils outside the cavity
- b. Coil inside the cavity
- c. Slotted cavity

The fraction of the a.c. magnetic field perpendicular to the axis of a conducting cylinder which penetrates this cylinder can be derived (S6). Calculations, based on this formula, show that at 500 kcs, for a brass cavity with 0.010 inch wall thickness and 0.50 inch diameter, less than one percent penetrates into the interior. Since the minimum line width of a dilute hydrated crystal is about ten gauss (3.7) (1.3), at least one thousand gauss would be required outside the cavity which could only be produced by a large current flowing in many turns. The power consumed by this and by the a.c. eddy current loss in the iron of the magnet which, of necessity, must surround the cavity to produce the required static magnetic field could only be generated by a very high power transmitter. Moreover, the power consumed by the a.c. eddy current loss would heat the iron to very high temperature,

FIGURE 12



SLOTTED RESONANT CAVITY
H₁₁₁ MODE

making field stabilization difficult. From these considerations, it can be seen that this is not a very fruitful approach. A small scale test was performed to check these conclusions. An improvement of ten in the signal-to-noise ratio was achieved when the resonance from a sample of "g" marker was examined which has a line width of four gauss (H5). The Q of the Helmholtz coils was very small making it difficult to match them to the transmitter and the iron of the magnet became too hot to touch.

The introduction of a conductor inside a 1.2 cm microwave cavity would reduce the Q of the cavity to such a low value as to negate completely any of the advantages derived from one (B11). It was also considered to be difficult to introduce the loop in such a manner as to keep the refrigerant out of the cavity. It should be noted that coils have been successfully introduced into large untuned cavities which are excited by many modes. This method was not considered seriously. Recently, Bleaney (B13) has reported a double modulation spectrometer using a half turn inside a 3 cm cavity. However, the sensitivity is reported to be inferior to that of the spectrometer described in this thesis.

If a narrow slot (0.020 inches) is cut down the axis of the cavity, as in Figure 12, then it is possible to introduce an a.c. magnetic field of any frequency inside the cavity. The a.c. current flows down the outside of one length of waveguide connected to the cavity, around both the inside

and outside of the cavity, and back up the other waveguide. The current flowing on the inside of the cavity produces an oscillating r.f. magnetic field in the interior of it. The current on the outside does not contribute for the same reason as advanced above. The cavity, from the point of view of the r.f., acts like a half turn with half of the current being effective. In this manner, it is possible to produce r.f. magnetic fields inside a cylindrical conducting cavity without affecting the microwave performance of the cavity (3.24). The split cavity can be clearly seen in the photograph in Plate VIII.

The power required to derive the high frequency modulation current through the split cavity is obtained from a 400 watt 462.5 kcs. transmitter which consists of a Clapp type, 6AC7 variable frequency oscillator, 807 Class C buffer and four 811A's in parallel. A low Q (10-15) tuned tank circuit is required to permit correct class C operation of the 811A's.

The a.c. impedance of the split cavity at 462.5 kcs is 1.6 ohms and the d.c. resistance is $0(10^{-2})$ ohms. The impedance match is obtained by tuning the split cavity to resonance at 462.5 kcs and connecting it to the appropriate tap point on the transmitter tank coil. 100 amperes r.m.s. of modulation current can easily be obtained using this procedure. It has been verified experimentally that the cavity is equivalent to a half turn with half of the r.f. current

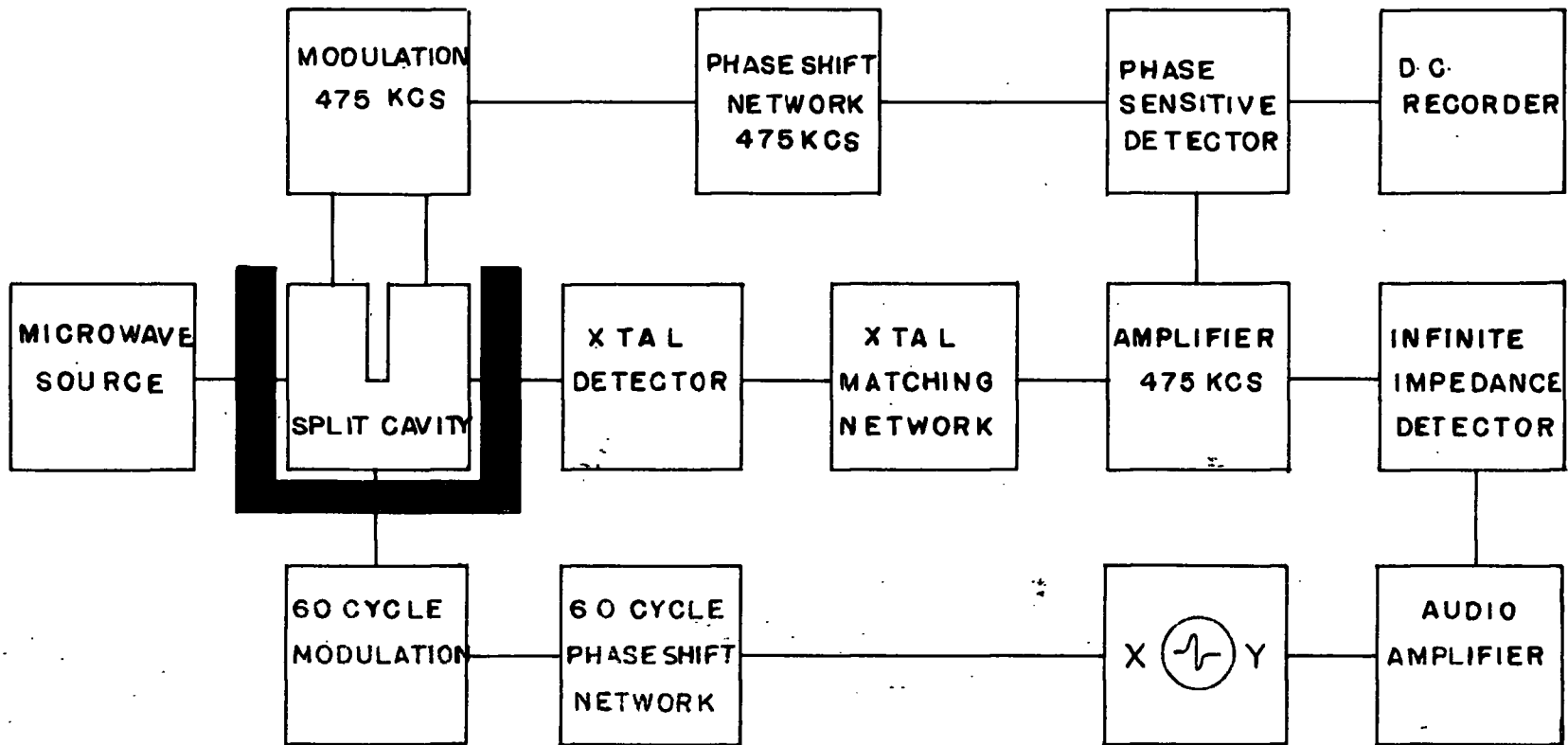
being effective in producing the r.f. magnetic field. Thus, 25 gauss r.m.s. or 79 gauss peak-to-peak can be obtained.

3.4. Detection Apparatus

3.4.1. Single Modulation

A two stage, low noise, variable gain amplifier of standard design is used to amplify the signals from the crystal converter to a sufficient level for presentation on an oscilloscope. It has been shown (S10) that the band width of a video amplifier should be about $100 f_1$ where f_1 is the modulation frequency if undistorted line shapes are to be reproduced. Since f_1 is 60 cycles in our arrangement, the amplifier was designed to be 3 db. down at 20 cycles and 15 kilocycles. The phase shift is then negligible from 40 cycles to 7 kilocycles. This was checked in operation by increasing the amplitude of the field modulation until the intensity of the signal began to decrease. This occurred at about twenty times the line width demonstrating that the frequency response of the amplifier was more than adequate. Since the overall noise figure of the system is primarily determined by the crystal converter, matching between it and the input stage was found to be non-critical. The maximum gain of the amplifier is 5000. Provision is made to mix electronically proton resonance and calibrating signals with the paramagnetic resonance signal.

FIGURE 13



BLOCK DIAGRAM OF DOUBLE MODULATION PARAMAGNETIC
RESONANCE SPECTROMETER

3.42. Double Modulation

A three stage low noise, stagger tuned, variable gain amplifier of standard design is used to amplify signals when the double modulation technique is employed. The band centre is 462.5 kcs., the bandwidth is 8 kcs. and the gain is 10^6 . The matching was found to be non-critical between crystal converter and input stage as in 3.41 (E1, S10, T2). The signal from the third stage is fed into either an infinite impedance linear detector or a phase sensitive detector and then onto the Y plates of an oscilloscope. The bandwidth of the output of either detector is $100 f_1$ or about 8 kcs. (S10). The signal obtained from the infinite impedance detector is the modulus of the derivative of the line shape of the resonance (H3, C1) while the phase sensitive detector yields the derivative. Figure 13 shows a block diagram of the detection system. It was found to be most essential that the crystal converter and the tuned amplifier be carefully shielded. The amplifier was constructed in a sealed brass box and then enclosed in another brass box with the crystal converter. The only ground point is the mounting of the crystal holder to this outer box. The photograph in Plate V shows the arrangement with the lids removed. The closed box can be seen in Plate III.

The amplifier box, all the controls and power and signal leads are insulated from the outer box. It was found to be possible, using this technique, to reduce the pickup from

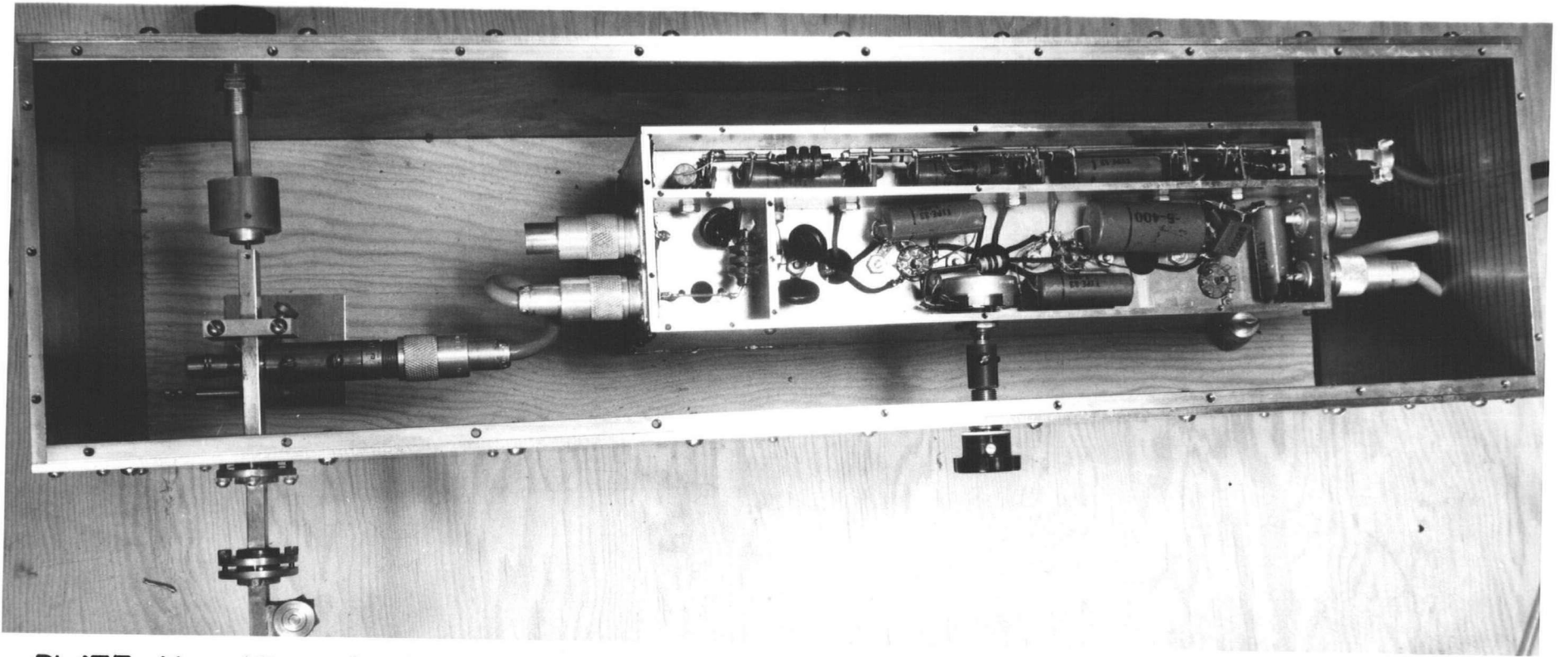


PLATE V. View showing shielding of r.f. amplifier and detector with cover plates removed.

the 400 watt 462.5 kcs. transmitter, used to drive the high frequency split cavity to below the input noise level of the amplifier which is 0.5 microvolts r.m.s. Pickup in excess of the noise will produce phase sensitive detection of signals of same magnitude in the linear detector. When strong signals are detected, the gain is reduced so that the signal does not block the second detector. In this condition, the noise in the absence of a signal is square - law detected while that on the signal is linearly detected which gives an apparent improvement in the signal-to-noise ratio. For weak signal detection, the gain is increased until linear detection occurs on the noise. Provision has been made to monitor the crystal current with a microammeter; this facilitates tuning the cavity in the absence of resonance signals.

3.43 Video Display

The resonance signals, from either the single or double modulation spectrometer are displayed on a 7 inch oscilloscope. The output of the phase shift network (3.35) drives the X plates while the Y plates are driven by (a) video amplifier (3.41); (b) phase-sensitive detector (3.42) or (c) linear detector (3.42). When photographs of the resonances on the oscilloscope screen are taken, a 5 inch Cossor double beam oscilloscope with 35 mm camera is used. This unit has been modified to enable only one half of the trace to be recorded. The beam trigger is controlled by 60 cycle

voltage of variable phase. By changing the phase, it can be arranged that one half of the trace is blanked out.

3.44. Narrow Band Operation

No narrow band operation has been attempted because insufficient time was available to construct the necessary apparatus required to sweep and stabilize the magnetic field. Moreover, the klystron frequency stabilizer (R2) has not yet been completed. The sensitivity of the double modulation spectrometer greatly reduces the necessity of employing narrow band operation because there is still considerable research to be performed ^{with} in the limit of its sensitivity. Moreover, narrow band is a slower method of collecting data.

3.5. Auxiliary Electronic Apparatus

3.51. Calibrator

It is useful to measure the relative and absolute intensities of resonance signals to permit comparison with theoretical transition probabilities. Provision has been made to inject "spikes" of calibrated amplitude in coincidence with resonance signals to perform these measurements. 60 cycle line voltage of variable phase is clipped by a blocked grid amplifier. The 60 cycle square wave so produced is differentiated and then either the positive or negative spikes are amplified; the spikes selection is accomplished by changing the d.c. level at which these spikes arrive on

the grid of the amplifier. One control sets the reference output amplitude of the spike, a resistance switching network permits multiplication or division by ten and another network divides the resulting amplitude by one hundred in units of one. These spikes are electronically mixed with the resonance signals (3.41) and then displayed on the oscilloscope (3.43).

3.52. Frequency Meter

A war surplus BC-221AH frequency meter is used to measure the frequency of the proton resonance signals when magnetic field measurements are performed. It is accurate to 1 part 10^5 over the frequency range 2-80 mcs. The output above 20 mcs has been improved by the addition of a harmonic amplifier and a cathode follower has been added to drive the cable that feeds the signal from this unit to the proton head.

3.53. Power Supplies

All the power required by the various electronic components in the two spectrometers is obtained from standard electronically regulated supplies (E4). The stabilization has been further improved in some cases by the addition of an electronic line voltage regulator. It has been found to be generally advisable to employ direct current heating of filaments to eliminate a.c. hum. This power is obtained from trickle-charged, lead storage cells.

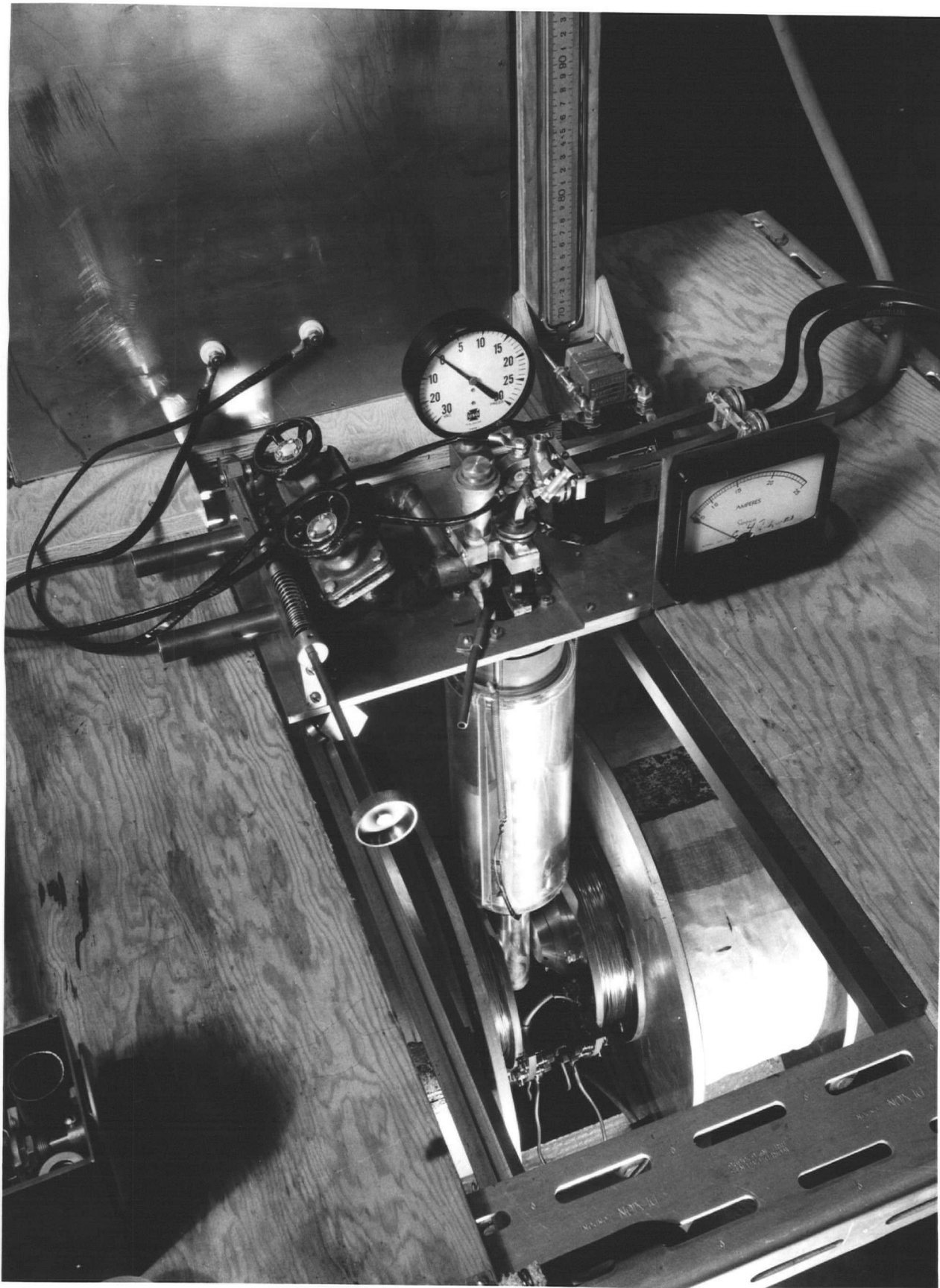


PLATE VI · View of the double modulation head with the dewars
in the magnetic field ·

facing page 74

3.6. Low Temperature Apparatus

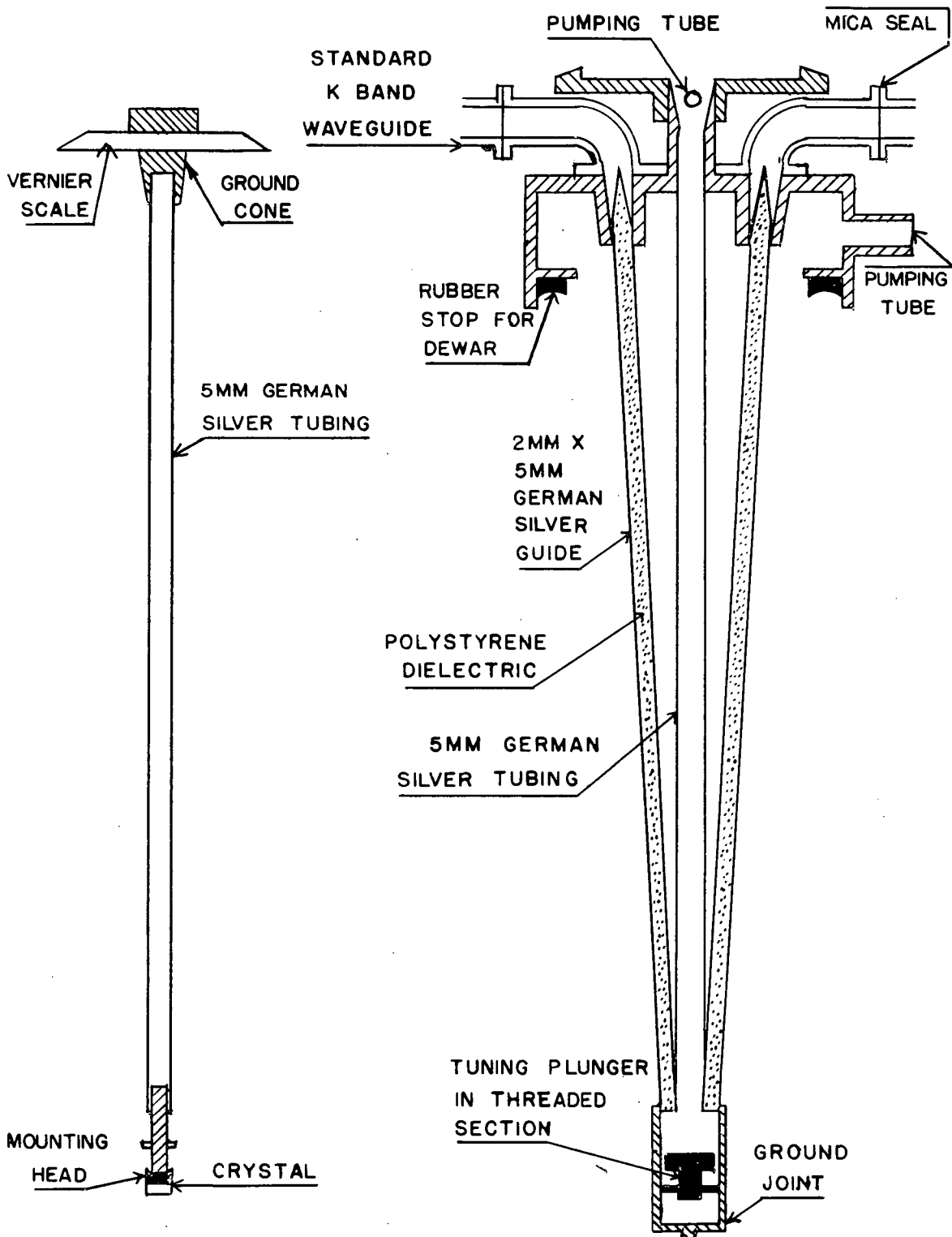
Both spectrometers have been expressly designed for operation at helium temperatures. Consequently, considerable effort has been devoted to the development of a flexible system which would enable measurements to be made accurately and quickly. The unit consisting of the cavity, connecting wave guide, pumping valves, dewars, etc. is hereafter referred to as the spectrometer head. As has already been mentioned (3.21) the head is mounted on bearings which rest on railway tracks permitting it to be smoothly rolled in and out of the magnetic field. The photograph in Plate VI clearly shows this aspect of the construction.

3.61. Single Modulation Head

Since the construction of a low temperature single modulation head presents fewer technical difficulties, it will be discussed first. If the head is to be used at oxygen or hydrogen temperatures then the system is greatly simplified. Figure 14 shows a cross-sectional drawing (S2) of such a head. A cylindrical cavity operated in the H_{111} mode and tuned with a threaded end plunger (3.24) is sealed with a coned cap coated with glycerine or silicone grease.

Elliptical holes couple the cavity to the rectangular waveguide ($1/8'' \times 1/4''$) which is constructed by drawing German silver tubing 6 mm diameter 0.1 mm wall thickness. German silver is used to reduce the heat leak into the

FIGURE 14



CROSS SECTION OF K BAND RESONATOR

refrigerant. The cut-off frequency of this waveguide is decreased by filling it with a dielectric. Teflon ($\epsilon = 2.00$) polystyrene, ($\epsilon = 2.50$) or fluorethene ($\epsilon = 2.2$) are suitable dielectrics, teflon being preferable because of its flexibility at low temperatures and chemical inertness. Electroformed tapered sections match the dielectric guide to the standard $1/4$ " x $1/2$ " O.D. K band guide. Thin mica sheets, beeswaxed to the ends of the tapered sections form a vacuum seal for the cavity without introducing serious discontinuity in the microwave system.

A 5 mm German silver tube mounted in a hole in the top of the cavity provides a sealed passage from the interior of the cavity to that portion of the head which is at room temperatures. The top end is terminated in a female ground cone. A male cone forms a rotatable vacuum seal. A scale plate engraved in five degree intervals and a vernier permit the rotation to be measured to one degree. A 3 mm German silver tube, connected to the male cone at the top, extends down the interior of the 5 mm tube to a crystal mount and choke which seals the cavity to microwaves. The sample is mounted on the end of the plunger with polystyrene cement. In this manner the crystal can be introduced flush with one end of the cavity and can be rotated in situ. Valves are provided to enable the cavity and wave guide to be evacuated and filled with a gas which does not freeze at the operating temperature. It is also possible, using this arrangement, to change crystals

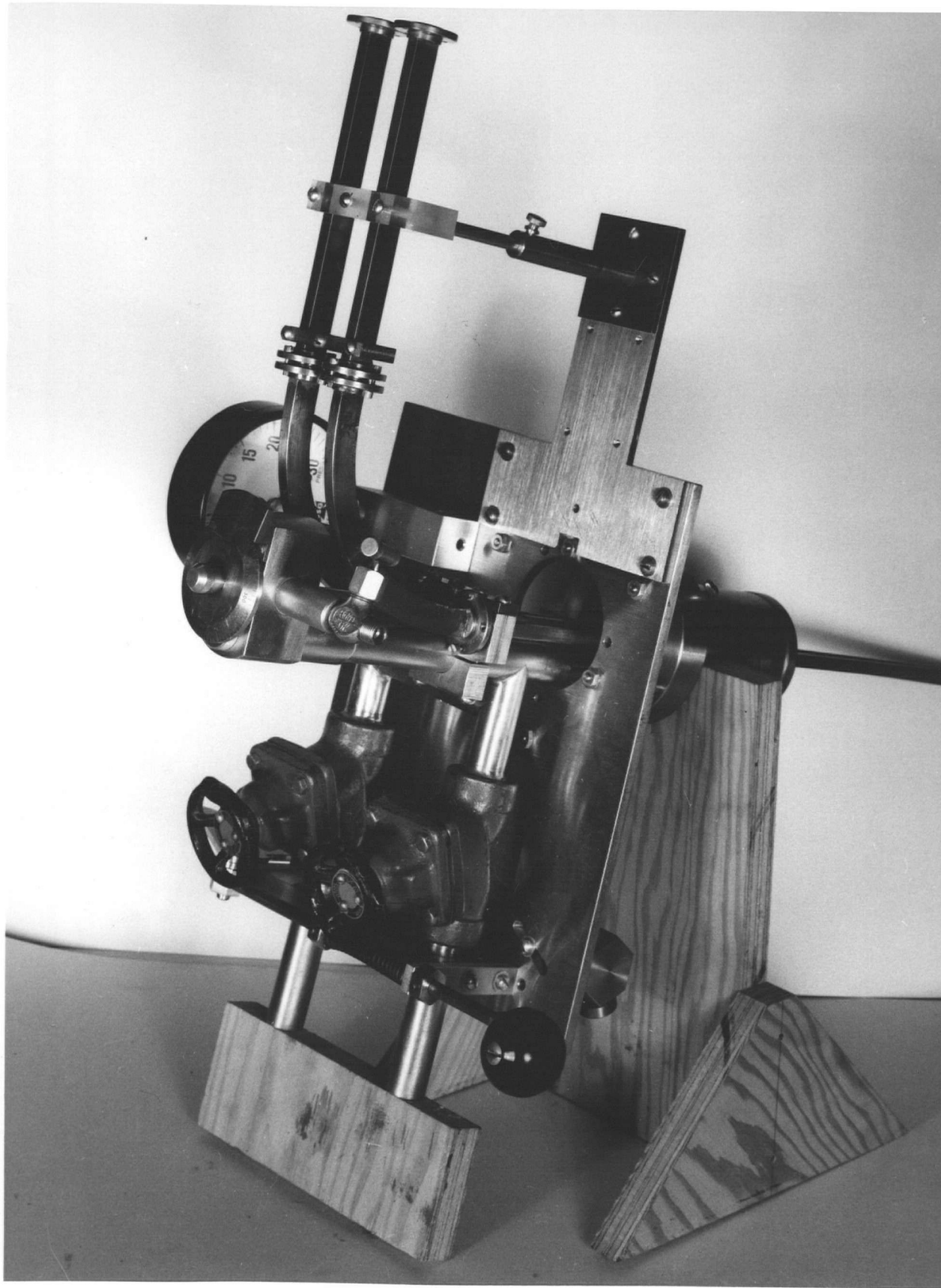


PLATE VII · VIEW OF HELIUM TEMPERATURE SINGLE
MODULATION HEAD ·

facing page 76

without warming the cavity.

A metal cap, through which the waveguide and central tube pass, fits over the dewar and is sealed to it by a section of a rubber inner tube. Other tubes which pass through the cap permit the refrigerant to be pumped when lower temperatures are required and the vapour pressure to be measured.

When helium temperatures are required, two coaxial dewars are used. The outer one which is filled with liquid oxygen or nitrogen, is suspended from the head in a spring loaded cradle. A tube is required to connect a syphon between the dewar to be filled and the liquid helium transport dewar. Additional pumping valves are required to facilitate the transfer by either pumping or blowing the liquid over. Moreover, since helium gas is expensive and, at times, difficult to obtain, a recovery system is required. A schematic diagram of the necessary pumping system is shown in Figure 15 and the pumping system and valves can be seen in the photographs in Plates II, VI, and IX. It is advantageous to maintain the top of the helium dewar at oxygen temperature to minimize the heat leak. The metal cap then involves a cup which can be filled with oxygen. A photograph of the helium temperature, single modulation head is shown in Plate VII.

3.62. Double Modulation Head

The application of the double modulation technique at temperatures which require liquid refrigerants introduces



PLATE VIII · VIEW OF THE DOUBLE MODULATION HEAD ·

numerous technical difficulties, which will be discussed in detail in this section. It is unfortunately necessary to report that some of these difficulties have not yet been solved in a satisfactory manner. Consequently, a considerable amount of time and effort has been expended on these problems and some of the solutions reported are still of a makeshift nature.

Plates VI and VIII contain photographs of the double modulation head. The pumping and filling system has already been discussed in 3.61. It should be noted that it is not possible, because of the nature of the construction of the double modulation cavity, to remove or rotate the crystal after the dewar has been positioned. Instead, the crystal is mounted on the tuning plunger before the cavity is tuned; no central tube, coned head, vernier scale, and mounting head are now required.

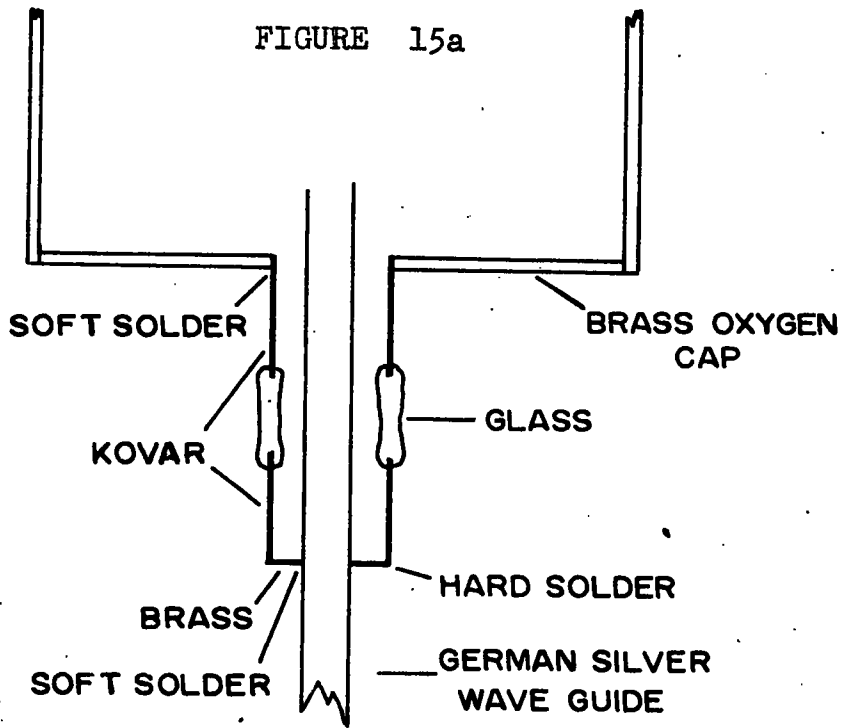
It is advantageous to prevent the refrigerant from entering the interior of the cavity because any bubbling of it due to boiling will produce a modulation of the microwave power which will result in very undesirable instabilities. Moreover, some refrigerants are very lossy at microwave frequencies. Since the cavity in the double modulation spectrometer has a slot in it, it is necessary for low temperature operation to seal the cavity to prevent the refrigerant from entering it.

Thermal setting Araldite, which has been used successfully in the low temperature laboratory at helium temperatures, was used to fill the slot. Initially, the slot in a finished cavity was filled with Araldite, however, it was found to be impossible to prevent some of it from entering the interior of the cavity. Since Araldite proved lossy at microwave frequencies, the Q of the cavity was drastically reduced. This difficulty could be surmounted by soldering the German silver waveguide to a brass cylinder with a slot milled in it. The slot was then filled with the adhesive which was cured by baking it in an oven at a suitable temperature for the recommended time. This assembly was then machined into a microwave cavity of the correct dimensions. Nonetheless, because the thermal setting Araldite contains a considerable quantity of occluded air, it was found, even after careful curing, to be porous, particularly after being immersed in liquid helium because small cracks developed. Consequently, this approach was abandoned; however, some subsequent work using cold setting Araldite which was heat cured in an oven indicates that it still might be successful.

A more successful approach is to enclose the cavity and associated waveguide below the oxygen cap in a rubber condom. They survive immersion in liquid helium without cracking even when stretched, however, they unpredictably develop small holes due to slight flaws in manufacture. Fortunately, it has been found that liquid helium can be allowed inside the cavity, although difficulty is experienced in

predicting the amount by which the resonant frequency is shifted by its presence. Part of the reason for this lies in the fact that although the heat of vaporization is small (4 calories/mole) the boiling takes place mostly at the surface particularly below the λ point. The same is definitely not true for either nitrogen or oxygen. Very anomalous effects occur which make operation almost impossible when they are present inside the cavity. Moreover, boiling occurs throughout the volume of these refrigerants.

Another problem which has proven difficult to solve arises from the fact that the wave guide must be insulated from the bottom of the oxygen cap, yet pass through it. This insulation must also form a vacuum seal capable of holding tight at oxygen temperature since it is undesirable to contaminate the helium gas with oxygen to facilitate easy cleaning of the recovered helium and also to reduce the helium boiling rate. Initially double Kovar seals, one end soldered to the oxygen cap and the other to the waveguide were tried. A diagram of one is shown in Figure 15a. These seals are vacuum tight and withstand liquid oxygen if they have been annealed in a hydrogen oven. Unfortunately Kovar is ferromagnetic and a poor electrical conductor and the induced eddy currents produce a large quantity of heat which is most undesirable. Similar units employing housekeeper seals were then tried, however they had a high breakage rate which occurred because of lack of mechanical strength and chemical



DOUBLE KOVAR SEAL

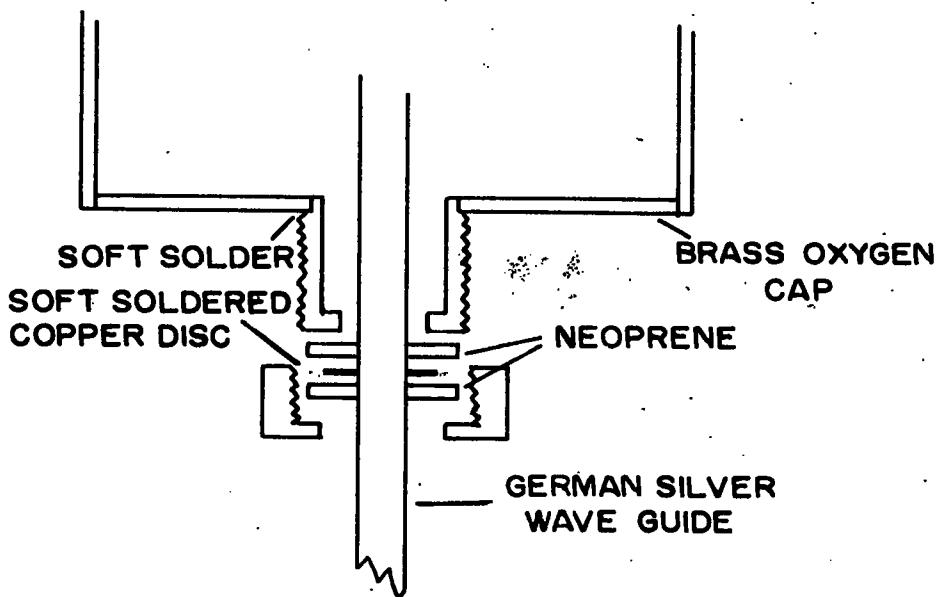


FIGURE 15b

SANDWICH TYPE INSULATED VACUUM SEAL

reaction with water and liquid oxygen. It was considered to be possible to minimize the heating effect in the Kovar by plating to the skin depth of 462.5 kcs with silver. This was tried without success because it was found to be impossible to obtain satisfactory bonding of the silver into the Kovar.

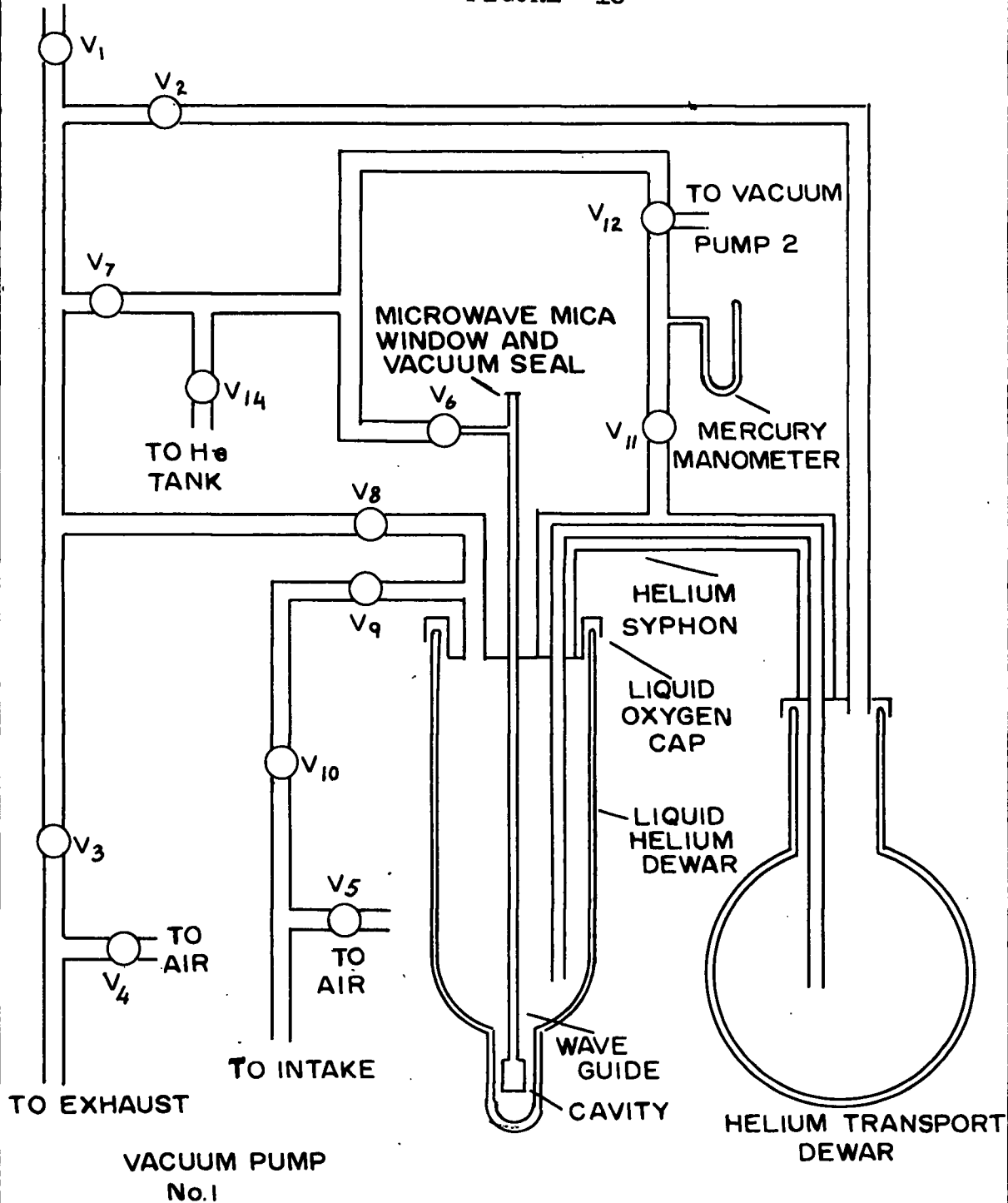
Bakelite discs which were Araldited to the cap and also to the waveguide were tried. Leaks developed in the Araldite for reasons similar to those mentioned in the discussion of sealing the cavity. Interfitting brass and bakelite cone sockets, again Araldited were unsuccessfully attempted for the same reasons. It was noted, during these efforts, that thermally cured cold setting araldite seals were much more reliable than the thermal setting variety. It is now felt that these methods might have been successful if the latter had been used.

In the meantime, another approach to this problem proved to be very successful. A thin circular disc of copper was soldered to each piece of waveguide. Discs of neoprene on each side of the copper of large diameter form a sandwich which is compressed, after lubrication with silicone grease, against a metal seat soldered in the bottom of the oxygen cap. The waveguide is insulated from the cap by the neoprene discs yet a vacuum seal is achieved. A drawing of this arrangement is shown in Fig. 15b.

HELIUM RECOVERY AND VACUUM SYSTEM

TO GAS HOLDER
IN CRYOSTAT ROOM

FIGURE 16



- V_1, V_2, V_3, V_4 : GLOBE VALVES
- V_5, V_6, V_7 : NEEDLE VALVES
- V_8, V_9, V_{10} : VACUUM VALVES
- V_{11}, V_{12}, V_{13} : GLASS STOP COCKS

V_{14} : REGULATOR VALVE

Since r.f. currents of up to 80 amperes rms, flow in the German silver wave guide in order to produce high frequency field modulation of sufficient amplitude, a considerable amount of heat is generated which boils off the liquid helium. The heat leak, in the absence of the modulation current, was found to be about 10 c.c. of liquid helium per hour (0.015 watts). When 25 amperes r.m.s. of r.f. current was passed through the system, the evaporation rate increased to 100 c.c. per minute (9.0 watts). Calculations based on these measurements indicated that this evaporation rate could be drastically decreased by electroplating the guide with silver to a thickness of about 0.0005 inches. At this thickness the conduction heat leak of the guide equals the heat generated by the r.f. current, i.e., the total heat input is minimized. The rate was then found to be about 4 c.c. per minute (0.36 watts).

3.63. Helium Recovery System

Due to the cost and the scarcity of helium gas, it is recovered by the low temperature laboratory. The vacuum system incorporates a recovery line so that when helium gas is being pumped, it can be returned to a reservoir. Figure 16 is a schematic diagram of the system employed. Some of the pumping arrangement can be seen in the photographs in Plates II and IX.

3.7. Crystals

The first step in the investigation of a paramagnetic ion is to choose a suitable crystal in which to carry out the study. This choice is governed by a number of requirements;

- (a) The crystal structure should be isomorphous throughout a group of similar ions to be studied. This decreases the work involved in calculation of the crystalline electric potentials and enables results on the ionic group to be correlated. This group must include a diamagnetic ion with which to 'dilute' the crystals.
- (b) The crystal structure should be known from X-ray analysis in order to simplify the determination of the form of the potential function which must be consistent with the crystal symmetry.
- (c) The structure should have preferably axial symmetry which facilitates the interpretation of the results.
- (d) It is advantageous for susceptibility and specific heat measurements to have been made. The results of the resonance experiments can be compared with these.
- (e) There should be only one ion in unit cell. This makes it easier to mount the crystal in the proper plane and gives maximum intensity in the spectrum.
- (f) Single crystals must grow easily in a desirable shape (in general one with a low surface to

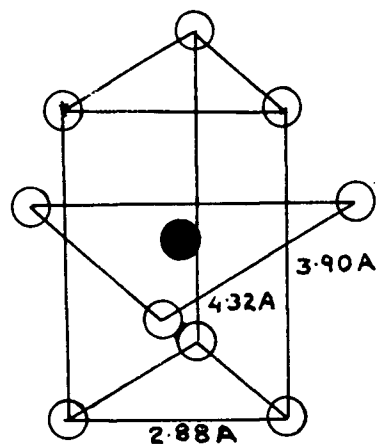
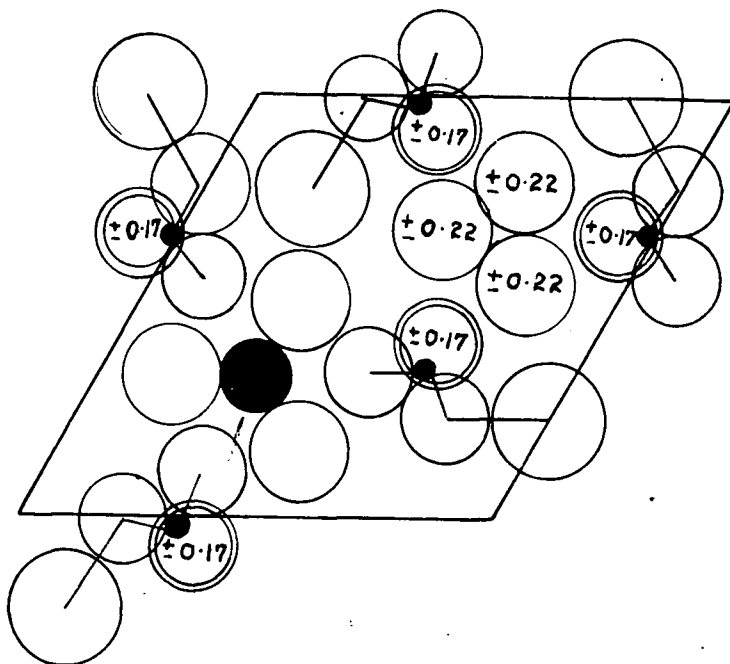
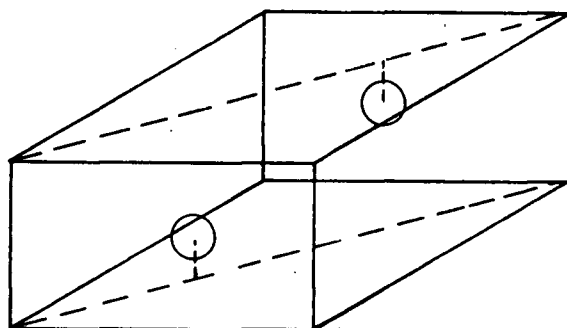


FIGURE 17

Elementary cell with the positions of the two metal ions.



Projection of the lower half of the elementary cell on a plane at right angles with the c-axis on 1/4 of its height.



Probable positions of the nine water molecules round the metal ion.

CRYSTAL STRUCTURE OF THE RARE EARTH ETHYL SULPHATES

volume ratio).

- (g) The crystal must withstand low temperatures without cracking and be chemically stable.

In the iron group, the alums, the fluosilicates and the Tutton salts have been found to be suitable for paramagnetic resonance investigations while in the rare earth group the ethyl sulphates and the magnesium nitrates are satisfactory. In Figure 17, the essential parts of the crystal structure, for the ethyl sulphate as determined by Ketelaar (K2), are illustrated.

In concentrated crystals, the width of the resonance line is determined by the spin-spin interaction (B11,P3). The resulting line width (\approx 200 gauss) is usually too great to resolve the hyperfine structure and certainly forbids the making of accurate measurements. Penrose (P2) found that the line width could be greatly reduced by diluting the salt with an isomorphous diamagnetic compound. The width is now limited by the fluctuating magnetic field of the protons in the neighbouring water molecules. The contribution of the protons to the line width can be calculated. It is 16 gauss in good agreement with the experimentally observed value. This is usually sufficiently small. It can be further reduced by growing the crystals from heavy water (B11). In order to reach the "proton" width, it is experimentally found that the ratio of the paramagnetic to diamagnetic ions must be about 1 part in 200 for the ethyl sulphates and 1 part in 20 for

the magnesium nitrates.

The mixed crystals are grown by adding appropriate amounts of concentrated solutions and then evaporating. The size of a suitable crystal for use in a 1.2 cm cavity is usually about one or two millimeters on edge i.e. 10^{-2} cm³. It was found that a considerable amount of time was spent in performing the necessary chemistry to prepare the various rare earth compounds. (L2,V6,Y1) are valuable references on the subject. The techniques, although straightforward, require considerable practice before they can be successfully employed.

3.8. Performance

The apparatus has been designed for ease, speed and accuracy of operation because of the large number of experimental runs which must be performed to do a complete investigation of a given crystal. The resonance phenomena of any crystal must be investigated at different temperatures, frequencies, and concentrations and also for many angles between the crystalline axis and the magnetic field. The apparatus discussed in this chapter performs most of these functions very well.

The chief limitation is the accuracy with which the magnetic field can be measured and stabilized. This could be greatly improved by the construction of a proton resonance magnetic field stabilizer. To justify the work involved, it would be necessary to build a magnet which would

give the required magnetic fields in the same gap but with larger diameter pole faces so that both the paramagnetic resonance and the proton resonance heads could be simultaneously placed in close proximity in a homogeneous field even when two dewars surround the paramagnetic resonance head. The field measurements could then be performed at the same time as the resonance measurements. With good field homogeneity, the correction for the different positions of the two heads should be small and easily measured.

The other limitation is not serious. It is desirable to be able to rotate the crystal in the cavity and also to be able to change crystals during a run. The mechanical nature of the double modulation spectrometer prevents this. In any case, a low temperature single modulation spectrometer has been constructed to allow this to be performed. Usually, the high sensitivity is only used to investigate the finer details of the resonances observed at lower sensitivity, in which case sufficient information is available to mount the crystal correctly.

It is possible to turn the machine on and perform room temperature measurements within fifteen minutes. Even when helium temperature experiments are performed the time lapse is only forty-five minutes. With the sensitivity available using the double modulation spectrometer

(10^{-9} grams) almost all resonance phenomena can be presented on an oscilloscope which permits a spectrum to be measured in a matter of minutes. This sensitivity is far in excess of that obtained in other magnetic measurements.

The greater sensitivity, available when narrow band operation is employed, was not felt to justify the complications which then arise, particularly for helium temperature operation.

CHAPTER IV

EXPERIMENTAL RESULTS

4.1. Introduction

The phenomenon of paramagnetic resonance was experimentally discovered by Zavoisky (Z1) in 1945. Concentrated crystals of the salts of the iron group were then rapidly studied. The experimental technique was greatly advanced by Penrose (P2) in 1949, who found that, by diluting copper potassium sulphate with the isomorphous diamagnetic magnesium salt, the spin-spin interaction was sufficiently reduced to make it possible to resolve the hyperfine structure of the copper ion. After this discovery, the experimental emphasis shifted to studies of diluted salts of the iron group.

In 1949, the Oxford group began a systematic study of the ions of the rare earth group in the ethyl sulphate crystal structure. These results are reported in Bleaney and Stevens (B11) and in Bowers and Owens (B16). In 1953, interest shifted to the rare earth double nitrates and coincided with the publication of the study of optical absorption in these double nitrates at helium temperatures by Hellwege and Hellwege (H2). The paramagnetic resonance measurements of the rare earth double nitrates have been

reported by Cooke and Duffus (C4,C5) and the crystal structure has been investigated by Jantsch (J2).

One of the primary motivations for the development of the paramagnetic resonance spectrometer with increased sensitivity described in this thesis (2.74) (S3) was the desire to attempt to measure the nuclear spin and quadrupole moment of radio-active isotopes of the rare earth ions. It was also realized that higher order effects in the previously observed spectra should be detectable. The experimental results obtained using this spectrometer are discussed in the remainder of this chapter (4.2 - 4.4) and summarized in 4.5

4.2. Gadolinium Ethyl Sulphate

The trivalent gadolinium ion, whose seven 4f electrons half fill this shell, has $^8S_{7/2}$ ground state by the Hundt rule. Its behaviour is very different from that of the other rare earth ions since it has zero orbital momentum. The crystalline electric field can affect its energy levels only through high-order interactions. The initial splitting of the $^8S_{7/2}$ level is very small (generally less than 1cm^{-1}) and the spin-lattice relaxation time is so long that narrow resonance lines can be observed even at room temperature.

4.21. Theory

The theory of the Gd^{3+} ion in the ethyl sulphate has been discussed by Elliott and Stevens (E1) (1.54). They show that it should be possible to fit the results, when the axis of the external magnetic field coincides with that of the crystalline electric field, to a spin-Hamiltonian of the form

$$\mathcal{H} = g \beta H \cdot S + A_2^0 P_2^0(S) + A_4^0 P_4^0(S) + A_6^0 P_6^0(S) + A_6^6 P_6^6(S) \quad (22)$$

where each P_n^m is an operator function which has the same transformation properties as the corresponding spherical harmonic Y_n^m .

The operator equivalents for the P_n^m s are

$$P_2^0(S) \equiv 3S_z^2 - S(S+1) \quad (23a)$$

$$P_4^0(S) \equiv 35S_z^4 - [30S(S+1) - 25] S_z^2 - 6S(S+1) + 3S^2(S+1)^2 \quad (23b)$$

$$P_6^0(S) \equiv 231S_z^6 - 105S_z^4 [3S(S+1) - 7] + S_z^2 [105S^2(S+1)^2 - 525S(S+1) + 294] - 5S^3(S+1)^3 + 40S^2(S+1)^2 - 60S(S+1) \quad (23c)$$

$$P_6^6(S) \equiv 1/2 (S_+^6 + S_-^6) \quad (23d)$$

$$P_2^2(S) \equiv 1/2 (S_+^2 + S_-^2) \quad (23e)$$

When the magnetic field H is perpendicular to the symmetry axis of the crystal, it is convenient in strong fields to use the direction of H as the axis of quantization and the spin-Hamiltonian (22) becomes

$$\begin{aligned} \hat{H} = & g\beta H \cdot S_z + A_2^0 (3/2 P_2^2 - 1/2 P_2^0) \\ & + A_4^0 (35/8 P_4^4 - 5/2 P_4^2 + 3/8 P_2^0) \\ & + A_6^0 (231/32 P_6^6 - 63/16 P_6^4 + 105/32 P_6^2 - 5/16 P_6^0) \\ & + A_6^6 (1/16 P_6^0 \cos 6\phi + 15/32 P_6^2 + 3/16 P_6^4 + 1/32 P_6^0) \end{aligned} \quad (24)$$

where ϕ is the angle between the magnetic field and a side of the hexagon formed by the cross-section of the crystal normal to the crystal axis. $\cos 6\phi = -1$ when the magnetic field is parallel to one of these sides.

The diagonal terms in (24) are

$$H_0 = g\beta H \cdot S_z - 1/2 A_2^0 P_2^0 + 3/8 A_4^0 P_4^0 + 1/16 (A_6^6 \cos 6\phi - 5A_6^0) P_6^0 \quad (25)$$

It is convenient, for computational purposes, to introduce new coefficients a_n^m related to the A_n^m as follows.

$$a_2^0 = 3A_2^0, \quad a_4^0 = 60A_4^0, \quad a_6^0 = 1260A_6^0, \quad a_6^6 = 1260A_6^6 \quad (26)$$

The seven strong transitions corresponding to $\Delta M = \pm 1$ have been studied by Bleaney, et al (B9, B12) parallel and perpendicular to the crystal symmetry axis and Scovil (S2) has verified that their angular dependence

is, to a first approximation, $(3\cos\theta - 1)$ as expected for the largest term P_2^0 , since it has the same transformation properties as the spherical harmonic Y_2^0 .

4.22. Experimental Results For Dilute Gadolinium Ethyl Sulphate

Transitions corresponding to $\Delta M = \pm 1$, ± 2 and ± 3 have been observed in crystals containing gadolinium ethyl sulphate diluted one part in about two hundred in the isomorphous, diamagnetic lanthanum salt at liquid oxygen temperature using the double field modulation spectrometer (2.74). Only the $\Delta M = \pm 1$ transitions were visible with the same crystal in the video spectrometer (2.73). Theoretically, the intensity of the $\Delta M = \pm 2$ transitions should be smaller than that of the $\Delta M = \pm 1$ transitions by a factor of about $(D/H)^2$ or about 0.006. The intensity of the $\Delta M = \pm 3$ transitions should be smaller than that of the $\Delta M = \pm 2$ transitions by a similar factor. Experimentally, it has been found that the relative intensities of the $\Delta M = \pm 1$, ± 2 , and ± 3 transitions are in the ratio $10^4 : 10^2 : 1$ in good agreement with the above calculation. The most intense $\Delta M = \pm 3$ transitions occurred at signal-to-noise ratios of 10:1 confirming the improvement in the sensitivity of the double modulation spectrometer of about 1000 over the video type.

The positions of the $\Delta M = \pm 1$ transitions in the parallel and perpendicular direction to the crystal

symmetry axis have been measured at 290°K., 90°K., and 20°K. by Scovil (S2,B12). His results at 290°K. and 90°K. are compared with ours in Table VII.

The positions of the energy levels for the parallel direction as predicted by the diagonal terms in the spin-Hamiltonian (III, 22) are

$$E(-7/2) = 7/2G + 7a_2^0 + 7a_4^0 + 1a_6^0$$

$$E(-5/2) = 5/2G + 1a_2^0 - 13a_4^0 - 5a_6^0$$

$$E(-3/2) = 3/2G - 3a_2^0 - 3a_4^0 + 9a_6^0$$

$$E(-1/2) = 1/2G - 5a_2^0 + 9a_4^0 + 5a_6^0$$

$$E(+1/2) = -1/2G - 5a_2^0 + 9a_4^0 - 5a_6^0$$

$$E(+3/2) = -3/2G - 3a_2^0 + 3a_4^0 + 9a_6^0$$

$$E(+5/2) = -5/2G + 1a_2^0 - 13a_4^0 - 5a_6^0$$

$$E(+7/2) = -7/2G + 7a_2^0 + 7a_4^0 + 1a_6^0$$

where $G = g_{\parallel} \beta H$

The transitions for the parallel direction corresponding to $\Delta M = \pm 1$ are,

$$E_{-7/2 \leftrightarrow -5/2} = G + 6a_2^0 + 20a_4^0 + 6a_6^0$$

$$E_{-5/2 \leftrightarrow -3/2} = G + 4a_2^0 - 10a_4^0 - 14a_6^0$$

$$E_{-3/2 \leftrightarrow -1/2} = G + 2a_2^0 - 12a_4^0 + 14a_6^0$$

$$E_{-1/2 \leftrightarrow +1/2} = G$$

$$E_{+1/2 \leftrightarrow + 3/2} = G - 2a_2^0 + 12a_4^0 - 14a_6^0$$

$$E_{+3/2 \leftrightarrow + 5/2} = G - 4a_2^0 + 10a_4^0 + 14a_6^0$$

$$E_{+5/2 \leftrightarrow + 7/2} = G - 6a_2^0 - 20a_4^0 - 6a_6^0$$

$\Delta M = \pm 2$ are,

$$E_{-7/2 \leftrightarrow - 3/2} = 2G + 10a_2^0 + 10a_4^0 - 8a_6^0$$

$$E_{-5/2 \leftrightarrow - 1/2} = 2G + 6a_2^0 - 22a_4^0$$

$$E_{-3/2 \leftrightarrow + 1/2} = 2G + 2a_2^0 - 12a_4^0 + 14a_6^0$$

$$E_{-1/2 \leftrightarrow + 3/2} = 2G - 2a_2^0 + 12a_4^0 - 14a_6^0$$

$$E_{+1/2 \leftrightarrow + 5/2} = 2G - 6a_2^0 + 22a_4^0$$

$$E_{+3/2 \leftrightarrow + 7/2} = 2G - 10a_2^0 - 10a_4^0 + 8a_6^0$$

and for $\Delta M = \pm 3$ are

$$E_{-7/2 \leftrightarrow - 1/2} = 3G + 12a_2^0 - 2a_4^0 + 6a_6^0$$

$$E_{-5/2 \leftrightarrow + 1/2} = 3G + 6a_2^0 - 22a_4^0$$

$$E_{-3/2 \leftrightarrow + 3/2} = 3G$$

$$E_{-1/2 \leftrightarrow + 5/2} = 3G - 6a_2^0 + 22a_4^0$$

$$E_{+1/2 \leftrightarrow + 7/2} = 3G - 12a_2^0 + 2a_4^0 - 6a_6^0$$

Similarly, the positions of the energy levels for the perpendicular direction as predicted by the diagonal terms in the spin-Hamiltonian (III,22) are,

$$\begin{aligned}
E(7/2) &= 7/2G + 7/2a_2^0 - 21/8a_4^0 - 1/16(a_6^6 \cos 6\theta - 5a_6^0) \\
E(5/2) &= 5/2G + 1/2a_2^0 + 39/8a_4^0 + 5/16(a_6^6 \cos 6\theta - 5a_6^0) \\
E(3/2) &= 3/2G - 3/2a_2^0 + 9/8a_4^0 - 9/16(a_6^6 \cos 6\theta - 5a_6^0) \\
E(1/2) &= 1/2G - 5/2a_2^0 - 27/8a_4^0 + 5/16(a_6^6 \cos 6\theta - 5a_6^0) \\
E(-1/2) &= -1/2G - 5/2a_2^0 - 27/8a_4^0 + 5/16(a_6^6 \cos 6\theta - 5a_6^0) \\
E(-3/2) &= -3/2G - 3/2a_2^0 + 9/8a_4^0 - 9/16(a_6^6 \cos 6\theta - 5a_6^0) \\
E(-5/2) &= -5/2G + 1/2a_2^0 + 39/8a_4^0 + 5/16(a_6^6 \cos 6\theta - 5a_6^0) \\
E(-7/2) &= -7/2G + 7/2a_2^0 - 21/8a_4^0 - 1/16(a_6^6 \cos 6\theta - 5a_6^0)
\end{aligned}$$

where $G = g_L \beta H$.

The transitions for the perpendicular direction corresponding to $\Delta M = \pm 1$ are

$$\begin{aligned}
E_{+7/2 \leftrightarrow +5/2} &= G + 3a_2^0 - 15/2a_4^0 - 3/8(a_6^6 \cos 6\theta - 5a_6^0) \\
E_{+5/2 \leftrightarrow +3/2} &= G + 2a_2^0 + 15/4a_4^0 + 7/8(a_6^6 \cos 6\theta - 5a_6^0) \\
E_{+3/2 \leftrightarrow +1/2} &= G + 1a_2^0 + 9/2a_4^0 - 7/8(a_6^6 \cos 6\theta - 5a_6^0) \\
E_{+1/2 \leftrightarrow -1/2} &= G \\
E_{-1/2 \leftrightarrow -3/2} &= G - 1a_2^0 - 9/2a_4^0 + 7/8(a_6^6 \cos 6\theta - 5a_6^0) \\
E_{-3/2 \leftrightarrow -5/2} &= G - 2a_2^0 - 15/4a_4^0 - 7/8(a_6^6 \cos 6\theta - 5a_6^0) \\
E_{-5/2 \leftrightarrow -7/2} &= G - 3a_2^0 + 15/2a_4^0 + 3/8(a_6^6 \cos 6\theta - 5a_6^0)
\end{aligned}$$

TABLE V

Experimental Data $\Delta M = \pm 1$ Transitions For Dilute Gadolinium Ethyl Sulphate at 290°K.

H parallel to crystal symmetry axis

$\nu = 24.250$ kmcs.

T = 290°K.

Transition $\Delta M = \pm 1$	Field (gauss)	Relative Position	Separation Between Transitions
-7/2 ↔ -5/2			
-5/2 ↔ -3/2	9567.2	+863.6	392.7
-3/2 ↔ -1/2	9174.5	+470.9	470.9
-1/2 ↔ +1/2	8703.6	0	473.0
+1/2 ↔ +3/2	8230.6	-473.0	395.3
+3/2 ↔ +5/2	7835.3	-868.3	298.7
+5/2 ↔ +7/2	7536.6	-1167.0	

H perpendicular to crystal symmetry axis

$\nu = 24.250$ kmcs.

T = 290°K.

Transition $\Delta M = \pm 1$	Field (gauss)	Relative Position	Separation Between Transitions	Correction (P_2^2)	Corrected Field
+7/2 ↔ +5/2	9373.8	+686.4		-15.1	9358.7
+5/2 ↔ +3/2	9093.0	+405.6	280.8	+ 2.5	9095.5
+3/2 ↔ +1/2	8883.8	+196.4	209.2	+14.2	8898.0
+1/2 ↔ -1/2	8687.4	0	196.4	+19.0	8706.4
-1/2 ↔ -3/2	8496.0	-191.4	191.4	+16.3	8512.3
-3/2 ↔ -5/2	8301.9	-385.5	194.1	+ 5.3	8307.2
-5/2 ↔ -7/2	8061.1	-626.3	240.8	-15.4	8045.7

TABLE VI

Experimental Data $\Delta M = \pm 1$ Transitions For Dilute
Gadolinium Ethyl Sulphate at 90°K.

H parallel to crystal symmetry axis

$\nu = 24.550$ kmcs. $T = 90^\circ\text{K}.$

Transition $\Delta M = \pm 1$	Field (gauss)	Relative Position	Separation Between Transitions
$-7/2 \leftrightarrow -5/2$			
$-5/2 \leftrightarrow -3/2$			
$-3/2 \leftrightarrow -1/2$	9,319.6	+500.2	500.2
$-1/2 \leftrightarrow +1/2$	8,819.4	0	496.3
$+1/2 \leftrightarrow +3/2$	8,323.1	-496.3	417.5
$+3/2 \leftrightarrow +5/2$	7,905.6	-913.8	321.2
$+5/2 \leftrightarrow +7/2$	7,584.4	-1235.0	

H perpendicular to crystal symmetry axis

$\nu = 24.375$ kmcs. $T = 90^\circ\text{K}.$

Transition $\Delta M = \pm 1$	Field (gauss)	Relative Position	Separation Between Transitions	Correction (P_2^2)	Corrected Field
$+7/2 \leftrightarrow +5/2$	9460.9	+728.2		-16.4	9454.5
$+5/2 \leftrightarrow +3/2$	9161.1	+428.4	299.8	+ 2.7	9163.8
$+3/2 \leftrightarrow +1/2$	8940.6	+207.9	220.5	+15.4	8956.0
$+1/2 \leftrightarrow -1/2$	8732.7	0	207.9	+20.7	8753.4
$-1/2 \leftrightarrow -3/2$	8529.5	-203.2	203.2	+17.7	8547.2
$-3/2 \leftrightarrow -5/2$	8324.7	-408.0	204.8	+ 5.8	8330.5
$-5/2 \leftrightarrow -7/2$	8071.7	-661.0	253.0	-16.8	8054.9

TABLE VII

"g" Values And Splitting Parameters For Dilute Gadolinium Ethyl Sulphate From $\Delta M = \pm 1$ Transitions

	290°K.		90°K.	
	Buckmaster	Scovil(S2)	Buckmaster	Scovil
g_{\parallel}	1.9908 ± 0.001	1.992 ± 0.002	1.9880 ± 0.001	1.992 ± 0.002
g_{\perp} (uncorrected)	1.9919 ± 0.001	1.992 ± 0.002	1.9915 ± 0.001	1.992 ± 0.002
g_{\perp} (corrected P_2^2)	1.9905 ± 0.001	1.992 ± 0.002	1.9901 ± 0.001	1.992 ± 0.002
$a_{2\parallel}^0$	$+193.2 \pm 2.0$	190	$+206.2 \pm 2.0$	204.7 ± 2.0
$a_{4\parallel}^0$	-3.84 ± 0.3	-3.62	-3.98 ± 0.3	-3.96 ± 0.3
$a_{6\parallel}^0$	$+0.44 \pm 0.3$	+0.538	$+0.41 \pm 0.3$	$+0.63 \pm 0.1$
$a_{2\perp}^0$ (uncorrected)	$+193.3 \pm 2$		+204.5	
$a_{4\perp}^0$ (uncorrected)	-3.83 ± 0.3		-4.05	
$(a_6^6 \cos 6\theta - 5a_6^0)_{\perp}$ (uncorrected)	-4.92 ± 0.5		-5.58	
$a_{2\perp}^0$ (corrected P_2^2)	$+192.8 \pm 2.0$	+191	$+204.7 \pm 2.0$	
$a_{4\perp}^0$ (corrected P_2^2)	-3.98 ± 0.3	-3.73	-4.50 ± 0.3	
$(a_6^6 \cos 6\theta - 5a_6^0)_{\perp}$ (corrected P_2^2)	-4.86 ± 0.5		-6.22 ± 0.5	
$a_{6\perp}^6$ (corrected P_2^2)	$+2.7 \pm 1.0$	+2.7	4.2 ± 1.0	$+3.5 \pm 0.5$

All values of a_n^m are in units of 10^{-4} cm^{-1} .

to $\Delta M = \pm 2$ are

$$E_{+7/2 \leftrightarrow +3/2} = 2G + 5a_2^0 - 15/4a_4^0 + 1/2(a_6^6 \cos 6\theta - 5a_6^0)$$

$$E_{+5/2 \leftrightarrow +1/2} = 2G + 3a_2^0 + 33/4a_4^0$$

$$E_{+3/2 \leftrightarrow -1/2} = 2G + a_2^0 + 9/2a_4^0 - 7/8(a_6^6 \cos 6\theta - 5a_6^0)$$

$$E_{+1/2 \leftrightarrow -3/2} = 2G - a_2^0 - 9/2a_4^0 + 7/8(a_6^6 \cos 6\theta - 5a_6^0)$$

$$E_{-1/2 \leftrightarrow -5/2} = 2G - 3a_2^0 - 33/4a_4^0$$

$$E_{-3/2 \leftrightarrow -7/2} = 2G - 5a_2^0 + 15/4a_4^0 - 1/2(a_6^6 \cos 6\theta - 5a_6^0)$$

and to $\Delta M = \pm 3$ are

$$E_{+7/2 \leftrightarrow +1/2} = 3G + 6a_2^0 + 3/4a_4^0 - 3/8(a_6^6 \cos 6\theta - 5a_6^0)$$

$$E_{+5/2 \leftrightarrow -1/2} = 3G + 3a_2^0 + 33/4a_4^0$$

$$E_{+3/2 \leftrightarrow -3/2} = 3G$$

$$E_{+1/2 \leftrightarrow -5/2} = 3G - 3a_2^0 - 33/4a_4^0$$

$$E_{-1/2 \leftrightarrow -7/2} = 3G - 6a_2^0 - 3/4a_4^0 + 3/8(a_6^6 \cos 6\theta - 5a_6^0)$$

Tables V and VI give the observed positions of the $\Delta M = \pm 1$ transitions at 290°K. and 90°K. for the parallel and perpendicular directions of the magnetic field with respect to the crystal symmetry axis. Table VII compares the values of the coefficients (a_n^m) and the "g" values as calculated from the above data with those of Scovil (S2,B12). The results are in agreement within the experimental error. The value of a_6^6 has been computed

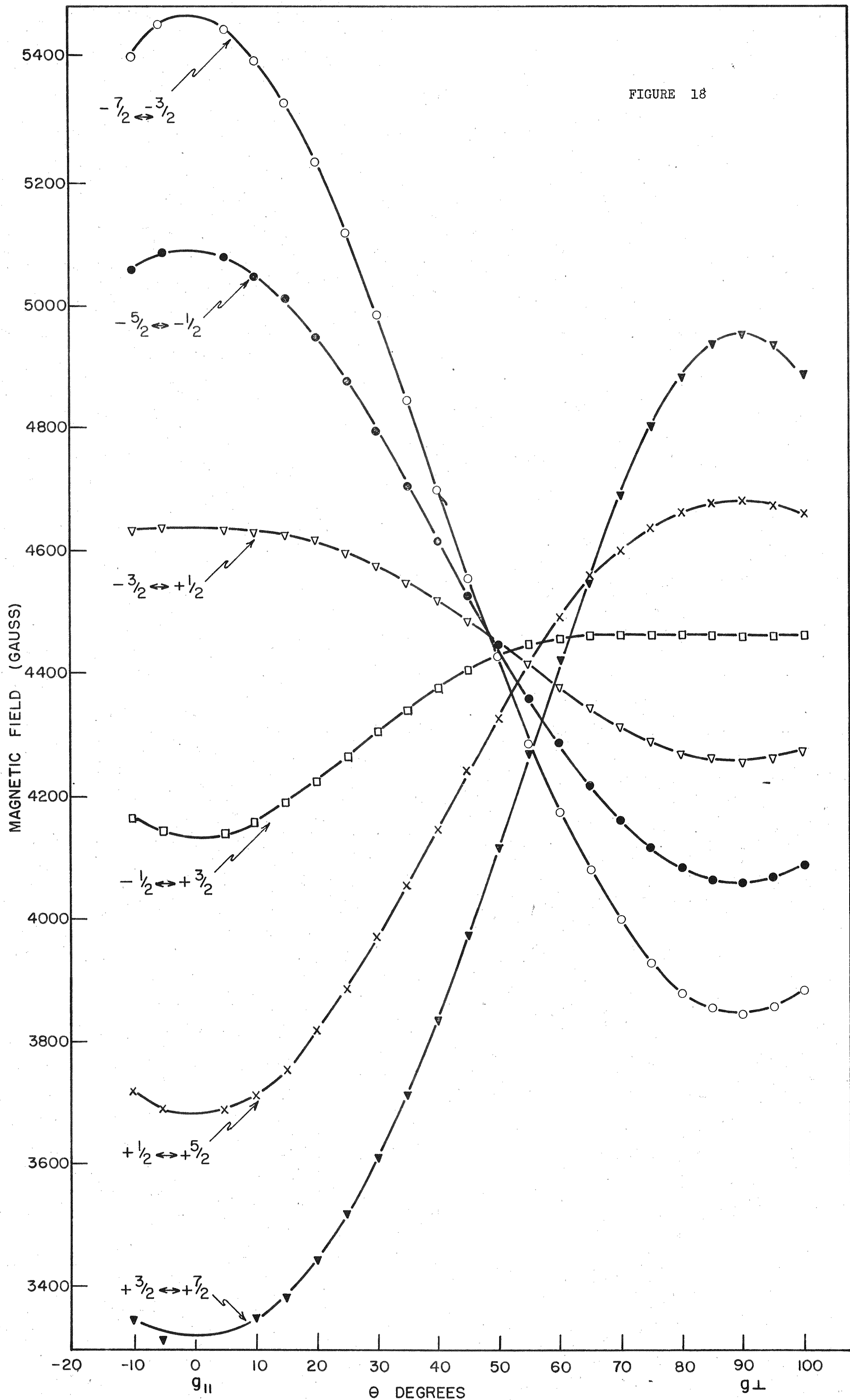


FIGURE 18

$\Delta M = \pm 2$ TRANSITION IN GADOLINIUM ETHYL SULPHATE AS A FUNCTION OF THE ANGLE WITH SYMMETRY AXIS OF THE CRYSTAL. $T = 90^\circ K.$ $\nu = 24.455$ kmcs.

TABLE VIII

Experimental Data $\Delta M = \pm 2$ Transitions For Dilute Gadolinium Ethyl Sulphate At 90°K .

H parallel to crystal symmetry axis

$\nu = 24.455$ kmcs.

$T = 90^\circ\text{K}$.

Transition $\Delta M = \pm 2$	Field (gauss)	Relative Position (Mean=4388)	Separation Between Transitions
$-7/2 \leftrightarrow -3/2$	5473	+1085	378
$-5/2 \leftrightarrow -1/2$	5095	+ 707	459
$-3/2 \leftrightarrow +1/2$	4636	+ 248	504
$-1/2 \leftrightarrow +3/2$	4132	- 256	450
$+1/2 \leftrightarrow +5/2$	3682	- 706	374
$+3/2 \leftrightarrow +7/2$	3308	-1080	

H perpendicular to crystal symmetry axis

$\nu = 24.455$ kmcs.

$T = 90^\circ\text{K}$.

Transition $\Delta M = \pm 2$	Field (gauss)	Relative Position (Mean=4388)	Separation Between Transitions	Correction (P_2^2)	Corrected Field
$+7/2 \leftrightarrow +3/2$	4954.5	+566.5	275.3	-14.8	4939.7
$+5/2 \leftrightarrow +1/2$	4679.2	+291.2	218.4	+15.3	4694.5
$+3/2 \leftrightarrow -1/2$	4460.8	+ 72.8	202.8	+34.8	4495.6
$+1/2 \leftrightarrow -3/2$	4258.0	-130.0	198.0	+39.0	4297.0
$-1/2 \leftrightarrow -5/2$	4060.0	-328.0	214.0	+26.0	4086.0
$-3/2 \leftrightarrow -7/2$	3846.0	-542.0		- 7.6	3834.4

TABLE IX

$\Delta M = \pm 2$ Transitions For Dilute
Gadolinium Ethyl Sulphate

$T = 90^\circ\text{K.}$ $\nu = 24.455$ kmcs. Error: ± 0.5 gauss

Angle θ°	$+\frac{7}{2} \leftrightarrow +\frac{3}{2}$	$+\frac{5}{2} \leftrightarrow +\frac{1}{2}$	$+\frac{3}{2} \leftrightarrow -\frac{1}{2}$	$+\frac{1}{2} \leftrightarrow -\frac{3}{2}$	$-\frac{1}{2} \leftrightarrow -\frac{5}{2}$	$-\frac{3}{2} \leftrightarrow -\frac{7}{2}$
-10	3,342.9	3,721.3	4,167.4	4,634.4	5,060.1	5,405.5
-5	3,309.7	3,693.1	4,146.0	4,638.2	5,089.4	5,456.5
g_H 0						
5		3,686.4	4,138.8	4,634.5	5,079.2	5,447.6
10	3,346.6	3,711.3	4,159.6	4,627.9	5,049.8	5,402.2
15	3,383.1	3,752.1	4,192.1	4,625.9	5,013.5	5,331.5
20	3,445.5	3,817.1	4,225.6	4,622.3	4,951.7	5,235.8
25	3,518.8	3,885.8	4,263.8	4,595.5	4,879.0	5,119.5
30	3,611.1	3,967.6	4,304.2	4,577.0	4,796.4	4,985.1
35	3,716.3	4,054.2	4,341.5	4,550.1	4,707.3	4,845.1
40	3,836.9	4,146.9	4,376.5	4,520.1	4,617.4	4,699.8
45	3,972.4	4,240.3	4,404.7	4,485.6	4,527.2	4,556.3
50	4,115.9	4,328.8	4,427.4	4,449.1	4,449.1	4,427.4
55	4,271.2	4,415.4	4,446.0	4,415.4	4,357.0	4,286.9
60	4,420.4	4,489.6	4,454.3	4,377.3	4,285.0	4,175.9
65	4,559.9	4,549.9	4,461.2	4,344.8	4,217.8	4,080.9
70	4,692.0	4,600.7	4,462.9	4,315.1	4,161.2	3,997.7
75	4,803.5	4,636.8	4,462.7	4,290.2	4,117.3	3,927.8
80	4,882.7	4,662.8	4,463.1	4,272.0	4,084.5	3,880.6
85	4,976.9	4,675.7	4,461.4	4,261.0	4,065.6	3,854.0
g_L 90	4,954.5	4,679.2	4,460.8	4,258.0	4,060.0	3,846.0
95	4,932.3	4,672.8	4,461.5	4,262.2	4,067.5	3,857.5
100	4,885.5	4,660.1	4,462.4	4,273.3	4,087.3	3,883.2

TABLE X

Values of g_{\parallel} And g_{\perp} And Splitting Parameters For Dilute Gadolinium Ethyl Sulphate From $\Delta M = \pm 2$ Transitions At 90°K.

Transition	Mean Field	g_{\parallel}
$\pm 7/2 \leftrightarrow \pm 3/2$	4,390.5	1.9897
$\pm 5/2 \leftrightarrow \pm 1/2$	4,3855	1,9906
$\pm 3/2 \leftrightarrow \mp 1/2$	4,384.0	1.9926

$$v = 24.455 \text{ kmcs.}$$

$$\text{Mean Value } g_{\parallel} = 1.9910 \pm 0.001$$

$$\text{Mean Value } g_{\parallel} \text{ Excluding } \pm 3/2 \leftrightarrow \mp 1/2 \text{ Transitions } 1.9902$$

Transition	Mean Field	g_{\perp}	Correction Factor (P_2^2)	Corrected Field	g_{\perp} Corrected
$\pm 7/2 \leftrightarrow \pm 3/2$	4400.3	1.9853	-11.2	4389.1	1.9903
$\pm 5/2 \leftrightarrow \pm 1/2$	4369.6	1.9992	+20.7	4390.3	1.9898
$\pm 3/2 \leftrightarrow \mp 1/2$	4309.4	2.0278	+36.9	4346.3	2.0100
Mean Value g_{\perp} Uncorrected		2.0041	± 0.001	Corrected	1.9967 ± 0.001

$$\text{Mean Value } g_{\perp} \text{ Corrected Excluding } \pm 3/2 \leftrightarrow \mp 1/2$$

$$\text{Transitions } 1.9901 \pm 0.001$$

	a_2^0	a_4^0	a_6^0	$(a_6^0 \cos 6\theta - 5a_6^0)$	a_6^6
Parallel	205.4 \pm 2.0	-3.61 \pm 0.2	0.98 \pm 0.3		
Perpendicular	204.7 \pm 2.0	-4.22 \pm 0.2		-4.59 \pm 0.3	
Perpendicular (Corrected)	202.2 \pm 2.0	-4.79 \pm 0.2		-5.10 \pm 0.3	

All values of a_n^m 's are in units of 10^{-4} cm^{-1} .

using $\phi = 90^\circ$ where $\cos 6\phi = -1$. However this value is subject to considerable error.

Table VIII summarizes the experimental data for the $\Delta M = \pm 2$ transitions for dilute gadolinium ethyl sulphate when the magnetic field is parallel and perpendicular to the symmetry axis of the crystal. The field values for the parallel direction are estimated from the rotational data given in Table IX and shown graphically in Figure 18, since the intensities of the $\Delta M = \pm 2$ transitions falls to zero as is expected from the fact that the $\Delta M = \pm 1$ transitions in this direction are symmetrical within experimental error as predicted by the diagonal terms in the spin-Hamiltonian (III,22). The behavior of the $\pm 7/2 \leftrightarrow \pm 3/2$ and $\pm 5/2 \leftrightarrow \pm 1/2$ transitions is in close agreement with that expected theoretically from the largest off-diagonal term P_2^2 in the spin-Hamiltonian. The behavior of the $\pm 3/2 \leftrightarrow \mp 1/2$ transitions is most clearly seen in Figure 18. No satisfactory explanation can be offered. Approximate calculations based on the second largest off-diagonal term P_4^2 do not improve the situation. The fact that these transitions occur at lower magnetic fields than expected indicates that the zero field splitting is greater than predicted by the present spin-Hamiltonian however this is not in agreement with the results of Bleaney, Scovil and Trenam (B11). The most striking features of the behavior of these transitions are their complete lack of symmetry with respect to each other. That each transition is relatively independent of the orientation

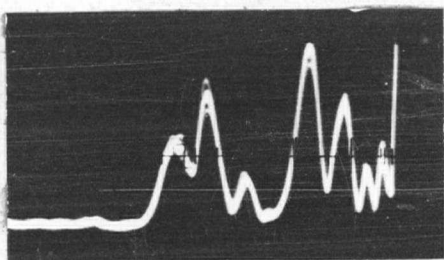


PLATE IXa
 Structure on $\Delta M = \pm 1$
 transitions due to
 lattice defects and pairs
 of Gd^{3+} ions

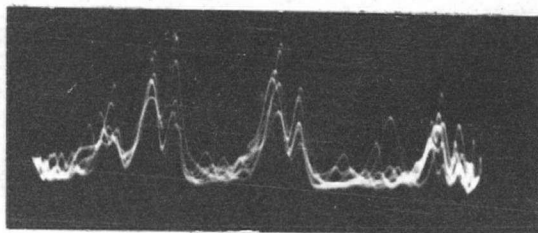


PLATE IXb
 4 of 5 $\Delta M = \pm 3$ transitions
 near crossover point

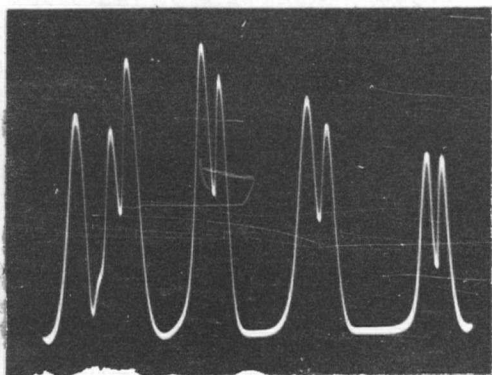


PLATE IXc
 $\Delta M = \pm 2$ transitions near
 crossover point

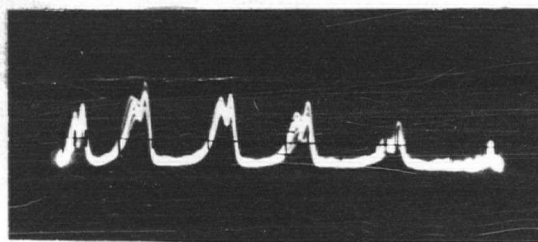


PLATE IXd
 6 $\Delta M = \pm 2$ transitions at
 magnetic field orientation
 where total separation is
 500 gauss

TABLE XI

$\Delta M = \pm 3$ Transitions For Dilute Gadolinium Ethyl Sulphate
As A Function Of Angle Between Direction Of Magnetic Field
And Crystal Symmetry Axis At 5° Intervals

$\nu = 24.52$ kmcs. $T = 90^\circ\text{K}$.

θ°	$-7/2 \leftrightarrow -1/2$	$-5/2 \leftrightarrow +1/2$	$-3/2 \leftrightarrow +3/2$	$-1/2 \leftrightarrow +5/2$	$+1/2 \leftrightarrow +7/2$
-10					
-6.5°					
-5					
0					
5					
10					
11		3372.7			
15					
16			2989.75		
20		3329.15	2975.97		
21		3319.66	2977.01		
25		3287.09	2986.43		
26		3277.44	2987.54	2634.47	
30	3413.19	3238.40	3001.65		
31	3227.74	3227.74	3003.37	2694.68	
35	3295.42	3178.99	3006.13	2742.02	
36	3269.14	3171.59	3009.95	2761.69	
40	3176.10	3119.78	3010.33	2811.02	
41	3149.28	3109.40	3011.91	2820.23	
45	3057.78	3057.78	3012.52	2866.60	
46	3045.87	3045.87	3008.25	2881.24	
50	2924.64	2992.81	3000.11	2924.64	
51	2934.72	2983.23	2997.49	2934.72	2735.04
55	2844.67	2933.54	2984.99	2984.99	2844.67
56	2830.17	2925.47	2985.75	2985.75	2830.17
60	2755.94	2872.75	2991.25	3011.11	2971.25
61	2744.07	2865.01	2968.80	3023.08	2968.80
65	2675.37	2820.92	2948.34	3049.09	3049.09
66	2666.98	2811.14	2947.69	3055.28	3079.98
70	2614.28	2778.29	2931.48	3075.68	3155.37
71	2600.07	2772.51	2927.63	3077.80	3172.76
75	2565.23	2744.77	2914.08	3087.74	3239.14
76	2557.41	2741.50	2910.07	3091.68	3253.13
80	2527.52	2722.22	2901.58	3096.11	3303.12
81	2514.91	2717.28	2899.99	3099.04	3314.84
85	2505.18	2700.54	2893.26	3099.42	3346.60
86		2697.41	2890.76	3100.07	3354.08
89	2500.03	2692.38	2889.59	3100.00	3363.66
91					
95	2502.47	2697.02	2893.43	3101.02	3356.60
96					
100	2522.03	2709.44	2901.03	3097.61	3319.47

TABLE XII.

Values of g_{\parallel} and g_{\perp} And Splitting Parameters For Dilute Gadolinium Ethyl Sulphate From $\Delta M = \pm 3$ Transitions At 90°K .

No value for g_{\parallel} can be calculated as no transitions were observed in this direction or sufficiently near to permit accurate extrapolation.

<u>Transition</u>	<u>Mean Field</u>	<u>g_{\perp}</u>	<u>Correction Factor P_2^2</u>	<u>Corrected Field</u>	<u>g_{\perp} Corrected</u>
$\pm 7/2 \leftrightarrow \pm 1/2$	2932	1.9915	$\cdot 4$	2936	1.9886
$\pm 5/2 \leftrightarrow \mp 1/2$	2897	2.0156	$+41$	2938	1.9875
$+3/2 \leftrightarrow -3/2$	2893	2.0184	$+54$	2947	1.9814

Mean Value g_{\perp} Uncorrected 2.0085 ± 0.001 Corrected 1.9858 ± 0.001

Mean Value g_{\perp} Corrected Excluding $+3/2 \leftrightarrow -3/2$ Transition 1.9881 ± 0.001

It is not possible to calculate the values of the a_n^m 's from the experimental data for the $\Delta M = \pm 3$ transitions since there are not a sufficient number of linearly independent equations. We, therefore, calculate the positions from the data for the $\Delta M = \pm 1$ and ± 2 transitions and compare with the observed positions

$$\nu = 24.520 \text{ kmcs. } T = 90^{\circ}\text{K.}$$

<u>Transition $\Delta M = \pm 3$</u>	<u>Measured Position</u>	<u>Correction Factor P_2^2</u>	<u>Corrected Field</u>	<u>Calculated $\Delta M = \pm 1$ Data</u>	<u>Calculated $\Delta M = \pm 2$ Data</u>
$+7/2 \leftrightarrow +1/2$	3364	$+ 1.7$	3366	3374	3369
$+5/2 \leftrightarrow -1/2$	3101	$+38.8$	3140	3141	3138
$+3/2 \leftrightarrow -3/2$	2893	$+53.8$	2947	2934	2934
$+1/2 \leftrightarrow -5/2$	2692	$+44.2$	2736	2727	2731
$-1/2 \leftrightarrow -7/2$	2500	$+ 6.8$	2507	2494	2500

of the magnetic field with the symmetry axis over a region of about 20° is the only similarity. The values of the splitting parameters given in Table X and calculated from the $\Delta M = \pm 2$ transitions are considered to be less reliable than those from the $\Delta M = \pm 1$ transitions because of the above-noted behavior of the $\pm 3/2 \leftrightarrow \mp 1/2$ transitions! This is most clearly seen in the "g" values where they appreciably increase the value of the mean for the three pairs of transitions. Consequently, the g values have also been calculated excluding the data for the $\pm 3/2 \leftrightarrow \mp 1/2$ transitions and these values are shown in Table X.

Table XI summarizes the experimental data for the $\Delta M = \pm 3$ transitions for dilute gadolinium ethyl sulphate and Table XII gives the values of the splitting parameters and spectroscopic splitting factors for the parallel and perpendicular directions. This data shows that the effects observed in the $\Delta M = \pm 2$ transitions are further magnified in the $\Delta M = \pm 3$ transitions. Unfortunately, not all of these transitions could be observed at each orientation so the data is incomplete and the calculations correspondingly less reliable. The relative intensities of the $\Delta M = \pm 3$ are quite asymmetric; the low field transition is always the weakest and the two high field transitions strongest. A similar effect was also observed in the $\Delta M = \pm 2$ transitions, however it was not so marked. The behavior of those transitions between the $+ 1/2$ and $- 1/2$ levels and the $+ 3/2 \leftrightarrow - 3/2$ transition as a

function of the angle between the direction of the static magnetic field and the symmetry axis of the crystal are very asymmetric. Consequently, the data in Table XII is not reliable although it has also been corrected for the effect of the largest off-diagonal term in the spin-Hamiltonian $P_2^2(S_z)$. Following a suggestion of Stevens (Bleaney, Scovill and Trenam B12), an attempt has been made to consider the effect of a term of the form $P_3^3(S_z)$ theoretically; however, this was unsuccessful. Moreover, the form of $P_3^3(S_z)$, when considered as a Legendre polynomial, is not correct to aid in symmetrizing the rotational data and hence is not considered as the correct interpretation of the asymmetry of these results.

4.3 Line Width Of Praseodymium Ethyl Sulphate At 4.2°K.

The paramagnetic resonance spectrum of Pr^{3+} [$4f^2; 3H_4$] has been studied at liquid hydrogen temperatures in the dilute ethyl sulphate by Bleaney and Scovill (B10) and at liquid helium temperatures in the dilute magnesium nitrate by Cooke and Duffus (C4). The experimental results have been fitted to the spin-Hamiltonian given in 1.55 (I,17) where a theoretical discussion is included which considers the asymmetry of the line shape.

Dilute praseodymium ethyl sulphate has been examined at liquid helium temperatures. Six asymmetric resonances were observed with maximum intensity when the direction of the static and r.f. magnetic fields were parallel in confirmation

of the above results. It was observed that the line width is considerably narrower at liquid helium temperature than reported by Bleaney and Scovil (B10). At 4.2°K. it has been found to be 35 ± 5 gauss whereas they report 200 gauss at 20°K. indicating that spin-lattice broadening must occur at the latter temperature. Unfortunately, the electromagnet broke down at this stage of the measurements and the experiment was stopped. It has not been repeated and thus no values for the splitting parameters are reported.

4.4. Excited State In Dysprosium Ethyl Sulphate At 4.2°K.

Recently, Bleaney (B13) has reported the detection of an excited state in dysprosium ethyl sulphate Dy^{3+} $[4f^9; 8H_{15/2}]$ at liquid hydrogen temperatures which disappeared above 20°K. due to spin-lattice broadening and below 13°K due to suggested depopulation of the excited level. Theoretically, the ground state is probably $J_z = \mp 9/2$ ($g_{\parallel} = 12$; susceptibility measurement $g_{\parallel} = 11.3 \pm 0.1$) with admixtures of $J_z = \pm 3/2$ and $\pm 15/2$ giving no allowed transitions. The observed "g" values for the excited level are $g_{\parallel} = 5.80 \pm 0.02$ and $g_{\perp} = 8.40 \pm 0.2$. They are in good agreement with the hypothesis that this level is an admixture of $J_z = \pm 7/2$ and $\mp 5/2$.

Dilute dysprosium ethyl sulphate has been examined at liquid helium temperatures. A weak resonance with a signal-to-noise ratio of 20:1 has been observed with the

double field modulation spectrometer (2.74) with $g_{\parallel} = 5.85 \pm 0.05$ in agreement with the above measurements. The weak intensity observed supports the depopulation hypothesis. Unfortunately, this experiment was also halted due to electromagnet troubles and consequently g_{\perp} was not measured.

4.5. Future Experiments

The apparatus has only recently been brought into successful operation at liquid helium temperatures. Unfortunately, whenever successful experiments have been underway at this temperature, the electromagnet gave trouble due to an intermittent short to one of the cooling coils. Consequently, although resonances have been observed in a number of substances very few measurements have been made and those reported in 4.3 and 4.4 have not been confirmed.

It would be worthwhile to study the intensity of the excited state transition in dysprosium ethyl sulphate as a function of the temperature in the liquid helium temperature range to carefully check the depopulation hypothesis.

An experiment has been planned to attempt to measure the spin and magnetic moment of the promethium isotope Pm^{3+} $147 [4f^4; 5I_4]$ in the magnesium nitrate crystal environment. This ion should exhibit the same resonance properties as praseodymium which has been discussed in 1.55. The ground state is not Kramer's degenerate however distortions from

trigonal symmetry due to the Jahn-Teller effect should produce transitions with maximum intensity when the direction of the r.f. magnetic is parallel to that of the static magnetic field. No naturally occurring isotopes of promethium are known. Isotope 147, which has a half-life of about four years, can be produced artificially by neutron bombardment of Nd 146 or as a fission product. Its spin is not known; however, from the nuclear shell model, it is probably $5/2$ with $7/2$ another possibility. Initially, 3 millicuries of promethium 147 should weigh $0(10^{-7})$ grams. It should be possible to obtain a lanthanum magnesium nitrate crystal containing $0(10^{-8})$ grams of promethium. Our spectrometer (2.74) possesses sufficient sensitivity to observe a resonance from such a crystal. Some lanthanum magnesium nitrate crystals have been prepared from atomic weight purity lanthanum to reduce the possibility of rare earth contamination. One of these crystals will be examined in the spectrometer at liquid helium temperatures to identify any such contamination and then redissolved in a solution of promethium nitrate and the mixed crystal grown. The promethium has been obtained from Atomic Energy of Canada Ltd. as a fission product to reduce the possibility of other rare earth ions being present. The spectroscopic analysis shows a maximum of 2.4 mg./ml. iron, 0.8 mg./ml. aluminum, 0.5 mg./ml. lead, 0.5 mg./ml. nickel and 1.5 mg./ml. cobalt.

If this experiment is successful, there are a number of other radioactive rare earth isotopes which have shorter half-lives which could be examined. The determination of their nuclear spins and magnetic moments would be most useful. It was for such experiments as these that the high sensitivity spectrometer was developed.

Resonances from impurities in semi-conductor crystals have been observed recently. It is hoped that resonances can be observed in some silicon crystals that have been doped with antimony, indium, arsenic, gallium and boron. Some preliminary theoretical work by Dr. J. M. Daniels supports this hope.

...

REFERENCES

- A1 Abragam, A. and Pryce, M.H.E., Proc. Roy. Soc., A, 205
135 (1951)
- B1 Bagguley, D.M.S. and Griffiths, J.H.E., Proc. Phys. Soc.
(London). A, 65, 594 (1952)
- B2 Beringer, R. and Castle, Jr. J.G., Phys. Rev. 78,
581 (1950)
- B3 Beringer, R. and Castle, Jr. J.G., Phys. Rev. 81,
82 (1951)
- B4 Bethe, H.A. Ann. Phys. 3, 133 (1929)
- B5 Bijl, D. Ph.D. Thesis, Leiden, (1950)
- B6 Bleaney, B. Rept. Prog. Phys. 11, 178 (1946-47)
- B7 Bleaney, B. Phil. Mag. 42, 441 (1951)
- B8 Bleaney, B. Physica 17, 175 (1951)
- B9 Bleaney, B., Elliott, R.J., Scovil, H.E.D. and
Trenam, R.S. Phil. Mag. 42, 1062 (1951)
- B10 Bleaney, B., and Scovil, H.E.D. Phil. Mag. 43, 999
(1952)
- B11 Bleaney, B. and Stevens, K.W.H., Rept. Prog. Phys. 16,
108 (1953)
- B12 Bleaney, B., Scovil, H.E.D., and Trenam, R.S., Proc. Roy.
Soc. A., 223, 15 (1954)
- B13 Bleaney, B., Private communication
- B14 Bleaney, B., Llewellyn, P.M., Pryce, M.H.E., and Hall, G.R.,
Phil. Mag. 45, 991 (1954)
- B15 Bloembergen, N., Nuclear Magnetic Relaxation, (Nijhoff.,
The Hague, 1948)
- B16 Bloembergen, N., Purcell, E.M., and Pound, R.V.,
Phys. Rev. 73, 679 (1948)
- B17 Bowers, K.D., and Owens, J., Rept. Prog. Phys. 18,
304 (1955)

- C1 Chance, B., Hughes, V., MacNichol, E.F., Sayre, D.,
Williams, F.C., Waveforms, Vol. 19 (1949)
- C2 Collins, T.L., Ph.D. Thesis, University of British
Columbia (1950) unpublished
- C3 Cooke, A., Rept. Prog. Phys. 13, 276 (1950)
- C4 Cooke, A.H. and Duffus, H.J., Proc. Roy. Soc. A, 229,
407 (1955)
- C5 Cooke, A.H., Duffus, H.J., and Wolf, N.P., Phil. Mag.
44, 623 (1953)
- E1 Elliott, R.J. and Stevens, K.W.H., Proc. Roy. Soc. A, 215,
437 (1952)
- E2 Elliott, R.J. and Stevens, K.W.H., Proc. Roy. Soc., A,
218, 553 (1953)
- E3 Elliott, R.J. and Stevens, K.W.H., Proc. Roy. Soc., A,
219, 387 (1953)
- E4 Elmore, W.C. and Sands, M., Electronics, Div. V, Vol. 1.
National Nuclear Energy Series, (McGraw-Hill,
New York, 1949)
- G1 Gordy, W., Rev. Mod. Phys., 20, 668 (1948)
- H1 Hartz, T.R. and Van der Ziel, A., Phys. Rev. 78, 473,
(1950)
- H2 Hellwege, A.M. and Hellwege, K.H., Z. Phys. 135,
92 (1953)
- H3 Hershberger, W.D., Journ. App. Phys. 19, 411 (1948)
- H4 Hirshon, J.M. and Fraenkel, G.K., R.S.I. 26, 34 (1955)
- H5 Holden, A.N., Kittel, C., Merritt, R.F., and Yager, W.A.,
Phys. Rev. 77, 147 (1950)
- J1 Jahn, H.A., and Teller, E., Proc. Roy. Soc. A, 161, 220
(1937)
- J2 Jantsch, Y., Z. anorg. Chem. 76, 303 (1912)
- J3 Judd, B.R., Proc. Roy. Soc. A, 227, 552 (1955)
- K1 Karplus, R., Phys. Rev. 73, 1027 (1948)
- K2 Ketelaar, J.A.A., Physica 4, 619 (1937)

- K3 Knight, W.D., and Pound, R.V., R.S.I. 21, 219 (1950)
- K4 Knipp, J.K., Kuper, J.B.H. and Hamilton, D.R.
Klystrons and Microwave Tubes. Vol. 7. M.I.T.
Radiation Lab. Series (McGraw-Hill, New York, 1948)
- K5 Knoebel, H.W., and Hahn, E.E., R.S.I. 22, 904 (1951)
- E1 Lawson, J.S. and Uhlenbeck, G.E., Threshold Signals
Vol. 24. M.I.T. Radiation Lab. Series (McGraw-Hill,
New York, 1948)
- L2 Levy, S.I., The Rare Earths - Their Occurrence, Chemistry
Technology, (Edward Arnold and Co., London, 1924)
- M1 Mann, C.R., Ph.D. Thesis, University of British Columbia,
(1952) unpublished
- M2 McLay, D., Ph.D. Thesis, University of British Columbia,
(1956) unpublished
- M3 Montgomery, C.A., Technique of Microwave Measurements
Vol. 11, M.I.T. Radiation Lab. Series (McGraw-Hill,
New York, 1947)
- P1 Penney, W.Y. and Schlapp, R., Phys. Rev. 41, 194 (1932)
- P2 Penrose, R.P., Nature, Lond., 163, 992 (1949)
- P3 Pound, R.V., R.S.I. 17, 490 (1946). Also Chapter 2 (M3)
- P4 Pryce, M.H.L. and Stevens, K.W.H., Proc. Phys. Soc. A,
63, 36 (1950)
- P5 Pryce, M.H.L., Phys. Rev. 80, 1107 (1950)
- R1 Rose, M.E., Phys. Rev. 53, 715 (1938)
- R2 Rundle, H.N., M.A. Thesis, University of British Colum-
bia (1955) unpublished
- S1 Schneider, E.E. and England, T.S., Physica 17, 221 (1951)
- S2 Scovil, H.E.D., D.Phil. Thesis, Oxford (1951).
unpublished
- S3 Scovil, H.E.D. and Buckmaster, H.A. (to be published)
- S4 Smaller, B., Phys. Rev. 83, 812 (1951)
- S5 Smaller, B. and Yasaitis, E.L., R.S.I. 24, 991 (1953)
- S6 Smythe, W.R., Static and Dynamic Electricity, 2nd ed.,
p. 417, No. 15 (McGraw-Hill, New York, 1950)

- S7 Stevens, K.W.H., Proc. Phys. Soc. A, 65, 209 (1952)
- S8 Stevens, K.W.H., Proc. Roy. Soc. A, 214, 237 (1952)
- S9 Stevens, K.W.H., Proc. Roy. Soc. A, 219, 542 (1953)
- S10 Strandberg, M.W.P., Microwave Spectroscopy (Methuen, London, 1954)
- T1 Thomas, H.A., Driscoll, R.E., and Hipple, J.A., Phys. Rev. 78, 787 (1950)
- T2 Torrey, H.C. and Whitmer, C.A., Crystal Rectifiers, Vol. 15, M.I.T. Radiation Lab. Series (McGraw-Hill, New York, 1948)
- T3 Townes, C.H. and Turkevitch, J., Phys. Rev. 77, 148 (1950)
- T4 Trenam, R.S., Proc. Phys. Soc. A, 66, 118 (1953)
- V1 Valley, Jr., G.E. and Wallman, H., Vacuum Tube Amplifiers, Vol. 18, M.I.T. Radiation Lab. Series (McGraw-Hill, New York, 1948)
- V2 Van der Ziel, A., Noise (Prentice-Hall, New York, 1954)
- V3 Van Vleck, J.H., The Theory of Electric and Magnetic Susceptibilities, (Oxford University Press, London 1932)
- V4 Van Vleck, J.H., Phys. Rev. 74, 1168 (1948)
- V5 Van Voorhis, S.N., Microwave Receivers. Vol. 23, M.I.T. Radiation Lab. Series (McGraw-Hill, New York, 1948)
- V6 Vickery, R.C., Chemistry of the Lanthanons, (Butterworths Scientific Publications, London, 1953)
- W1 Weidner, R.S., and Whitmer, C.A., R.S.I. 23, 75 (1952)
- Y1 Yost, D.M., Russel, Jr. H., and Garner, C.S., The Rare-Earth Elements and Their Compounds (John Wiley and Sons., Inc., New York, 1947)
- Z1 Zavoisky, E., J. Phys. U.S.S.R. 9; 211 (1945)

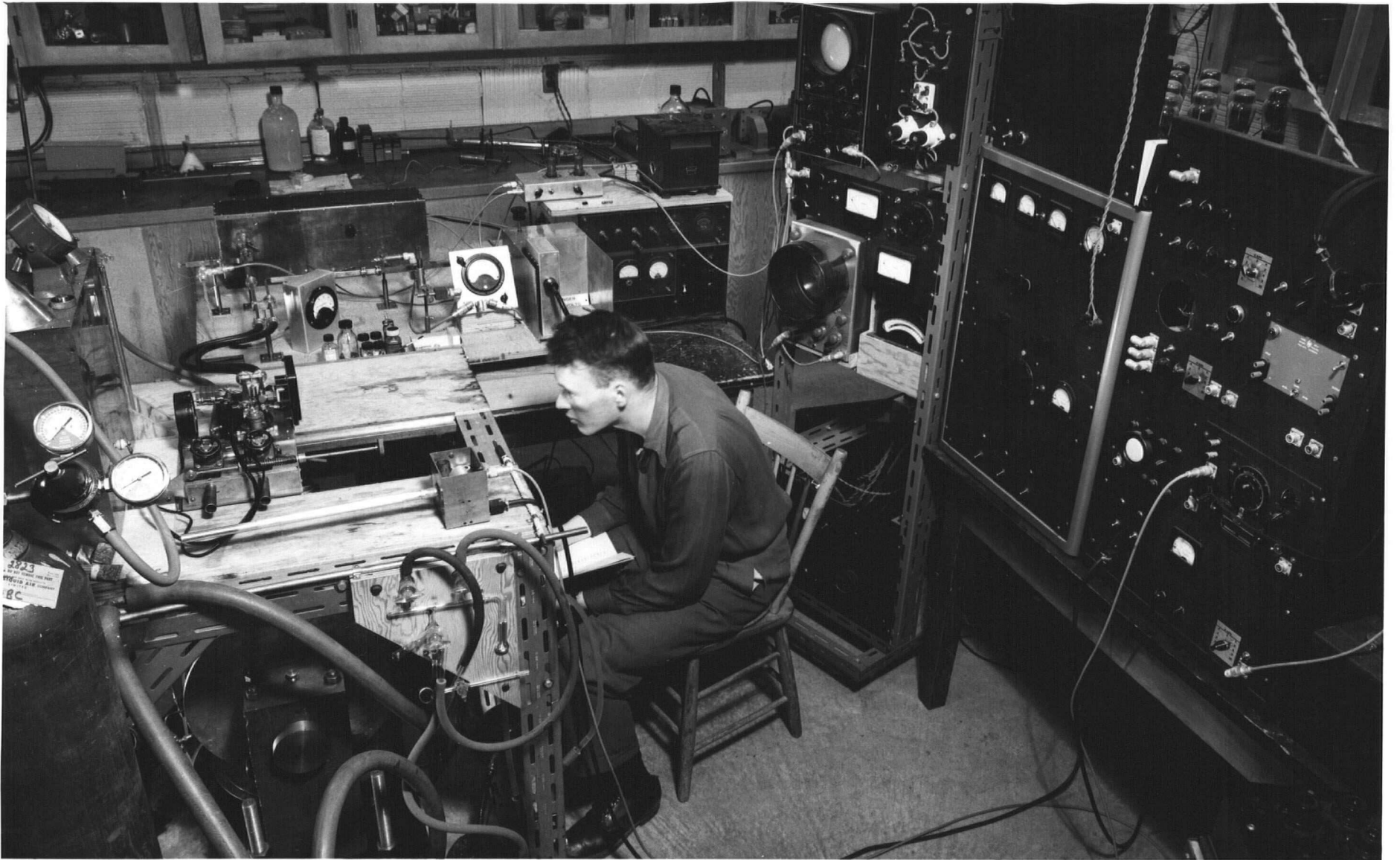
APPENDIX I

The electronic circuit diagrams of the components of the single and double modulation paramagnetic resonance spectrometers described in this thesis are collected together in this appendix together with several photographs of the equipment.

	Page
Plate X A general view of the apparatus	109
Plate XI A general view of the microwave bench showing the 462.5 kcs. amplifier with the shielding cover plates removed	110
Figure 19 Circuit diagram for proton resonance detector r.f. head	111
Figure 20 Circuit diagram for proton resonance low noise audio amplifier and cathode follower	112
Figure 21 Circuit diagram for proton resonance r.f. level V.T.V.M. and oscillator level control and stabilizer	113
Figure 22 500 kcs. class C. power amplifier and variable load matching section to split cavity	114
Figure 23 Oscillator and buffer for high frequency modulation	115
Figure 24 Circuit diagram for 500 kcs. transmitter power supply	116

	Page
Figure 25 Circuit diagram of video amplifier . . .	117
Figure 26 Circuit diagram of calibrator	118
Figure 27 Circuit diagram of typical low ripple, high regulation power supply	119
Figure 28 Circuit diagram for high voltage reg- ulated klystron power supply	120
Figure 29 Block diagram of magnet field control circuit	121
Figure 30 Circuit diagram of current controls for electromagnet and 60 cps. field modulation	122

....



facing page 109

PLATE X · GENERAL VIEW OF EXPERIMENTAL APPARATUS

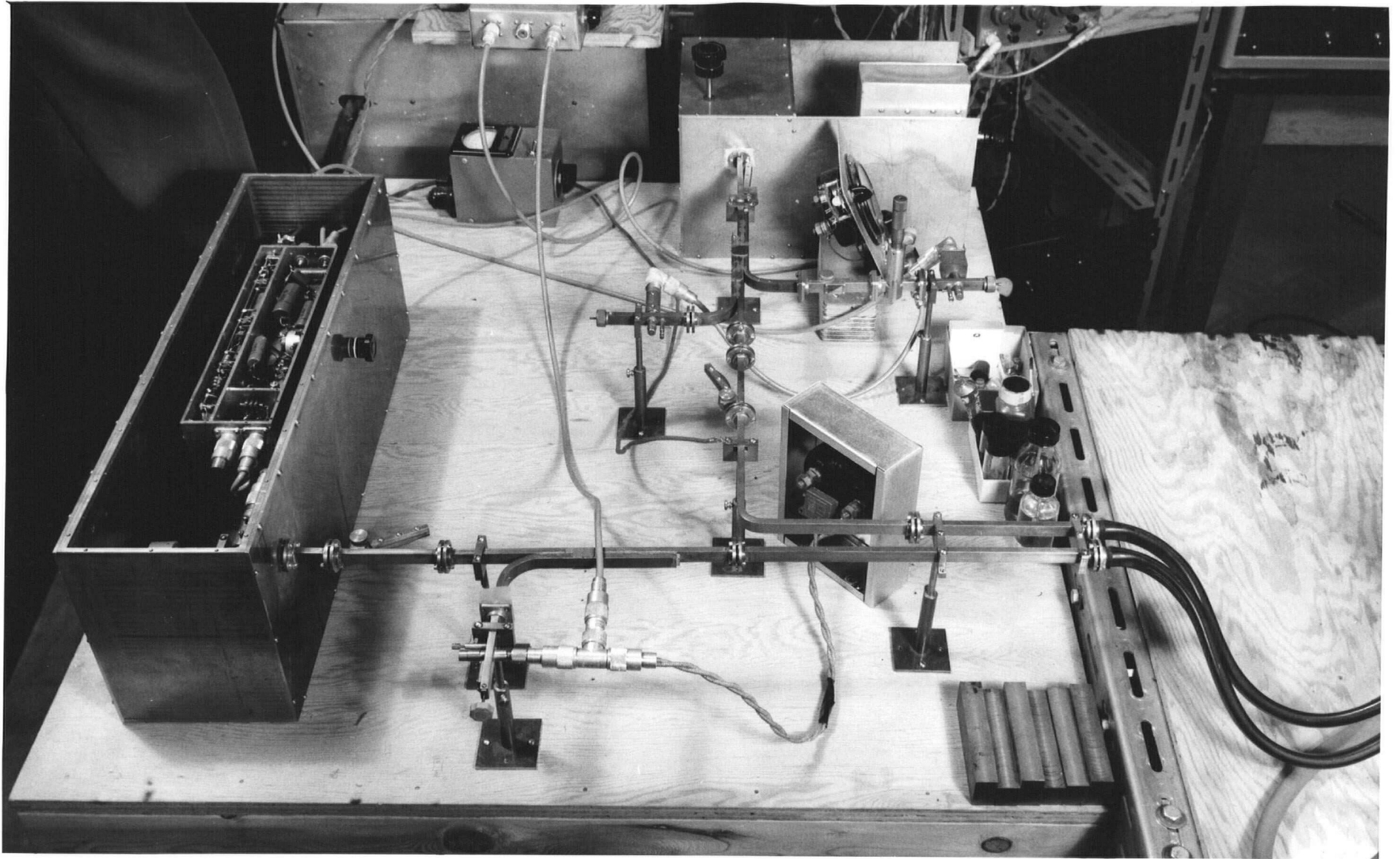
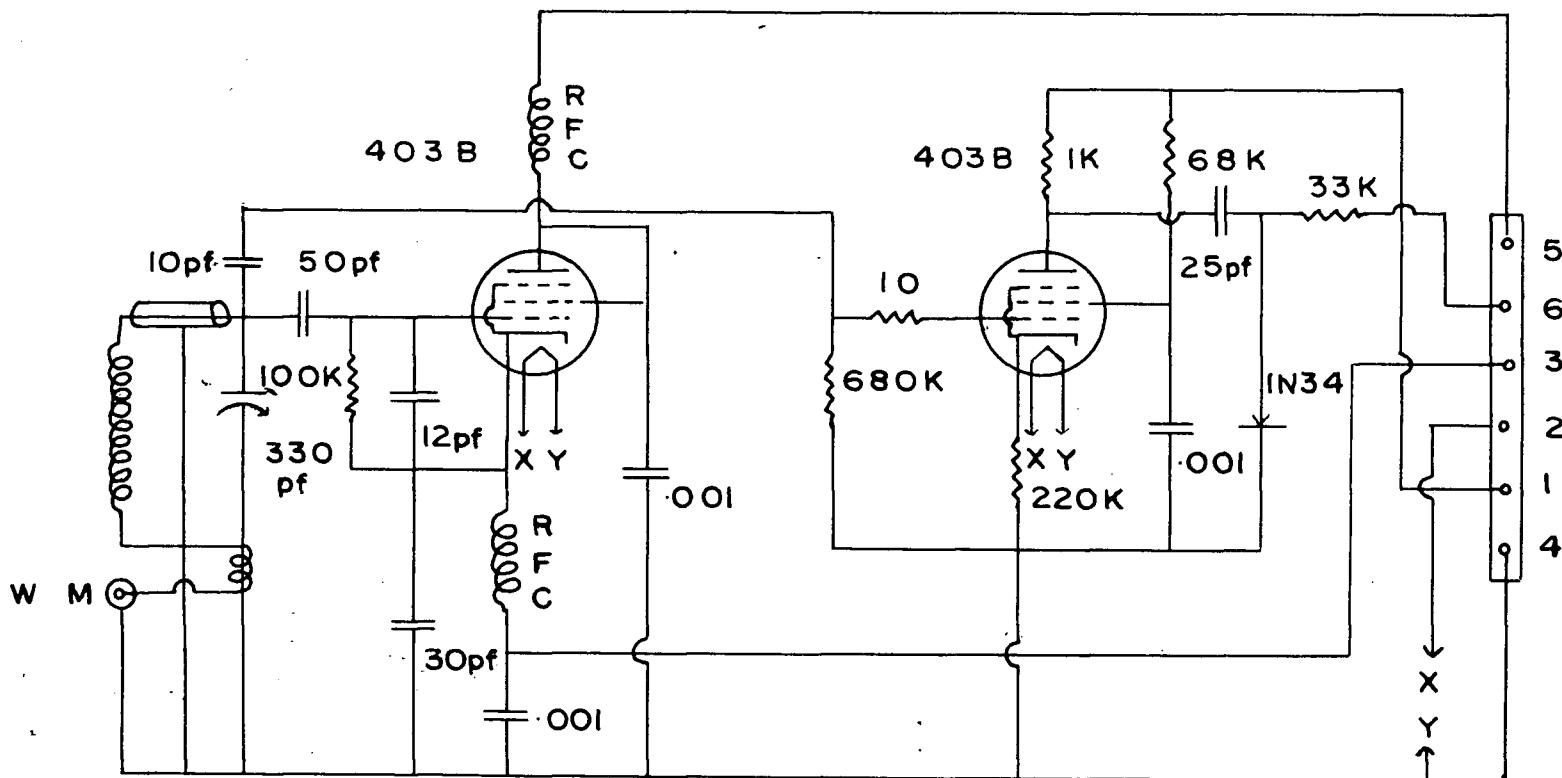


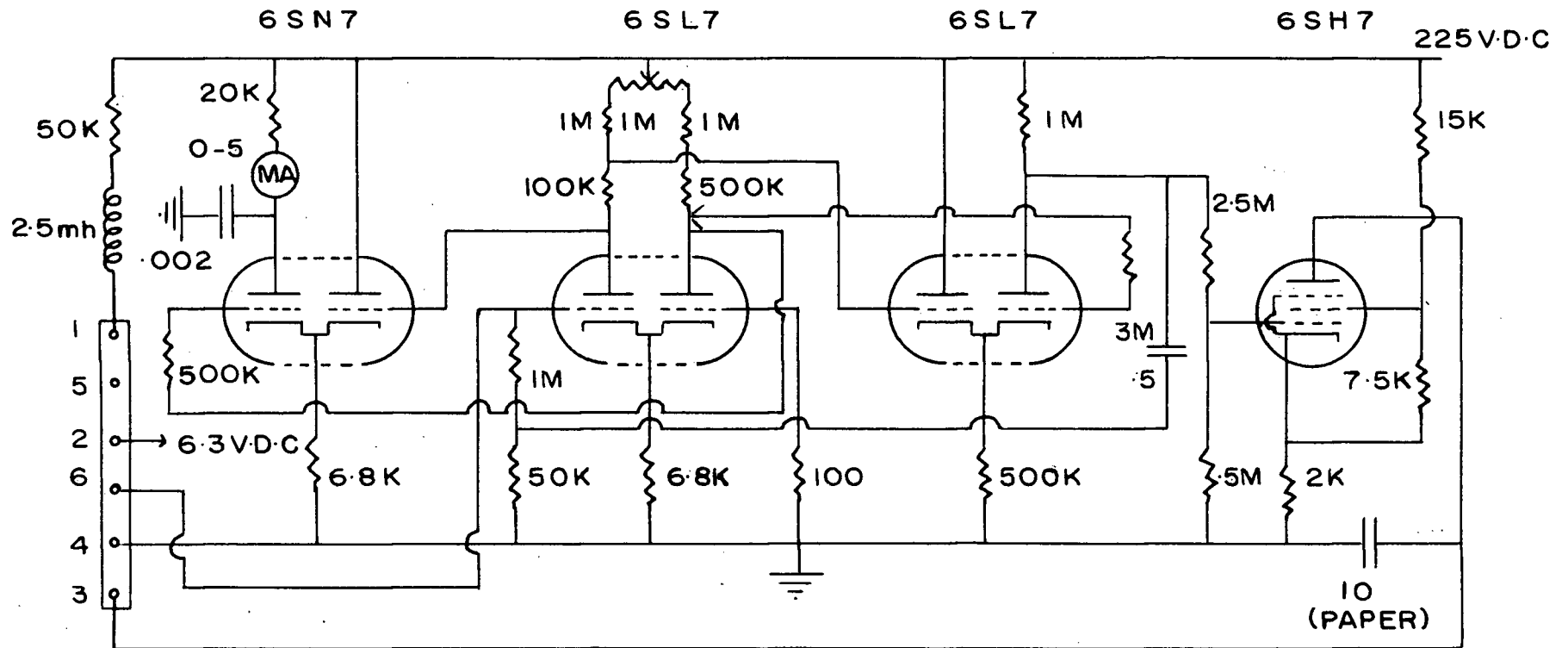
PLATE XI · GENERAL VIEW OF MICROWAVE BENCH ·

FIGURE 19



CIRCUIT DIAGRAM FOR PROTON RESONANCE
DETECTOR R.F. HEAD

FIGURE 21



CIRCUIT DIAGRAM FOR PROTON RESONANCE
R.F. LEVEL V.T.V.M AND OSCILLATION LEVEL
CONTROL AND STABILIZER

FIGURE 22

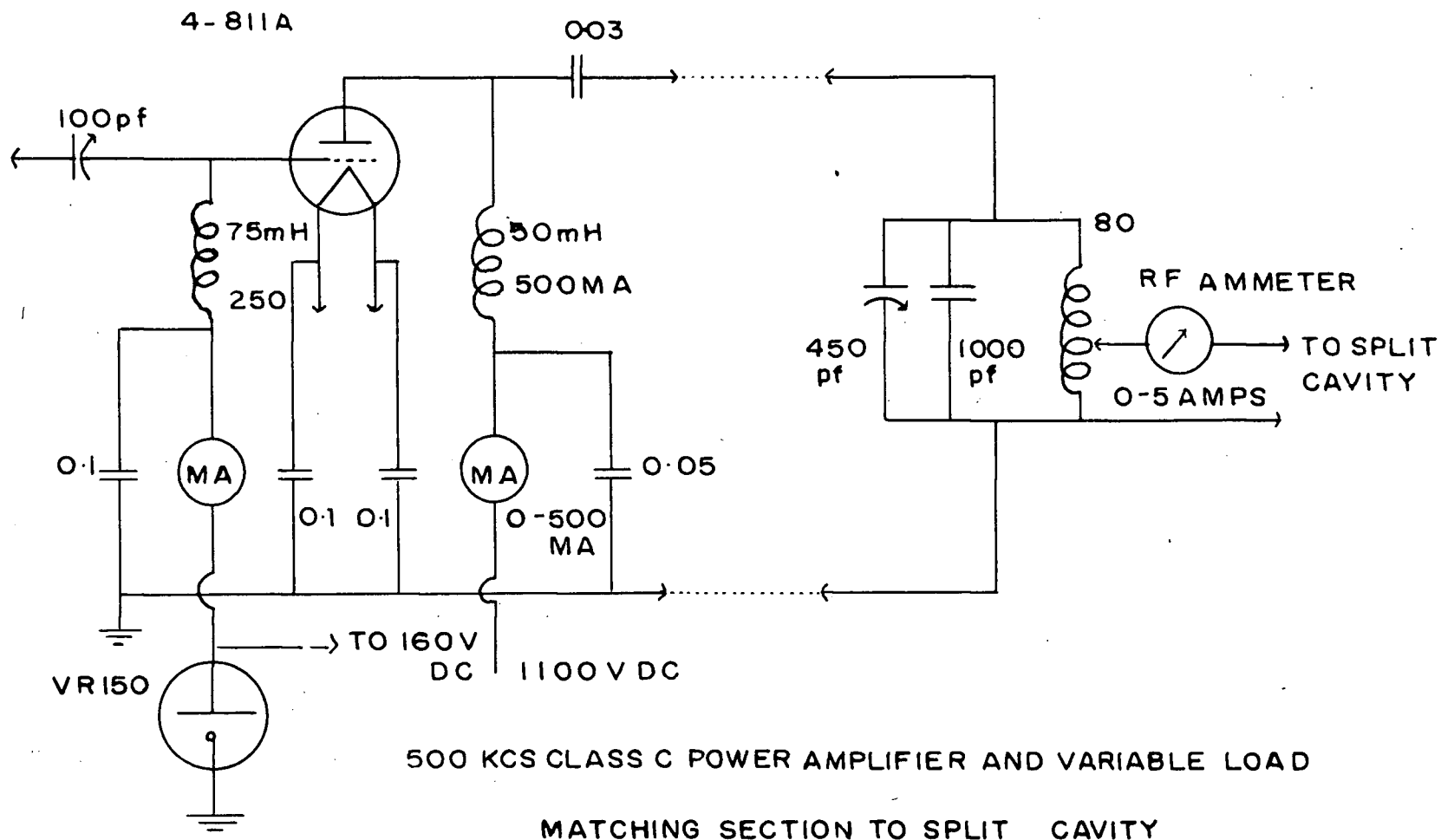
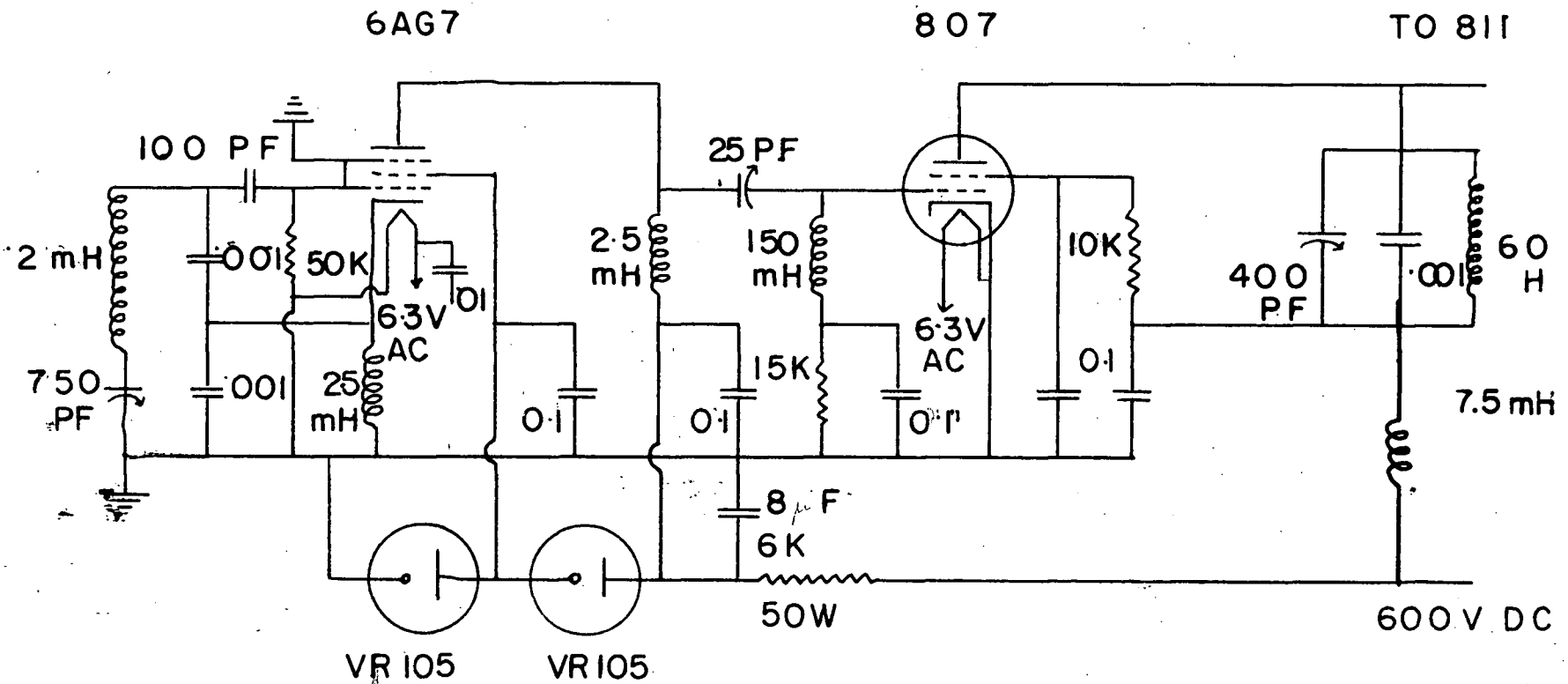
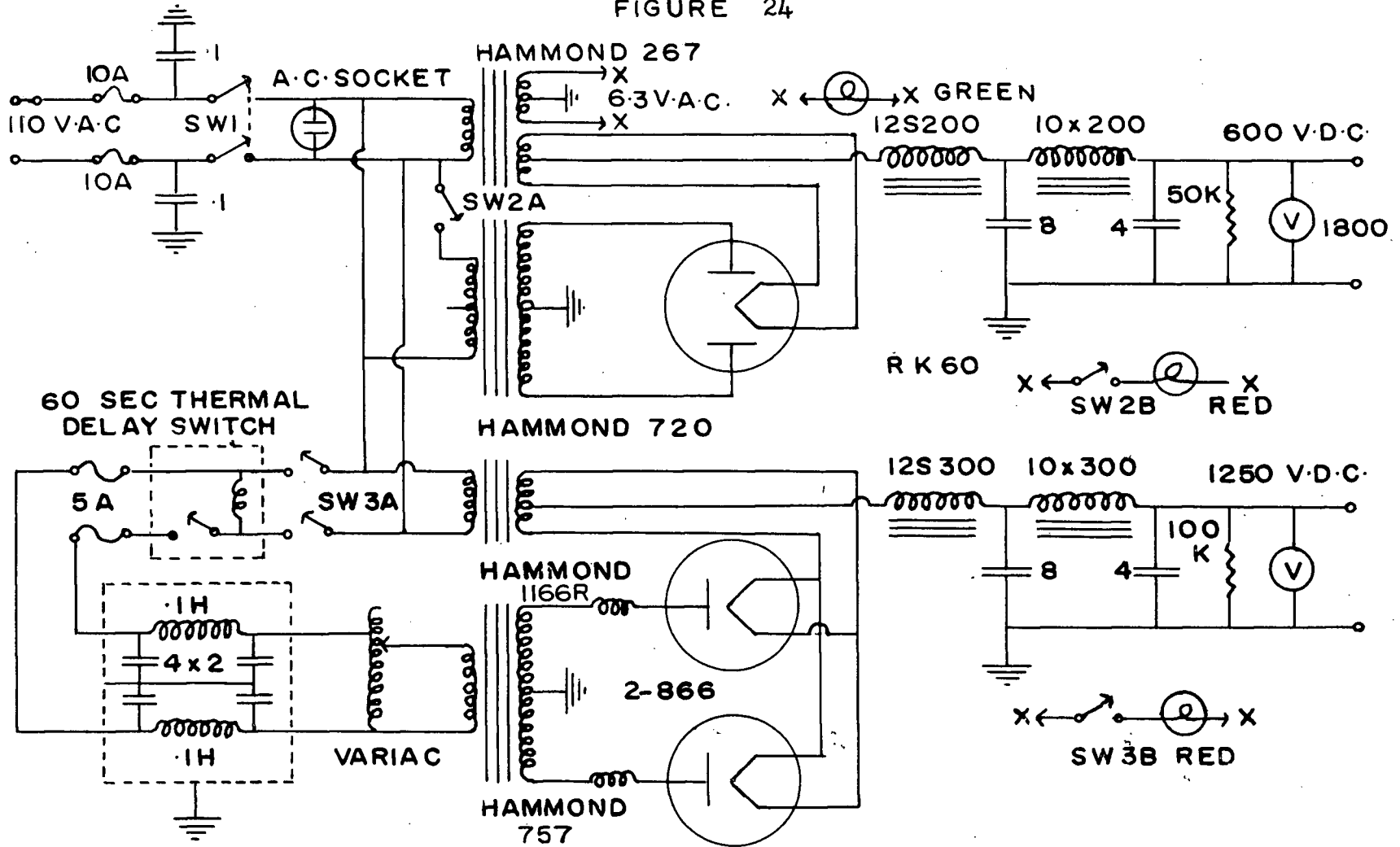


FIGURE 23



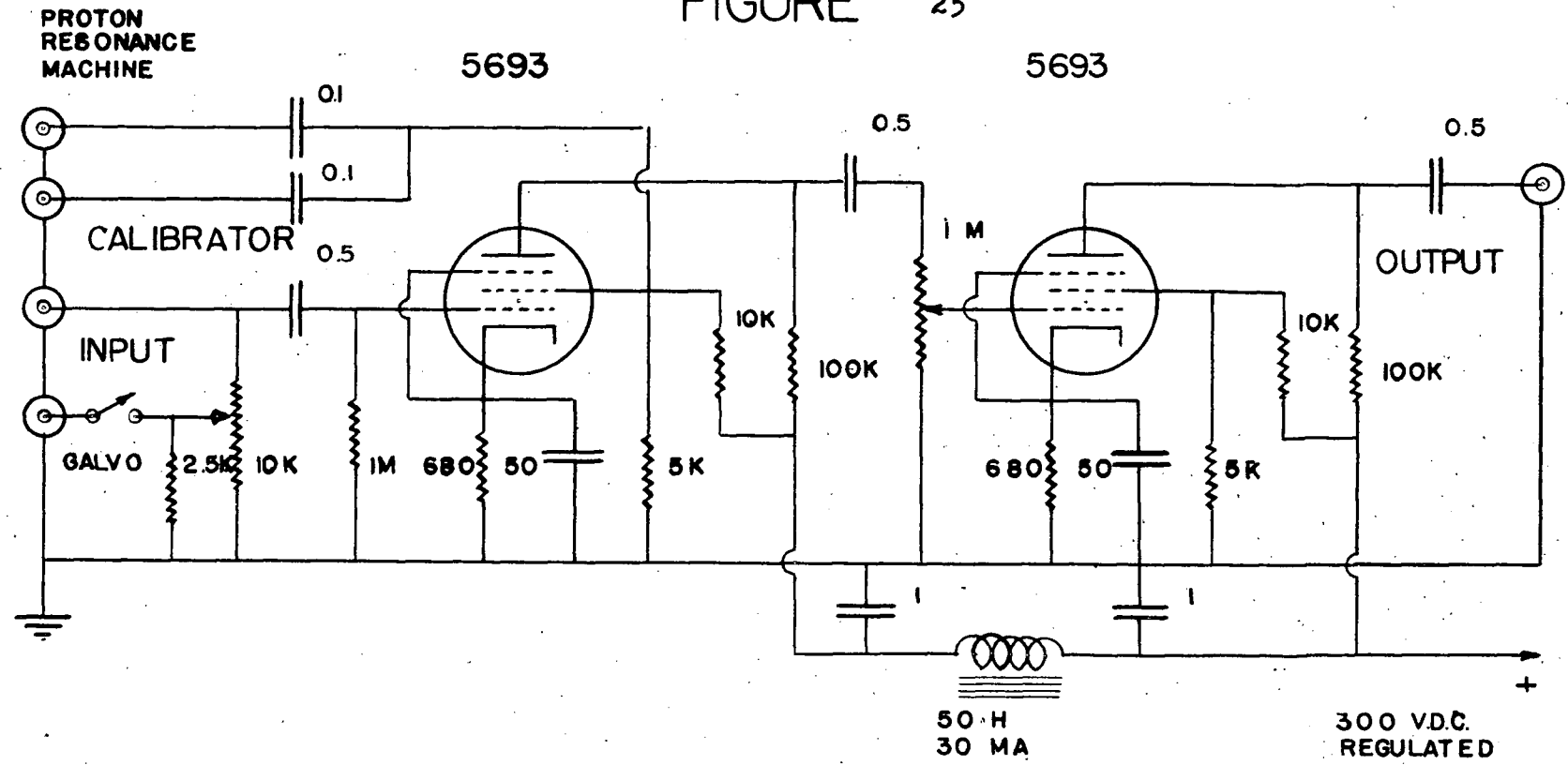
OSCILLATOR AND BUFFER FOR
HIGH FREQUENCY MODULATION
FREQUENCY RANGE 100 KCS.-1MCS.

FIGURE 24



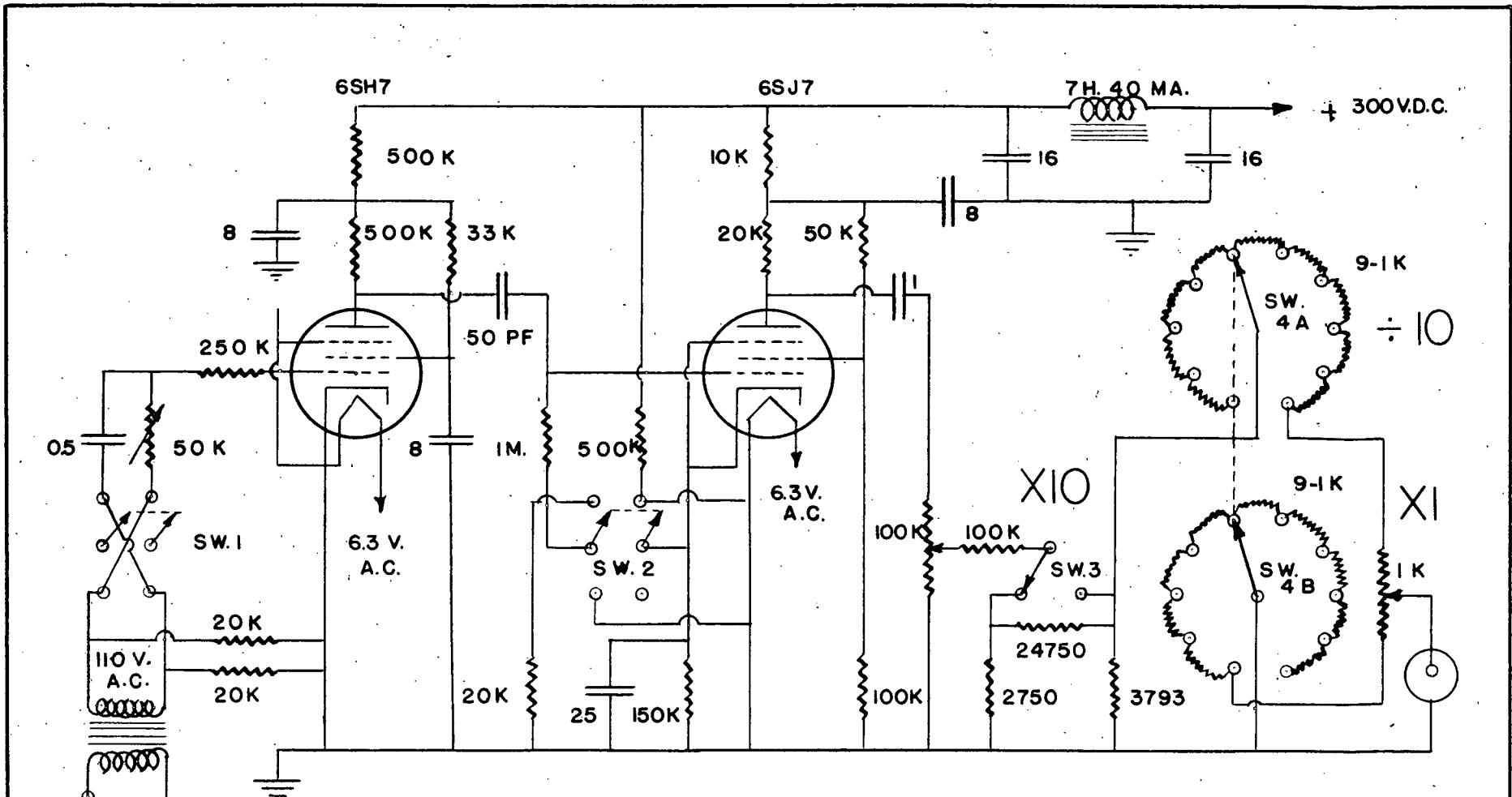
CIRCUIT DIAGRAM FOR 500 KCS TRANSMITTER POWER SUPPLY

FIGURE 25



6.3 V.D.C. FILAMENT SUPPLY PIN 2 GROUNDED

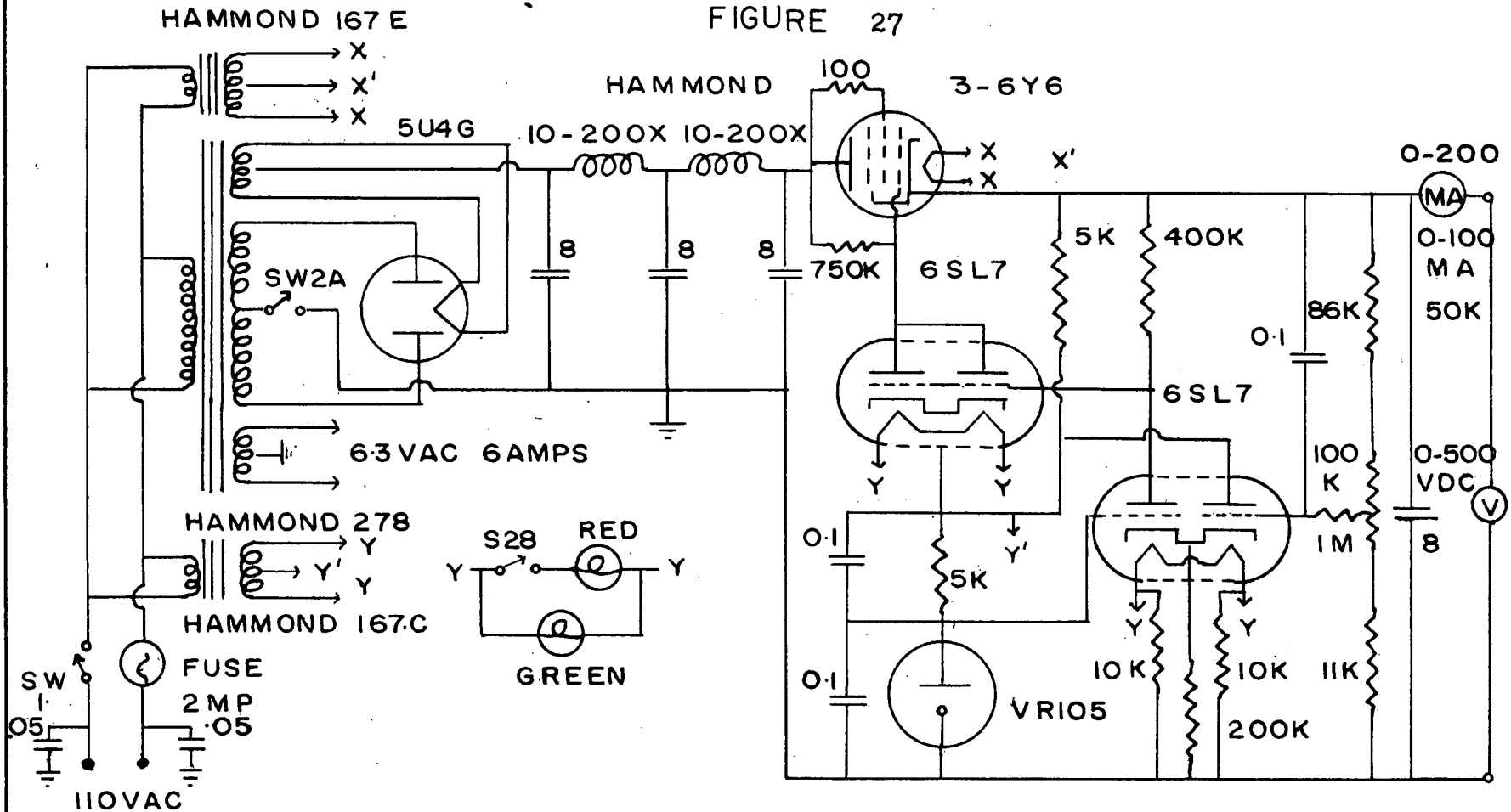
VIDEO AMPLIFIER



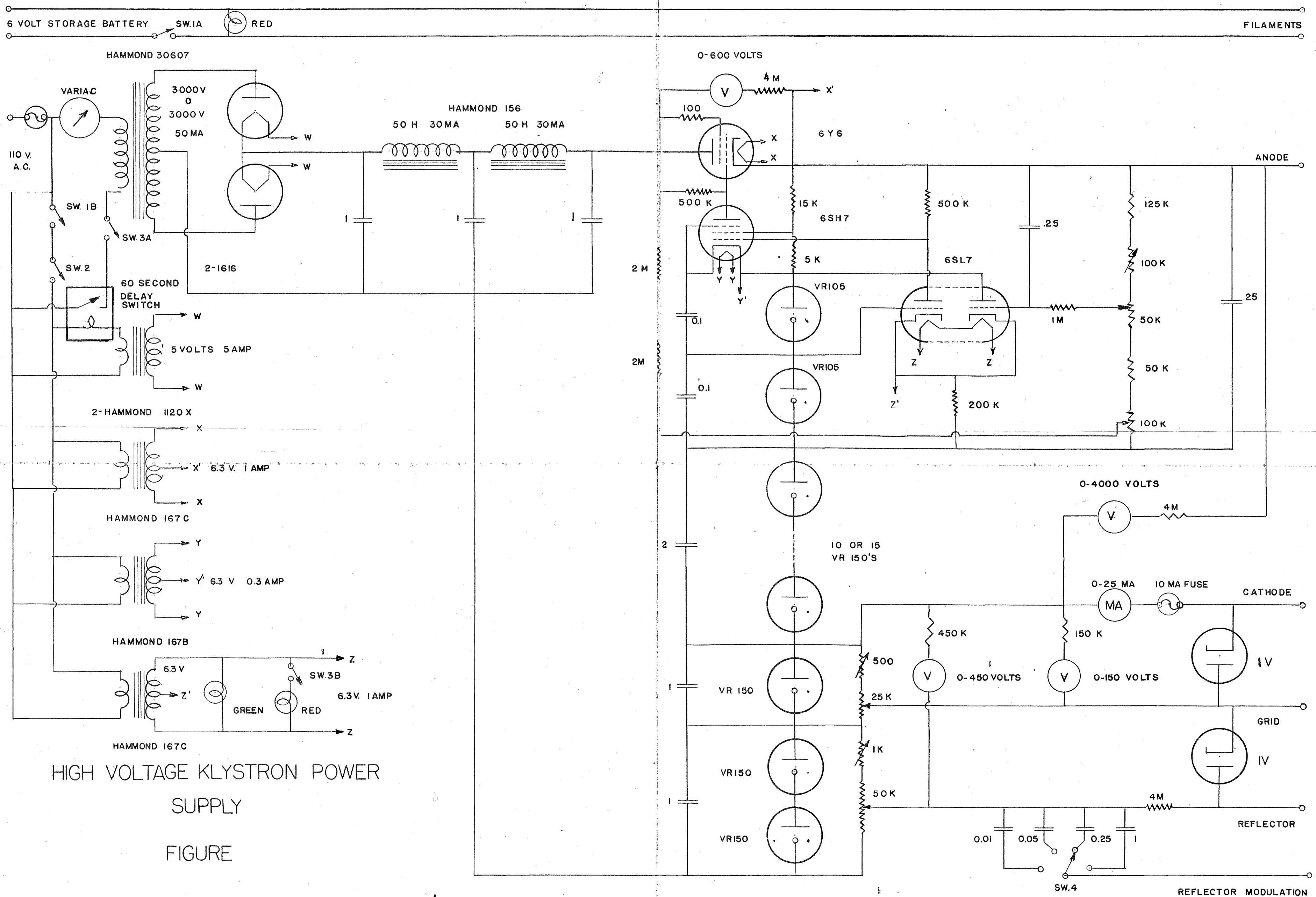
CALIBRATOR

FIGURE 26

FIGURE 27



TYPICAL LOW RIPPLE, HIGH REGULATION POWER SUPPLY
250-375 VOLTS D.C. 25-200 MA



HIGH VOLTAGE KLYSTRON POWER SUPPLY
 SUPPLY
 FIGURE

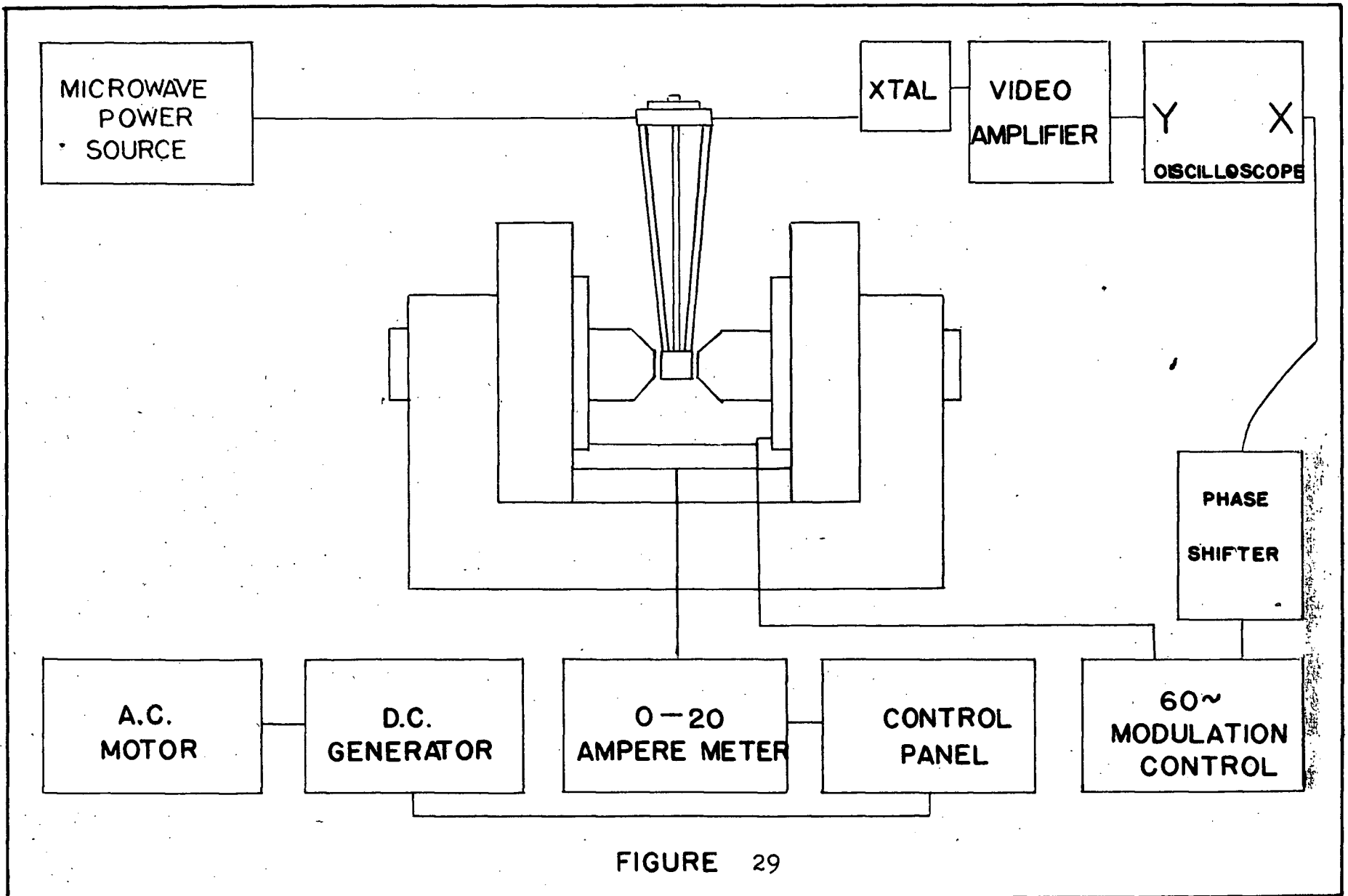
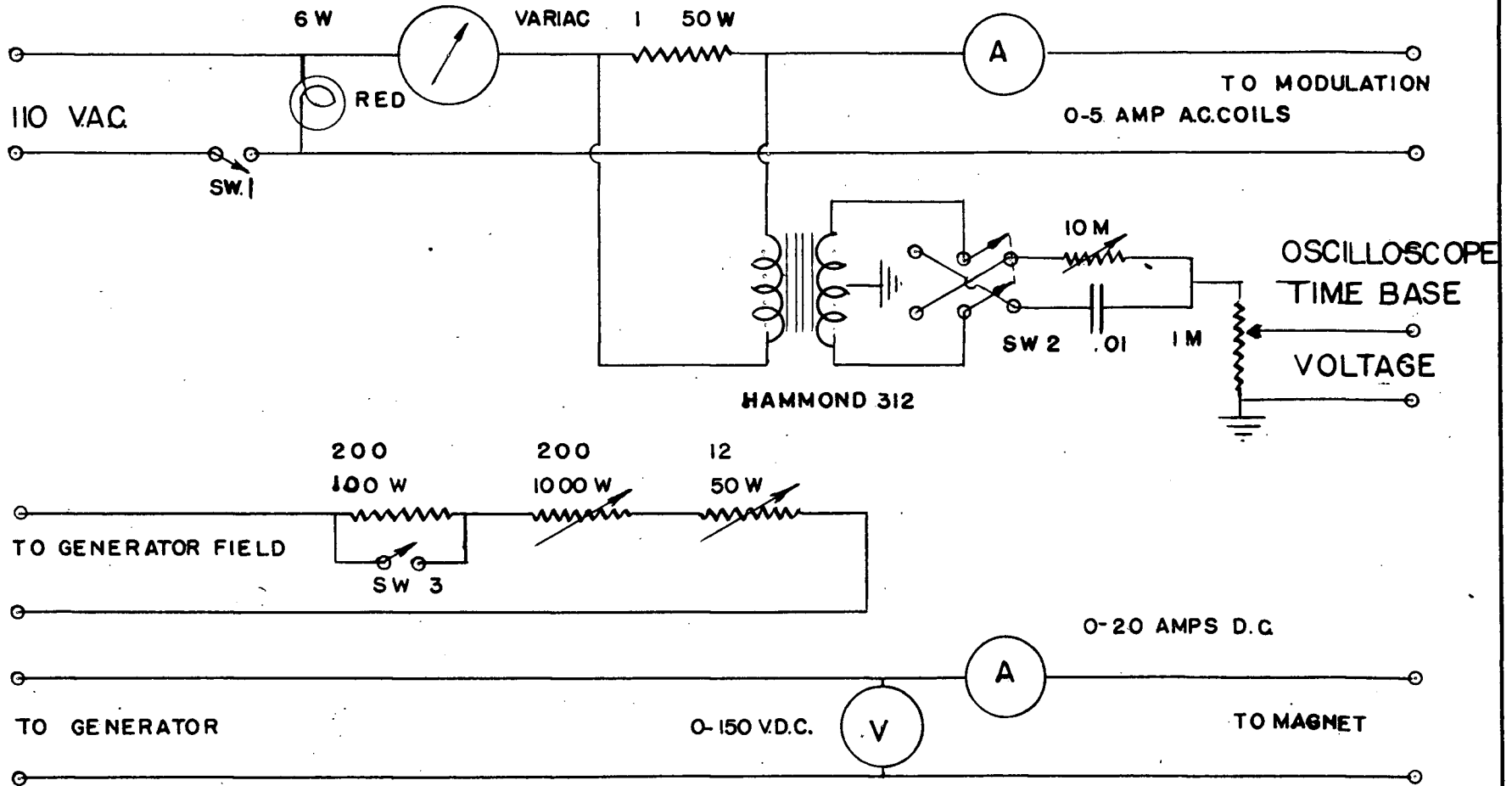


FIGURE 29

FIGURE 30



CURRENT CONTROL CIRCUITS FOR DIRECT CURRENT
MAGNETIZATION AND 60 CYCLE MODULATION COILS
ON PARAMAGNETIC RESONANCE ELECTROMAGNET